

A Compendium of Far-Infrared Line and Continuum Emission for 227 Galaxies Observed by the Infrared Space Observatory

James R. Brauher¹, Daniel A. Dale², George Helou¹

ABSTRACT

Far-infrared line and continuum fluxes are presented for a sample of 227 galaxies observed with the Long Wavelength Spectrometer on the *Infrared Space Observatory*. The galaxy sample includes normal star-forming systems, starbursts, and active galactic nuclei covering a wide range of colors and morphologies. The dataset spans some 1300 line fluxes, 600 line upper limits, and 800 continuum fluxes. Several fine structure emission lines are detected that arise in either photodissociation or H II regions: [O III] 52 μm , [N III] 57 μm , [O I] 63 μm , [O III] 88 μm , [N II] 122 μm , [O I] 145 μm , and [C II] 158 μm . Molecular lines such as OH at 53 μm , 79 μm , 84 μm , 119 μm , and 163 μm , and H₂O at 58 μm , 66 μm , 75 μm , 101 μm , and 108 μm are also detected in some galaxies. In addition to those lines emitted by the target galaxies, serendipitous detections of Milky Way [C II] 158 μm and an unidentified line near 74 μm in NGC 1068 are also reported. Finally, continuum fluxes at 52 μm , 57 μm , 63 μm , 88 μm , 122 μm , 145 μm , 158 μm , and 170 μm are derived for a subset of galaxies in which the far-infrared emission is contained within the \sim 75'' ISO LWS beam. The statistics of this large database of continuum and line fluxes, including trends in line ratios with the far-infrared color and infrared-to-optical ratio, are explored.

Subject headings: infrared: galaxies — infrared: interstellar medium

1. Introduction

Far-infrared wavelengths provide the opportunity to observe dust-enshrouded galaxies without large extinction effects and offer many diagnostics of the physical conditions in the interstellar medium of these galaxies. The *Kuiper Airborne Observatory* provided early data on the far-infrared fine structure lines that arise in photodissociation regions (PDRs) and

¹California Institute of Technology, MC 314-6, Pasadena, CA 91101

²Department of Physics and Astronomy, University of Wyoming, Laramie, WY 82071; ddale@uwyo.edu

H II regions in galaxies. With the launch of the *Infrared Space Observatory* (*ISO*; Kessler et al. 1996; Kessler et al. 2003) the far-infrared properties of galaxies were observed with greater sensitivity than ever before. The Long Wavelength Spectrometer (LWS; Clegg et al. 1996; Gry et al. 2003) on *ISO* allowed the large-scale study of far-infrared atomic and molecular lines that supply new insight into the understanding of the interstellar medium of these sources. Our next opportunities for far-infrared spectroscopic studies of galaxies will come with the *Stratospheric Observatory for Infrared Astronomy* and the *Herschel Space Observatory*.

The LWS data presented in this paper were taken from the *ISO* archive.¹ A variety of extragalactic observing programs used the LWS to obtain spectra of the primary diagnostic lines of the interstellar medium in the far-infrared. These lines include [O III] 52 μm , [N III] 57 μm , [O I] 63 μm , [O III] 88 μm , [N II] 122 μm , [O I] 145 μm , and [C II] 158 μm . Among these atomic and ionic fine structure lines, [C II] 158 μm and [O I] 63 μm are the dominant cooling lines for neutral interstellar gas. Observations of [C II] 158 μm in NGC 6946 (Madden et al. 1993; Contursi et al. 2002) suggest that a significant fraction of the [C II] 158 μm emission might also originate in diffuse ionized gas in some galaxies, while the far-infrared emission lines from ionized species ([O III] 52 μm , [N III] 57 μm , [O III] 88 μm , and [N II] 122 μm) predominantly originate in H II regions (see also Sauvage, Tuffs, & Popescu 2005). Combined with models of PDRs and H II regions (e.g., Tielens & Hollenbach 1985; Rubin 1985; Wolfire, Tielens & Hollenbach 1990; Hollenbach, Takahashi, & Tielens 1991; Spinoglio & Malkan 1992; Rubin et al. 1994; Kaufman et al. 1999; Abel et al. 2005; Le Petit et al. 2006; Meijerink, Spaans, Israel 2007; Groves et al. 2008), these fine structure transitions can be used to derive gas temperatures, densities, and the intensity of the radiation fields in galaxies. The LWS was also used to observe a suite of molecular lines in galaxies (Fischer et al. 1999) including hydroxyl (OH; 53 μm , 65 μm , 79 μm , 84 μm , 119 μm , 163 μm), water (H₂O; 59 μm , 67 μm , 75 μm , 101 μm , 108 μm), and the LWS range contains a plethora of high level rotational lines of carbon monoxide (Varberg & Evenson 1992). From the detections of multiple transitions of these molecules, the column densities and abundances for OH, H₂O, and CO can be determined (e.g., Skinner et al. 1997; González-Alfonso et al. 2004; Spinoglio et al. 2005; González-Alfonso et al. 2008).

This contribution reports on LWS observations of seven far-infrared fine structure atomic and ionic lines, far-infrared lines from three molecular species, and the far-infrared continuum of 227 galaxies, in addition to serendipitous detections of Milky Way [C II] 158 μm emission. The collection of far-infrared line fluxes in this paper comprise the largest sample

¹<http://www.iso.vilspa.esa.es/ida/index.html>

ever assembled and reduced in a uniform manner. These line fluxes are used to compare the relationship of the far-infrared fine structure lines, normalized to either another far-infrared line or the far-infrared continuum level, to two indicators of star formation activity: the $60\ \mu\text{m}/100\ \mu\text{m}$ ratio and far-infrared-to- B ratio. The properties of these emission lines are compared to findings from previous LWS emission line studies (Malhotra et al. 1997, 2001; Leech et al. 1999; Fischer et al. 1999; Luhman et al. 1998; Negishi et al. 2001; Luhman et al. 2003). The LWS continuum fluxes derived in this work are compared to *IRAS* $60\ \mu\text{m}$ and $100\ \mu\text{m}$ fluxes, ISOPHOT $170\ \mu\text{m}$ fluxes (Stickel et al. 2000), and infrared spectral energy distribution models for normal star-forming galaxies (Dale & Helou 2002).

These data can form an important framework for studies of global extragalactic interstellar media including the derivation of average gas temperatures, densities, abundances, and radiation fields integrated over entire galaxy systems. The line and continuum fluxes presented here can also supply the data for studies of the individual components (H II regions, spiral arms, disk regions) of large galaxies resolved by the LWS. Contursi et al. (2002), for example, examine the physical conditions of these different galaxy components in NGC 1313 and NGC 6946 using PDR models (Kaufman et al. 1999), and Johnson et al. (in preparation) explore the relationships between the far- and mid-infrared cooling lines observed respectively by *ISO* and the *Spitzer Space Telescope*. LWS studies of individual galaxies have also been carried out for NGC 4038/4039, M 82, NGC 253, Cen A, NGC 1068, Arp 220, and Mrk 231 (Fischer et al. 1996; Colbert et al. 1999; Unger et al. 2000; Bradford et al. 1999; González-Alfonso et al. 2004; Spinoglio et al. 2005; González-Alfonso et al. 2008).

Section 2 describes the sample of galaxies, while § 3 describes the observations and data analysis. In § 4, the far-infrared continuum data are presented and assessed from comparisons to *IRAS* 60 and $100\ \mu\text{m}$ data, ISOPHOT $170\ \mu\text{m}$ data, and galaxy infrared spectral energy distribution models. The far-infrared line data and properties are presented in § 5. In § 6, the statistical trends seen in the line data are described and these trends are related to those found from previous studies. A summary of the main results is given in § 7. The Appendix provides a description of the extended source correction and how it may be applied to the line and continuum fluxes for sources that are extended compared to the $\sim 75''$ LWS aperture.

2. The Sample and Data

The ISO LWS sample of galaxies selected from the *ISO* archive for this paper is presented in Table 1 and lists the galaxy positions, recession velocities, morphologies, optical sizes, and the flux densities of these galaxies in the four *IRAS* bands along with the $IRAS$ $60\ \mu\text{m}/100\ \mu\text{m}$

ratios. The positions, optical sizes, and velocities were taken from the NASA Extragalactic Database (NED) in mid-2004.

The sample includes both normal and Seyfert galaxies that were initially selected by identifying galaxies in the *IRAS* Cataloged Galaxies and Quasars Observed in the *IRAS* Survey (CGQ; Fullmer & Lonsdale 1989). The galaxies identified from the CGQ range in 60 μm and 100 μm flux density from 1 to 1300 Jy. The *ISO* Data Archive was queried using this list, from which 198 galaxies were observed in the LWS L01 “spectral range” or L02 “line” observing modes. Later, galaxies with *IRAS* fluxes less than 1 Jy or those with no cataloged *IRAS* flux were added to the sample in order to enlarge the sample. With these considerations, another 29 galaxies were identified within the *ISO* Archive. Photometric mode L02 observations in which the grating remained in a fixed position are excluded from this sample. The large, nearby galaxies M 31 and the Small and Large Magellanic Clouds are excluded from this sample because the size of these three galaxies is over 100 times larger than the LWS beam.

Among these 227 galaxies there are two distinct subsets, distinguished by the far-infrared size of the galaxy. The 181 galaxies in the first subset are unresolved in the far-infrared with respect to the $\sim 75''$ LWS beam. This unresolved subset of galaxies is an extension of the combined sets of smaller samples observed with the LWS (Malhotra et al. 2001; Pierini et al. 1998; Luhman et al. 2003; Negishi et al. 2001) with additional sources added from the *ISO* Data Archive. The second subset consists of 46 galaxies resolved by the LWS beam in the far-infrared. The data from this resolved subset of galaxies can be used to complement past studies (Stacey et al. 1991; Madden et al. 1993, 1997) of large galaxies with data taken from the *Kuiper Airborne Observatory* and *ISO*. The resolved galaxies are denoted as such in Table 1. The *IRAS* flux densities presented in Table 1 are selected from either Rice et al. (1988) or Dale et al. (2000) for the large, nearby galaxies in the resolved subset. For the unresolved subset of galaxies, the *IRAS* fluxes in Table 1 are taken from SCANPI co-additions of the *IRAS* survey scans.

The galaxies in this sample are distributed across the entire sky. Figure 1 displays the galaxy distribution in Galactic coordinates. The clump of galaxies at $(l, b) \sim (280^\circ, 74^\circ)$ is the Virgo Cluster. Approximately 40 galaxies lie within the Zone of Avoidance, where $|b| < 20^\circ$. Although there may be some serendipitous Galactic line and continuum emission in all directions of the sky, this serendipitous contamination is more likely toward galaxies within the Zone of Avoidance in either the galaxy spectra or the spectra of an off-source position taken during these observations. This contamination of the observed line measurements by Milky Way emission is a concern, and a discussion of detected Galactic emission lines is found in Section 5.

The *Palomar Observatory Sky Survey* plates and other observations found within NED were used to reexamine the optical morphology for each galaxy (Harold Corwin, private communication). In Figure 2, the distribution of the optical morphological types for the two subsets is shown. Both the resolved and unresolved subsets span the range of early- to late-type galaxies. The unresolved subset contains a relatively large number of S0 galaxies while the resolved subset contains no elliptical, S0/a, or peculiar galaxies.

Most of the galaxies in both the unresolved and resolved subsets are relatively nearby, and Figure 3 shows the redshift distribution for both subsets. All galaxies in the resolved subset have an absolute redshift less than 2000 km s^{-1} . With the exception of a large bin (22/181) of galaxies with redshifts greater than 10000 km s^{-1} , most galaxies in the unresolved subset have redshifts less than 6000 km s^{-1} .

Figure 4 shows the distribution of measured flux densities at $60 \mu\text{m}$ and $100 \mu\text{m}$ for the resolved and unresolved galaxies in this contribution, with *IRAS* detections taken from Table 1. At $60 \mu\text{m}$, the resolved galaxies span a more elevated flux density range ($\sim 1 - 1300 \text{ Jy}$) than the unresolved galaxies ($\sim 0.2 - 150 \text{ Jy}$), with the median flux density for unresolved galaxies smaller by a factor of roughly 4.5. At $100 \mu\text{m}$, the unresolved and resolved galaxy subsets have similar distributions over flux density, covering the range ~ 0.5 to 1000 Jy with the median flux density of unresolved galaxies smaller by only a factor of 1.6.

The distributions of the $60 \mu\text{m}/100 \mu\text{m}$ ratio and far-infrared flux are displayed in Figure 5. The $60 \mu\text{m}/100 \mu\text{m}$ ratio is an indicator of the typical heating intensity of dust in galaxies and may also suggest the relative star formation activity level of a galaxy. Lower $60 \mu\text{m}/100 \mu\text{m}$ ratios typically correspond to quiescent galaxies, whereas higher $60 \mu\text{m}/100 \mu\text{m}$ ratios indicate either a higher rate of star formation or perhaps the presence of an AGN (Helou 1986). The far-infrared flux is defined as $FIR = 1.26 \cdot 10^{-14} [2.58f_{\nu}(60\mu\text{m}) + f_{\nu}(100\mu\text{m})] \text{ W m}^{-2}$, where $f_{\nu}(60 \mu\text{m})$ and $f_{\nu}(100 \mu\text{m})$ are the $60 \mu\text{m}$ and $100 \mu\text{m}$ *IRAS* flux densities in Jy (Helou et al. 1988). The unresolved and resolved galaxy subsets peak near $60 \mu\text{m}/100 \mu\text{m}$ ratios of 0.5 and 0.4, respectively, and the resolved subset does not contain many warm galaxies with $60 \mu\text{m}/100 \mu\text{m}$ ratios greater than 0.7. It is not surprising that resolved galaxies are on average closer and more quiescent than unresolved galaxies. The larger subset of unresolved (\sim distant) systems should include more galaxies exhibiting extreme luminosities and activity levels. The distribution of *FIR* values for the two subsets spans five orders of magnitude with a peak between 10^{-12} and $10^{-13} \text{ W m}^{-2}$. The resolved galaxies reach *FIR* values as large as $10^{-10} \text{ W m}^{-2}$, an order of magnitude larger than the brightest unresolved galaxies. In Figure 6, the *IRAS* $12 \mu\text{m}/25 \mu\text{m}$ ratio is plotted against the $60 \mu\text{m}/100 \mu\text{m}$ ratio for the resolved and unresolved subsets. The sequence of infrared

colors in Figure 6 is associated with a sequence of star formation activity in galaxies (Helou 1986) and dust-heating intensity (Boulanger et al. 1988), with the upper left populated by quiescent galaxies and the lower right by warmer, more actively star-forming galaxies.

3. Observations and Data Analysis

Observations were made using the LWS in grating mode (L01, L02, 43–197 μm , $\lambda/\Delta\lambda \sim 200$). The LWS consists of ten detectors with spectral overlap for adjacent detectors. In the grating mode of the LWS, the spectral resolution is about 0.29 μm for the 10 μm -wide short-wavelength detectors (SW1–SW5) and 0.60 μm in the 20 μm -wide long-wavelength detectors (LW1–LW5). The L01 Astronomical Observation Template (AOT) is a range scan of the grating that results in 10 spectra covering a significant range of the LWS. The L02 AOT produces spectra for up to ten wavelengths, specified by the observer. In this mode, data are recorded for all ten detectors while the specified wavelengths are being scanned, producing spectra with significant gaps across the range of the LWS.

All guaranteed and open time observations for 227 galaxies were extracted from the *ISO* Data Archive and processed through the LWS Pipeline Version 7.0 or 8.7. Slight improvements in the photometric model are made beyond Pipeline Version 7.0, but these changes have minor effects on the calibration of the L01 and L02 grating mode AOTs. These changes yield improvements in the flux accuracies by a few percent but do not significantly alter the line and continuum fluxes that are derived from Pipeline 7.0.

Further data manipulation is then carried out using the LWS Interactive Analysis (LIA; Hutchinson et al. 2001) and the *ISO* Spectral Analysis Package (ISAP; Sturm et al. 1998). The continuum fluxes in the LWS spectra are significantly affected by the uncertainties in the dark current, which can be of the same order as the source continuum. Many of the galaxies in this sample are in this faint flux regime ($f_\nu(60\mu\text{m}) < 50$ Jy in the 75'' LWS beam). As the dark currents are only additive in nature across the whole band, they do not affect the line flux estimates. The dark currents are re-estimated and removed one at a time by hand through visual inspection using the LIA. The data are then corrected detector by detector for any evident instrumental responsivity variations and flux calibrated to the LWS calibration source Uranus, applied using LIA. Glitches due to cosmic rays are removed by hand from the data using ISAP by plotting spectral scans as a function of time and identifying bad data points through the characteristic appearance of falling glitch trails. Depending on the quality of the observation of a galaxy, between 15% and 20% of the data are typically discarded. Spectral scans are co-added and averaged together using a 3σ clip in spectral bins of about 0.05 μm . For extended sources or for sources that are off-center

with respect to the LWS aperture, a sinusoidal fringe associated with internal reflection and interference within the LWS instrument may arise (Gry et al. 2003; Swinyard et al. 1998). The fringes are usually less than 5% of the continuum and do not severely affect the line and continuum measurements. For full-grating L01 observations, these fringes can be removed using a defringing algorithm available within ISAP. The LWS data also suffer from transients. When the grating is scanned between the forward and reverse directions, a small (<5%) detector memory effect (Gry et al. 2003) may be visible between the two scan directions. This memory effect is due to different response times for the detectors depending on whether the signal increases or decreases with time and is most visible in the SW1, SW2, and LW2 detectors during L01 observations. No correction is applied for these memory effects. When these memory effects are present in the data, each scan direction is averaged separately, and the line and continuum fluxes for each scan direction are measured before estimating the final fluxes and uncertainties (see Sections 4 and 5 for further details). An additional source of uncertainty occurs for extended sources where the variation in the LWS beam from detector to detector might cause a mismatch between adjacent detectors by up to 30% depending on the extent and structure of the galaxy. With the application of an extended source correction, this mismatch can be partially corrected. The data presented in this paper are based on the point source calibration of the pipeline and no correction for extended sources has been applied due to the uncertainty in this correction. See the Appendix for the definition and discussion of the extended source correction.

Through the use of LIA and ISAP, the improvement in the overall quality of the data from the original pipeline Auto-Analysis Result product is substantial. By re-estimating the dark currents, the appearance of negative fluxes in most of these observations is removed. Through the re-estimation of the dark currents and gain corrections and careful glitch removal, the match between overlapping detectors is improved, thus producing more continuous spectra, shown in Figure 7. Any remaining spectral mismatch between adjacent detectors may be the result of residual errors in the dark current subtraction or beam uncertainties from detector to detector. Using LIA and ISAP, the line and continuum calibration uncertainties decrease from 20%–30% to 10%–20%, on average, for faint sources ($f_\nu(60\mu\text{m}) < 50 \text{ Jy}$) as illustrated in Figure 7.

4. The Continuum Data

The “monochromatic” continuum fluxes are derived from the LWS spectra by fitting a 2–5 μm linear baseline through the spectra surrounding the wavelengths 52 μm , 57 μm , 63 μm , 88 μm , 122 μm , 145 μm , 158 μm , and 170 μm . Continuum fluxes are measured

only for the well-calibrated LWS spectra when spectra are available at these wavelengths. Continuum fluxes could not be derived in some L02 observations that had no spectra at these wavelengths. If the observations were affected by changes in the responsivity and dark current caused by warm-ups in the long wavelength detectors, no continuum flux is derived. These continuum fluxes and associated uncertainties are listed in Table 2. Because of the uncertainty of off-axis continuum contributions in extended sources, only fluxes for galaxies unresolved by the LWS beam are listed.

Since the L02 observations do not have much overlap between detectors, it is difficult to properly estimate the dark current, and thus the continuum, for faint sources. In order to test the consistency of the continuum of the L02 observations, the continuum data are compared with observations of the 158 μm and 63 μm lines for galaxies that had a pointing at the same position in both the L01 and L02 AOTs. The continuum flux is taken from the linear baseline that is used for the fit to the lines at 158 μm and 63 μm for these observations. The continuum in the L02 observations accurately reproduces the continuum measured in the L01 AOT to within 5% for continuum fluxes down to 10 Jy. The continuum correlation between the two AOTs holds for fluxes below 10 Jy, but the dispersion in this relation increases by a factor of two. Thus, the L02 continuum appears to be consistent with the L01 continuum although some uncertainties exist from the dark or gain calibration due to the lack of overlapping spectra from adjacent detectors.

The continuum uncertainties quoted in Table 2, typically 15–20%, are a combination of the measurement and calibration uncertainties. In most observations, the calibration uncertainties are the dominant source of uncertainty in the continuum fluxes, but in the low flux limit (<10 Jy), the measurement uncertainties become dominated by uncertainties in the dark current. The detector dark currents are of the same order as the continuum in this flux regime. The effect of these uncertainties in the dark current for continuum levels below 10 Jy is described below in Sections 4.1 and 4.2. Although the comparisons to *IRAS* and ISOPHOT data show an excellent overall agreement with the LWS continuum fluxes within the LWS 20% uncertainties down to fluxes below 10 Jy, the dispersion in these relationships increases by as much as a factor of two below 10 Jy. Although there may be large uncertainties, the measured continuum fluxes below 10 Jy are included in Table 2 because there are no biases in the agreement of the LWS fluxes with *IRAS* and ISOPHOT in this low-flux limit.

4.1. Comparison with *IRAS* 60 and 100 μm Data

An extensive comparison of the LWS continuum fluxes and *IRAS* catalog fluxes was carried out for galaxies unresolved by the LWS. The following criteria were applied to this study: 1) galaxies must have an *IRAS* Point-Source Catalog detection, 2) the far-infrared emission must be concentrated within the 75'' LWS beam, and 3) LWS data must exist in the vicinity of 60 μm and 100 μm wavelengths to be used for a continuum estimation. Using these three criteria, 41 galaxies were observed in the L01 AOT and 104 galaxies in the L02 AOT.

For L01 observations, the 60 μm and 100 μm continua are estimated by performing synthetic photometry with an algorithm provided in ISAP. This photometry is performed on the spectra by integrating across the *IRAS* passbands. The 60 μm and 100 μm flux densities are then derived using the *IRAS* assumption that the source spectral energy distribution is of the form $\lambda f_\lambda = \text{constant}$. For the comparison at 60 μm a correction must be introduced because the LWS does not cover the entire *IRAS* 60 μm filter (43–197 μm vs. 27–87 μm). The galaxies used for this comparison span a wide range of 60 μm /100 μm ratios (0.2–1.4), so the amount of the integrated flux in the *IRAS* 60 μm filter missed by the LWS varies depending on the shape of the infrared spectral energy distribution of the galaxy. Dale & Helou (2002) present a sequence of galaxy spectral energy distributions sorted across a range of 60 μm /100 μm ratios. Using these models, the amount of the total integrated flux in the *IRAS* 60 μm filter missed by the LWS between 27 μm and 43 μm varies from 3% to 7% for these 60 μm /100 μm ratios. This correction based on the 60 μm /100 μm ratio of the galaxy is applied to the LWS 60 μm fluxes derived from L01 observations.

For L02 observations, synthetic photometry cannot be used because of the gaps between the multiple short scan spectra. Instead, a monochromatic flux is estimated by fitting a linear baseline to a 2–5 μm slice of spectra surrounding the wavelengths 60 μm and 100 μm . The L02 60 μm and 100 μm monochromatic continuum fluxes must also have a secondary correction applied because these monochromatic fluxes cannot be directly compared to the *IRAS* fluxes. Since the fluxes derived from the L02 observations are taken by fitting a linear baseline through the *IRAS* filter central wavelengths, the assumption would be that the flux at these wavelengths is equal to the flux over the entire *IRAS* passband for galaxies of these 60 μm /100 μm colors. A calculation of the difference between the monochromatic fluxes, estimated by fitting a linear baseline to the spectra at 60 μm and 100 μm and the synthetic photometry fluxes from integrating over the *IRAS* filters, is done using a set of pointed observations in which the same sky position on a galaxy was observed in both the L01 and L02 AOTs. The monochromatic fluxes overestimate the integrated spectral photometry on average by 11% at 60 μm and 9% at 100 μm . The monochromatic L02 fluxes are corrected

for these overestimations from using linear fits to the spectra.

After these two corrections are applied, the background is estimated using IRSKY and then removed from the LWS data. Figure 8 shows a comparison of the LWS and *IRAS* data. The LWS error bars are a combination of the uncertainties associated with the baseline fit to the line and the pipeline calibration uncertainties. The *IRAS* error bars are taken directly from the *IRAS* Point Source Catalog as given by NED. The LWS fluxes are, on average, 1% lower and 2% higher than *IRAS* at 60 μm and 100 μm , respectively, for *IRAS* fluxes above 10 Jy, a remarkable agreement. Below 10 Jy, the dispersion increases from 20% to 50%, not surprising since the dark current is comparable to 10 Jy for these sources. Both the L01 and L02 continuum fluxes show similar offsets and dispersions in the LWS–IRAS comparison.

4.2. Comparison with ISOPHOT 170 μm Continuum Data

For galaxies where the infrared continuum peaks near 60 μm , the continuum level at 170 μm is a factor of 2 or more lower compared to the peak. For galaxies with 60 μm flux densities less than 10 Jy, the detection limit of the LWS may be reached, and the reliability of the 170 μm continuum is once again subject to uncertainties in the dark current. Using published fluxes from ISOPHOT pointed observations at 180 μm (Klaas et al. 2001) and 170 μm Serendipity Survey (Stickel et al. 2000), 25 galaxies constrained to the LWS beam are compared to 170 μm fluxes measured by the LWS.

Both ISOPHOT studies referenced above utilized the broad C_160 filter. Therefore, two corrections must be applied to the LWS monochromatic fluxes. These monochromatic fluxes are compared to 170 μm fluxes derived by integrating over the ISOPHOT C_160 filter using the synthetic photometry algorithm in ISAP. On average, the monochromatic LWS fluxes are 11% higher than their synthetic counterparts, and this correction is applied to the LWS monochromatic fluxes. The second correction applied adjusts for the difference in wavelength spanned by the LWS and ISOPHOT C_160 filter (43–197 μm vs. 100–240 μm). The flux missed by the LWS in the ISOPHOT filter depends upon the spectral shape of the galaxy, and this flux is estimated by assuming the Dale & Helou (2002) spectral shape of a galaxy for a given 60 μm /100 μm ratio. Typically, this correction is approximately 3% for the range of 60 μm /100 μm ratios of these galaxies.

The total correction applied to LWS flux densities is approximately 14%, and Figure 9 is the resulting plot of this comparison. The ISOPHOT and LWS flux densities track each other well between 1 and 100 Jy, particularly if just ISOPHOT Pointed data are considered, although the dispersion increases significantly below 10 Jy. This effect is due to the

large uncertainties in the dark current at this wavelength and flux regime. The ISOPHOT Serendipity Survey (SS) flux densities are systematically a bit high compared to the LWS data. Serendipitous Survey sources were observed as they streamed by the instrument field-of-view; the fluxes reconstructed from the glancing scans may have been slightly overestimated. Considering the differences in beam size and calibration between the LWS and ISOPHOT instruments, the 30% overall agreement is consistent with the uncertainties of the two instruments at this wavelength.

4.3. Comparison with Models of Galaxy Infrared Spectral Energy Distributions

The data for the subset of galaxies smaller than the LWS aperture discussed in the previous section are compared to a semi-empirical model for the infrared spectral energy distributions of normal star-forming galaxies between 3 and 1100 μm (Dale et al. 2001; Dale & Helou 2002). The comparison of the LWS and model flux densities provides a consistency check of the LWS continuum flux densities, especially at the longer wavelengths where few continuum measurements from other observatories exist. The model is based on the combination of emission curves for large and very small grains and aromatic feature carriers for varying interstellar radiation fields, and are combined assuming a variable power-law distribution of dust mass over heating intensity. The model is constrained by *IRAS* and *ISO* observations of a sample of 60 normal, star-forming galaxies (Dale et al. 2000). According to this model, a sequence of global star formation activity level is formed as galaxies are sorted according to their 60 μm /100 μm ratio; the *IRAS* 60 μm /100 μm ratios are used in conjunction with the models to predict the LWS continuum levels at various wavelengths. The observed LWS continuum agrees with the predicted model flux densities (anchored by 60 and 100 μm *IRAS* photometry) for these galaxies to within 25% at 52 μm , 57 μm , 63 μm , 88 μm , 122 μm , 145 μm , 158 μm , and 170 μm and is presented in Figure 10. The spectral energy distribution models and the comparison with the LWS continuum are explored further in Dale & Helou (2002).

5. The Line Data

All spectral lines in this paper are unresolved ($\Delta v \sim 1500 \text{ km s}^{-1}$). Thus, the line fluxes are calculated assuming the line profile to be dominated by a Gaussian instrumental profile (FWHM=0.29 μm for $\lambda < 93 \mu\text{m}$, 0.60 for $\lambda > 80 \mu\text{m}$; for wavelengths between 80 and 93 μm , the spectral resolution depends on which of the two overlapping detectors (SW5, LW1) the

line was measured). A Gaussian has been shown to fit the LWS instrumental profiles to within 2% (Gry et al. 2003). Example line scans from this sample with various signal-to-noise ratios are displayed with a Gaussian fit in Figure 11. A detected line in this sample is defined as one that has a peak flux at the 3σ or higher confidence level. The statistical uncertainty associated with each line is $\Delta\lambda f_\lambda(\text{r.m.s.})$, the spectral resolution times the root mean square variations in the flux density of the local continuum. The dominant uncertainty for most observations is the systematic flux uncertainty that is taken from the pipeline processing. This uncertainty is a combination of the dark current, illuminator, and Uranus model calibration uncertainties. The total uncertainty is calculated by adding the statistical and systematic uncertainties in quadrature. The total uncertainty is typically between 10% and 20% of the line flux measurement, depending on the quality of the observation. In the case of non-detections, 3σ upper limits are calculated by multiplying the local statistical uncertainty described above by 3.² The data for galaxies from previous studies are included as a subset of the larger sample presented here, but are independently reduced in the manner described in § 3. In general, the line fluxes presented here agree with literature values to within 30%. The lines, rest wavelengths, and transitions for this sample are listed in Table 3.

5.1. Far-Infrared Fine Structure Lines

A number of studies have produced models that predict the strength of far-infrared fine structure lines such as [C II] 158 μm , [O I] 145 μm , and [O I] 63 μm as a function of the density and radiation intensity in PDRs (e.g., Tielens & Hollenbach 1985; Wolfire, Tielens & Hollenbach 1990; Hollenbach, Takahashi, & Tielens 1991; Spinoglio & Malkan 1992; Kaufman et al. 1999; Abel et al. 2005; Le Petit et al. 2006; Dopita et al. 2006; Dopita et al. 2006; Meijerink, Spaans, Israel 2007; Groves et al. 2008). The [C II] 158 μm and [O I] 63 μm lines act as the primary coolants to the dense ($n \sim 10 - 10^5 \text{ cm}^{-3}$ or more), warm ($T \sim 100 - 1000 \text{ K}$), neutral media. Other far-infrared fine structure lines probed by *ISO*, such as [N II] 122 μm , [O III] 52 μm and 88 μm , and [N III] 57 μm , are important to understanding H II regions. From these H II region lines, the electron densities n_e and the effective temperature of the ionizing stars can be determined. The fluxes and associated uncertainties for these seven far-infrared fine structure line measurements are given in Table 4 with the resolved and unresolved subsets noted in the table.

²Upper limits are also available via L01 range scans, though they are not presented here.

5.1.1. $[C\,II]$ 158 μm

The C⁺ fine structure transition at 157.74 μm is the dominant coolant of the neutral interstellar medium and traces PDRs. Because of the low ionization potential of neutral carbon (11.26 eV), [C II] 158 μm will emanate from neutral surface layers of far-ultraviolet illuminated neutral gas clouds. C⁺ is also easy to excite ($\Delta E/k \sim 91$ K and $n_{\text{crit}} \sim 3 \cdot 10^3$ cm⁻³) and therefore cools the warm, neutral gas (Tielens & Hollenbach 1985; Wolfire et al. 1990). In addition to PDRs, significant contributions to [C II] 158 μm emission can arise from ionized gas in diffuse H I and H II regions, although it is unclear how much [C II] 158 μm comes from these regions (Madden et al. 1993, 1997; Petuchowski & Bennett 1993; Heiles 1994; Sauty, Gerin & Casoli 1998; Malhotra et al. 2001; Contursi et al. 2002; Sauvage, Tuffs, & Popescu 2005). [C II] 158 is detected in 153 unresolved galaxies and 3σ upper limits are determined in another 17 galaxies in the unresolved subset of galaxies. [C II] 158 μm is detected in all 46 galaxies in the resolved sample.

5.1.2. $[O\,I]$ 63 μm & OI 145 μm

Neutral oxygen has two fine structure transitions at 63 μm and 145 μm and has an ionization potential of 13.62 eV. Atomic oxygen is only found in neutral regions and exists deeper into clouds than C⁺. [O I] 63 μm becomes the main coolant in warmer and denser environments ($T > 200$ K and $n > 10^5$ cm⁻³) due to its higher excitation energies and critical densities ($\Delta E/k \sim 228$ K; $n_{\text{crit}} \sim 8.5 \cdot 10^5$ cm⁻³ for [O I] 63 μm at $T \sim 100$ K and $\Delta E/k \sim 325$ K; $n_{\text{crit}} \sim 1 \cdot 10^5$ cm⁻³ for [O I] 145 μm at $T \sim 100$ K). The [O I] 63 μm line may be particularly strong in the X-ray dissociated regions surrounding active galactic nuclei (Maloney, Hollenbach, & Tielens 1996; Dale et al. 2004). In this sample, the [O I] transitions are always observed in emission except in the ultraluminous infrared galaxy Arp 220, where the 63 μm line is observed in absorption. The case of Arp 220 is discussed as part of a progression of emission and absorption line characteristics in a spectroscopic survey of infrared bright galaxies (Fischer et al. 1999) and its absorption spectrum is discussed in detail in González-Alfonso et al. (2004). In the unresolved galaxy sample, the [O I] 63 μm line is detected in 93 galaxies with 3σ upper limits available for an additional 25, while in the resolved galaxy sample it is detected in 28 galaxies with 3σ upper limits available for an additional three galaxies. In the unresolved galaxy sample, the much fainter [O I] 145 μm line is detected in 20 galaxies and 3σ upper limits are measured for another 15. In the resolved galaxy sample, the [O I] 145 μm line is detected in nine galaxies and 3σ upper limits are available for another two resolved systems.

5.1.3. $[N\ II]$ 122 μm

Neutral nitrogen has an ionization potential of 14.53 eV. One of the brighter lines of singly-ionized nitrogen, the $[N\ II]$ 122 μm line has a critical electron density of $3.1 \cdot 10^2$ cm $^{-3}$. The $[N\ II]$ 122 μm transition arises only in diffuse, ionized H II regions. The *Cosmic Background Explorer (COBE)* and the *Kuiper Airborne Observatory* provided the first astronomical detections of the $[N\ II]$ 122 μm line (Wright et al. 1991; Colgan et al. 1993). This sample greatly expands the number of extragalactic $[N\ II]$ detections from earlier studies (Malhotra et al. 2001). The $[N\ II]$ 122 μm line is detected in 38 unresolved galaxies and 3σ upper limits are measured for an additional 41 of the galaxies in the unresolved subset. For the resolved subset of galaxies, $[N\ II]$ is detected in 16 galaxies and 3σ upper limits are reported for another two.

5.1.4. $[O\ III]$ 52 μm & 88 μm

An ionizing energy of 35.12 eV is required to create O $^{++}$ from singly-ionized oxygen. Due to this high ionization potential, the $[O\ III]$ 52 μm and 88 μm transitions occur in H II regions. Using the methodology of Rubin et al. (1994), the ratio of these two lines, $[O\ III] 88\ \mu m/[O\ III] 52\ \mu m$, can be used to derive the average electron density n_e of these regions within galaxies (Duffy et al. 1987; Carral et al. 1994; Lord et al. 1996; Fischer et al. 1996; Colbert et al. 1999; Unger et al. 2000; Malhotra et al. 2001; Hunter et al. 2001). The $[O\ III]$ 88 μm line is detected in 52 galaxies and 3σ upper limits are available for 14 galaxies in the unresolved subset. The $[O\ III]$ 88 μm line is detected in 16 galaxies in the resolved galaxy sample while 3σ upper limits are available for an additional galaxy in the resolved subset. The lower signal-to-noise $[O\ III]$ 52 μm line is detected in 11 unresolved galaxies with 3σ upper limits for another 22 available, whereas the $[O\ III]$ 52 μm line is detected in five resolved galaxies and there are an additional six 3σ upper limits for the resolved galaxy subset.

5.1.5. $[N\ III]$ 57 μm

N $^+$ has a high ionization potential of 47.45 eV and therefore, the 57 μm transition of N $^{++}$ is only found in the ionized H II regions of the galaxies in this sample. The ratio $[N\ III] 57\ \mu m/[N\ II] 122\ \mu m$ provides a measure of the effective temperature T_{eff} (Rubin et al. 1994). The LWS allowed a more detailed study of the faint $[N\ III]$ 57 μm line since there are few detections of this line in the literature (Duffy et al. 1987; Malhotra et al. 2001). For

the unresolved subset of galaxies, the [N III] 57 μm line is detected in nine galaxies and 3σ upper limits are available for another 24 galaxies. The [N III] 57 μm line is detected in two resolved galaxies and 3σ upper limits are determined for six additional galaxies resolved by the LWS aperture.

5.2. Molecular Lines

Molecular line fluxes are reported in Table 5 for several of the brightest galaxies observed in this sample with *IRAS* 60 μm fluxes typically higher than 100 Jy. Molecular lines are observed in both emission and absorption for these galaxies.

5.2.1. H_2O

Water (H_2O) has been reported in two galaxies in this sample. The unresolved 101 μm ortho-para- H_2O pair is found in absorption for NGC 4945. All five H_2O transitions reported in this paper are observed in absorption in Arp 220. Detailed analysis of the far-infrared H_2O lines in Arp 220 and Mrk 231 are presented in González-Alfonso et al. (2004, 2008).

5.2.2. OH

Six transitions of Hydroxyl (OH) have been detected in this sample. The OH 53 μm transition is measured in absorption and the 163 μm transition in emission for NGC 253 and Arp 220. All galaxies in Table 5 show OH from the ground level at 119 μm , and with the exception of the archetypical Seyfert 2 galaxy NGC 1068, this transition is measured in absorption. In fact, the OH lines detected for NGC 1068, at 79, 119, and 163 μm , are observed in emission, suggesting a unique excitation environment (Spinoglio et al. 2005). The ultraluminous Seyfert 1 galaxy Mrk 231 shows an absorption line spectrum very similar to that of the ultraluminous galaxy Arp 220. The multiple OH detections in NGC 253, NGC 1068, Mrk 231, and the megamaser galaxies IRAS 20100-4156 and III Zw 35 have been previously reported and analyzed in detail (Bradford et al. 1999; Kegel et al. 1999; Goicoechea, Martín-Pintado, & Cernicharo 2005; Spinoglio et al. 2005; González-Alfonso et al. 2008). In Arp 220, all six transitions of OH reported in this paper are detected. A detailed analysis of the far-infrared absorption spectrum of Arp 220 and the implications for understanding the “[C II] 158 μm deficit” (see § 6.1, Luhman et al. 2003) is discussed in González-Alfonso et al. (2004).

5.3. Unidentified Line

An unidentified emission line at $74.24\text{ }\mu\text{m}$, also reported in NGC 7027 (Liu et al. 1996) and RWC 103 (Oliva et al. 1999), is detected in NGC 1068. The line flux and associated uncertainty for this line is listed in Table 5.

5.4. Serendipitous Galactic [C II] $158\text{ }\mu\text{m}$

The Far-Infrared Absolute Spectrophotometer (FIRAS) on the *COBE* satellite conducted an unbiased survey of the far-infrared emission from our Galaxy. The FIRAS spectral line survey included the emission lines from [C II] $158\text{ }\mu\text{m}$, [N II] $122\text{ }\mu\text{m}$ and $205\text{ }\mu\text{m}$, [C I] $370\text{ }\mu\text{m}$ and $609\text{ }\mu\text{m}$, and CO $J = 2 - 1$ through $J = 5 - 4$ with a resolution of 7° and were first reported by Wright et al. (1991). The [C II] $158\text{ }\mu\text{m}$ line had sufficient strength to be mapped by FIRAS, and Bennett et al. (1994) present detailed maps of this emission line. The all-sky maps of the [C II] $158\text{ }\mu\text{m}$ line show the highest concentration at low Galactic latitudes ($|b| < 20^\circ$). The cosecant relation provided by Bennett et al. (1994) for Galactic [C II] $158\text{ }\mu\text{m}$ emission based on *COBE* data is

$$I(\text{[C II]} \text{ } 158\mu\text{m}) = (1.43 \pm 0.12) \cdot 10^{-6} \csc |b| \text{ ergs cm}^{-2} \text{ s}^{-1} \text{ sr}^{-1}, \quad (1)$$

nominally applicable for $|b| > 15^\circ$.

There are approximately 40 galaxies in this sample that reside at low Galactic latitudes of $|b| < 20^\circ$. Galactic [C II] $158\text{ }\mu\text{m}$ contamination for low Galactic latitude galaxies can be a concern, particularly if they have recessional velocities smaller than the velocity resolution of the LWS ($|v| < 1500\text{ km s}^{-1}$). The impact of Galactic [C II] $158\text{ }\mu\text{m}$ contamination in such systems can be directly addressed via off-galaxy/sky observations made in concert with the targeted extragalactic observations. Table 6 lists six galaxies with $|v| < 1500\text{ km s}^{-1}$ for which sky observations are available. These off-galaxy positions were typically carried out $4' - 6'$ away from the targeted extragalactic direction. The level of Galactic [C II] $158\text{ }\mu\text{m}$ contamination is between 10% and 25% of the total [C II] $158\text{ }\mu\text{m}$ in the LWS aperture for these six galaxies. The [C II] $158\text{ }\mu\text{m}$ line fluxes listed in Table 4 for these six galaxies have had the foreground Milky Way [C II] $158\text{ }\mu\text{m}$ from Table 6 removed.

Equation 1 provides another method for estimating the Galactic [C II] $158\text{ }\mu\text{m}$ contamination for galaxies with $|v| < 1500\text{ km s}^{-1}$. To enhance the comparison between LWS observations and predictions from the *COBE* relation, an additional six galaxies have been added to Table 6, galaxies with recessional velocities large enough such that Milky Way [C II] $158\text{ }\mu\text{m}$ contamination is not an issue. The maps at $100\text{ }\mu\text{m}$ and the LWS line spectra

containing both Galactic C⁺ and extragalactic C⁺ for three higher redshift galaxies are presented in Figure 12. The C⁺ line associated with each target galaxy is located at the redshift of the galaxy, whereas the foreground Milky Way C⁺ is at the rest wavelength of 157.74 μm . The [C II] 158 μm intensities predicted from Equation 1 agree with the observations to within a factor of 2 for all galaxies in Table 6 except Maffei 2, which lies a half degree from the Galactic plane. For the remaining dozen or so galaxies with $|v| < 1500 \text{ km s}^{-1}$ and $|b| < 20^\circ$ that lack off-galaxy/sky observations, the contamination from Milky Way [C II] 158 μm is predicted from Equation 1 to be no more than 25%. For the 55 higher latitude ($|b| > 20^\circ$) galaxies with $|v| < 1500 \text{ km s}^{-1}$ and no off-source observation, any Milky Way [C II] 158 μm contamination is likely much less than 10%.

The four high latitude detections of Galactic [C II] 158 μm listed in Table 6 may either be due to the warm ionized medium (Petuchowski & Bennett 1993) or high latitude molecular clouds (Magnani et al. 1996). The *IRAS* Sky Survey Atlas images at 60 μm and 100 μm reveal extended Galactic emission in the same direction as the four high latitude [C II] 158 μm detections. Reach et al. (1998) describe the location of the UGCA 332 observation as a high latitude warm infrared excess H II region around the nearby B star Spica using far-infrared (60–240 μm) data from the *COBE* Diffuse Infrared Background Experiment and the Leiden-Dwingeloo H I survey (Hartmann & Burton 1997), and the spectrum for this object in Figure 12 confirms the foreground nature of this line emission.

6. Statistical Trends in the Line Data

In this section the trends in the far-infrared fine structure line fluxes are examined for the subset of 181 galaxies unresolved by the LWS beam. Line-to-line and line-to-far-infrared ratios are examined across a broad range of 60 $\mu\text{m}/100 \mu\text{m}$ and *FIR/B* values. The 60 $\mu\text{m}/100 \mu\text{m}$ ratio is an indicator of the dust heating intensity in galaxies, which is related to the star formation activity in a galaxy. The *FIR/B* ratio compares the luminosity reprocessed by dust to that of escaping starlight, indicating star formation activity along with the effects of extinction. The intent here is to identify major trends or lack thereof, as opposed to carrying out a detailed physical analysis with model comparisons.

6.1. [C II] 158 $\mu\text{m}/\text{FIR}$

Previous studies (Malhotra et al. 1997, 2001; Luhman et al. 1998, 2003; Leech et al. 1999; Negishi et al. 2001) of the [C II] 158 $\mu\text{m}/\text{FIR}$ ratio for galaxies reveal a trend

with dust heating intensity as measured by $60 \mu\text{m}/100 \mu\text{m}$ and/or FIR/B . Figure 13 shows this trend for the 181 unresolved galaxies, a trend that broadly holds for all morphological types. A $[\text{C II}]/\text{FIR}$ ratio that decreases from 1% to 0.1% with increasingly warm infrared color is typical of normal and starburst galaxies, confirming earlier studies based on smaller samples (Crawford et al. 1985; Stacey et al. 1991; Malhotra et al. 1997, 2001; Luhman et al. 2003; Verma et al. 2005). As the dust temperature increases for the most actively star-forming galaxies in this sample ($60 \mu\text{m}/100 \mu\text{m} \geq 0.8$), the $[\text{C II}]/\text{FIR}$ ratio reaches levels as low as 0.01%. The elliptical galaxies NGC 6958 and NGC 1052 are a factor of 2–5 lower than typical values of $[\text{C II}]/\text{FIR}$ for normal galaxies as first reported by Malhotra et al. (2000). However, the remaining early-type galaxies (ellipticals and lenticulars) appear to have $[\text{C II}]/\text{FIR}$ ratios similar to those of the other morphological types. $[\text{C II}]$ $158 \mu\text{m}$ emission in irregular galaxies is higher relative to the $[\text{C II}]$ $158 \mu\text{m}$ emission in spiral galaxies of the same far-infrared color temperature shown in Figure 13, as was also noted by Hunter et al. (2001).

There is a large spread in the $[\text{C II}]/\text{FIR}$ ratio for a given $60 \mu\text{m}/100 \mu\text{m}$ and FIR/B ratio. Despite this, there are several observed trends in the $[\text{C II}]/\text{FIR}$ shown in Figure 13 and several possible explanations for these trends in galaxies.

1. The $[\text{C II}]/\text{FIR}$ peaks for normal, star-forming galaxies with a $60 \mu\text{m}/100 \mu\text{m}$ ratio of 0.3–0.6 and FIR/B ratio between 0.01 and 1, consistent with the earlier studies mentioned above. These galaxies may have a higher fraction of intermediate-mass stars that are efficient at producing ultraviolet and $[\text{C II}]$ $158 \mu\text{m}$ line emission, thus, causing the peak for these galaxies. Alternatively, the high $[\text{C II}]/\text{FIR}$ values for at least the early-types may simply due to a dearth of far-infrared emission.
2. The $[\text{C II}]/\text{FIR}$ ratios for quiescent galaxies below a $60 \mu\text{m}/100 \mu\text{m}$ ratio of 0.3 and FIR/B ratio of 0.1 are, on average, similar to or slightly less than those for normal, star-forming galaxies. There is some evidence for lower $[\text{C II}]/\text{FIR}$ ratios in the quiescent galaxies of the Virgo Cluster as suggested in this study and Leech et al. (1999). Quiescent galaxies with this range of $60 \mu\text{m}/100 \mu\text{m}$ and FIR/B have a larger old low-mass stellar population than normal galaxies, and produce less ultraviolet and $[\text{C II}]$ $158 \mu\text{m}$ line emission, possibly causing a decrease in the observed $[\text{C II}]/\text{FIR}$ ratio.
3. The $[\text{C II}]/\text{FIR}$ decreases with increasing $60 \mu\text{m}/100 \mu\text{m}$ and FIR/B ratio (Malhotra et al. 1997, 2001). This trend has been seen within our Galaxy (Nakagawa et al. 1995; Bennett et al. 1994) and is not surprising for a sample of galaxies spanning a large range of $60 \mu\text{m}/100 \mu\text{m}$ and FIR/B ratios. Galaxies with $60 \mu\text{m}/100 \mu\text{m}$ ratios greater than 0.6 and FIR/B ratios greater than unity have increasingly warmer dust temperatures, most likely due to more extreme star formation. These actively star-forming galaxies have a large

proportion of massive O stars that produce hard ultraviolet radiation. Several explanations from previous studies have been offered for the decrease in the [C II]/*FIR* ratio in galaxies with the warmest dust temperatures. Malhotra et al. (2001) propose that the decrease in [C II]/*FIR* is due to the dust grains becoming more positively charged and less efficient at heating the gas for high ratios of ultraviolet flux-to-gas density (G_0/n) according to PDR models. Negishi et al. (2001) attribute this decrease in [C II]/*FIR* to either an increase in the collisional de-excitation of the [C II] 158 μm transition at high densities or a decrease in the ionized component of the [C II] 158 μm emission. For a sample of 15 ultraluminous infrared galaxies Luhman et al. (2003) report a deficiency of [C II] 158 μm , consistent with the decrease in the [C II]/*FIR* ratio at high 60 μm /100 μm ratios and explain this deficiency as the result of non-PDR contributions to the far-infrared continuum, possibly from dust-bounded ionized regions.

6.2. [O I] 63 μm /*FIR*

The [O I] 63 μm /*FIR* ratio for galaxies shows no trend with 60 μm /100 μm and a decreasing trend with *FIR/B* as displayed in Figure 14 for the 181 galaxies of the unresolved subset, plotted according to morphological type. An [O I] 63 μm /*FIR* of 0.05%–1% characterizes these galaxies. Although [C II] 158 μm /*FIR* tends to decrease with increasing 60 μm /100 μm , the same is not found for [O I] 63 μm /*FIR*, consistent with earlier studies by Malhotra et al. (2001) and Negishi et al. (2001). Therefore, as the heating environment in galaxies gets warmer, [C II] 158 μm becomes less dominant while [O I] 63 μm becomes more important in the cooling of the interstellar medium (see Section 6.5).

6.3. [N II] 122 μm /*FIR*

The [N II] 122 μm /*FIR* ratio for galaxies reveals a trend with dust temperature as measured by the 60 μm /100 μm ratio (Malhotra et al. 2001). The [N II] 122 μm /*FIR* for the 181 galaxies of the unresolved subset in this sample, plotted according to morphological type, is presented in Figure 15. A [N II] 122 μm /*FIR* of 0.01%–0.1% characterizes these galaxies. The [N II] 122 μm /*FIR* follows a similar decreasing trend as [C II] 158 μm /*FIR* with 60 μm /100 μm and *FIR/B* as suggested in Figure 15. There is a clear decrease in [N II] 122 μm /*FIR* as 60 μm /100 μm and *FIR/B* increase for spirals and irregulars. For morphologies other than spirals and irregulars, there are few detections of [N II] 122 μm and no trend is discernible. From *COBE* observations of the Milky Way, a correlation between [C II] 158 μm and [N II] 205 μm was found (Bennett et al. 1994), therefore, it is not surprising

that [N II] 122 μm and [C II] 158 μm in galaxies exhibit some of the same characteristics over a broad range of heating environments.

6.4. [O III] 88 $\mu\text{m}/\text{FIR}$

The [O III] 88 $\mu\text{m}/\text{FIR}$ ratio for the galaxies in the unresolved subset is presented in Figure 16. An [O III] 88 $\mu\text{m}/\text{FIR}$ of 0.03%–2% characterizes this sample. While there is a large scatter among the data and a small number of [O III] 88 μm detections above 60 $\mu\text{m}/100 \mu\text{m}$ ratios of 0.9, there seems to be a weak increasing trend in [O III] 88 $\mu\text{m}/\text{FIR}$ as the 60 $\mu\text{m}/100 \mu\text{m}$ ratio increases in Figure 16a. On average, there is relatively more [O III] 88 μm emission in warmer galaxies, presumably due to a higher density of H II regions in these galaxies. This overall increase in the [O III] 88 $\mu\text{m}/\text{FIR}$ ratio is also noted in Negishi et al. (2001) for a smaller set of galaxy observations. In Figure 16b, the [O III] 88 $\mu\text{m}/\text{FIR}$ appears to decrease as the FIR/B ratio increases. Malhotra et al. (2001) point out this anticorrelation between [O III] 88 $\mu\text{m}/\text{FIR}$ and FIR/B , but they attribute the effect to the observations of two irregular galaxies in their sample. In this study, many new observations of the [O III] 88 μm line are included, and a decreasing trend in [O III] 88 $\mu\text{m}/\text{FIR}$ with increasing FIR/B is discovered.

6.5. [O I] 63 $\mu\text{m}/[\text{C II}] 158 \mu\text{m}$

In Figures 13 and 14, [C II] 158 $\mu\text{m}/\text{FIR}$ is shown to decrease with increasing 60 $\mu\text{m}/100 \mu\text{m}$ and FIR/B while [O I] 63 $\mu\text{m}/\text{FIR}$ remained steady with 60 $\mu\text{m}/100 \mu\text{m}$ and FIR/B . In Figure 17, the [O I] 63 $\mu\text{m}/[\text{C II}] 158 \mu\text{m}$ ratio is plotted against 60 $\mu\text{m}/100 \mu\text{m}$ and FIR/B , and a rise in [O I] 63 $\mu\text{m}/[\text{C II}] 158 \mu\text{m}$ ratio is found as 60 $\mu\text{m}/100 \mu\text{m}$ increases for all morphologies but no conclusive trend in the [O I] 63 $\mu\text{m}/[\text{C II}] 158 \mu\text{m}$ ratio is found as FIR/B increases. From Figure 17a, [O I] 63 μm begins to dominate cooling in the interstellar medium of warmer galaxies ($60 \mu\text{m}/100 \mu\text{m} \geq 0.8$), consistent with the results reported by Malhotra et al. (2001).

6.6. [N II] 122 $\mu\text{m}/[\text{C II}] 158 \mu\text{m}$

The [N II] 122 $\mu\text{m}/[\text{C II}] 158 \mu\text{m}$ ratio remains relatively constant across a broad range of 60 $\mu\text{m}/100 \mu\text{m}$ and FIR/B for all morphological types as shown in Figure 18. The median value of [N II] 122 $\mu\text{m}/[\text{C II}] 158 \mu\text{m}$ for this sample is 0.11 when both lines have

been detected, consistent with what *COBE* observed for the Milky Way (Wright et al. 1991; Bennett et al. 1994), but lower than what models predict if [C II] 158 μm were only produced in H II regions (Rubin 1985). The similar decreasing behaviors in the [C II] 158 μm /*FIR* and [N II] 122 μm /*FIR* ratios with increasing 60 μm /100 μm and *FIR/B* ratios shown in Figures 13 and 15 along with Figure 18 suggests that a significant fraction of [C II] 158 μm arises from H II regions where N⁺ originates. Thus, the [N II] 122 μm /[C II] 158 μm ratio, on average, is nearly constant across a broad range of heating environments (Malhotra et al. 2001).

6.7. [O I] 145 μm /[O I] 63 μm

In general, the [O I] 63 μm line goes optically thick for lower column densities than the [O I] 145 μm line does. The [O I] 145 μm /[O I] 63 μm measures the gas temperature and the optical depth in the 63 μm line and rises as the gas temperature increases (Tielens & Hollenbach 1985; Kaufman et al 1999). There are few [O I] 145 μm line observations presented in this paper, most of low signal-to-noise. The low signal-to-noise [O I] 145 μm line has few detections in this sample. Therefore, the [O I] 145 μm /[O I] 63 μm ratio has no clear trend with the 60 μm /100 μm or *FIR/B* ratios as displayed in Figure 19. Hunter et al. (2001) noted an increase in the [O I] 145 μm /[O I] 63 μm with increasing *FIR/B* ratios between 0.5 and 10 and attributed this increase to an indication of the optical depth effects for [O I] 63 μm .

6.8. ([O I] 63 μm + [C II] 158 μm) / *FIR*

The gas heating efficiency of PDRs in galaxies is measured by ([O I] 63 μm + [C II] 158 μm)/*FIR* (Hollenbach & Tielens 1997) and is plotted against the 60 μm /100 μm ratio and *FIR/B* for the unresolved subset of galaxies in the sample discussed in this paper in Figure 20. The ([O I] 63 μm + [C II] 158 μm)/*FIR* ratio shows no trend with 60 μm /100 μm and a decreasing trend with *FIR/B*. For a sample of normal galaxies dominated by spirals, Malhotra et al. (2001) noted a decrease in this ratio as 60 μm /100 μm increased. Although the entire sample of galaxies does not appear to decrease in ([O I] 63 μm + [C II] 158 μm)/*FIR* as the 60 μm /100 μm ratio increases, the spiral galaxies show evidence for a decline in this ratio in warmer dust environments. The decrease in the ([O I] 63 μm + [C II] 158 μm)/*FIR* with increasing *FIR/B* is a result of the decrease in [C II] 158 μm emission shown in Figure 13.

6.9. [O III] 88 μm /[C II] 158 μm

In Figures 13a and 16a, a decrease in [C II] 158 μm /*FIR* and an increase in [O III] 88 μm /*FIR* emission are shown with increasing 60 μm /100 μm ratio. Accordingly, the [O III] 88 μm /[C II] 158 μm ratio increases with increasing 60 μm /100 μm ratio, as presented in Figure 21a. This is an interesting correlation since O⁺⁺ originates in higher density H II regions than does N⁺. While the [N II] 122 μm /[C II] 158 μm ratio did not show a correlation with the 60 μm /100 μm ratio in Figure 18a, the [O III] 88 μm /[C II] 158 μm ratio does. This suggests that the contribution to the C⁺ emission from H II regions originates in lower density, N⁺ and O⁺ regions rather than the highly ionized, more dense O⁺⁺ regions that produce [O III] 88 μm . In comparison, [C II] 158 μm /*FIR* and [O III] 88 μm /*FIR* are shown to decrease with increasing *FIR/B* ratio in Figures 13b and 16b. In Figure 21b, the [O III] 88 μm /[C II] 158 μm ratio is plotted against the *FIR/B* ratio. There is evidence for a decreasing trend in [O III] 88 μm /[C II] 158 μm with increasing *FIR/B*. The irregulars, for example, show a decrease in [O III] 88 μm /[C II] 158 μm due to a larger decrease in [C II] 158 μm than [O III] 88 μm emission with increasing *FIR/B* ratio. The irregulars also have higher [O III] 88 μm /[C II] 158 μm ratios than most spirals as noted by Hunter et al. (2001) and shown in Figure 21. The higher [O III] 88 μm /[C II] 158 μm ratios observed in irregulars are likely due to stars with higher effective temperatures found in the H II regions of these galaxies that produce doubly ionized oxygen but little C⁺.

6.10. [O III] 88 μm /[O I] 63 μm

In Figure 14, the [O I] 63 μm emission remains relatively constant when normalized to far-infrared across a broad range of interstellar medium environments measured by the 60 μm /100 μm ratio. The relative drop seen in [C II] 158 μm emission is not observed for [O I] 63 μm . By comparison, [O III] 88 μm /*FIR* shows a weak, increasing trend with increasing 60 μm /100 μm ratio in Figure 16a. The [O III] 88 μm /[O I] 63 μm ratio is plotted against the 60 μm /100 μm ratio in Figure 22a. The [O III] 88 μm /[O I] 63 μm ratio has no obvious trend that spans all 60 μm /100 μm ratios, unlike [O III] 88 μm /[C II] 158 μm . In Figures 14b and 16b, the [O I] 63 μm /*FIR* ratio shows little trend with *FIR/B* while the [O III] 88 μm /*FIR* ratio falls as the *FIR/B* ratio increased. A slight decline in the [O III] 88 μm /[O I] 63 μm ratio is observed as the *FIR/B* ratio increases and is shown in Figure 22b. Similar to the [O III] 88 μm /[C II] 158 μm ratio, the [O III] 88 μm /[O I] 63 μm ratio for irregulars decreases noticeably with increasing *FIR/B*. Irregular galaxies also show an elevated [O III] 88 μm /[O I] 63 μm ratio when compared to spirals as mentioned by Hunter et al. (2001).

6.11. [O III] 88 μm /[N II] 122 μm

[O III] 88 μm originates in higher density H II regions (excitation potential=35 eV), and [N II] 122 μm originates in lower density H II regions (excitation potential=14.5 eV). The [O III] 88 μm /[N II] 122 μm ratio is plotted against the 60 μm /100 μm and FIR/B ratios in Figure 23 for galaxies unresolved by the LWS. Perhaps there are correlations for [O III] 88 μm /[N II] 122 μm with the 60 μm /100 μm and FIR/B ratios, though too few data are available to have confidence in these trends.

7. Summary

ISO LWS far-infrared line and continuum fluxes for a sample of 227 galaxies selected from the *ISO* Data Archive spanning an *IRAS* 60 μm /100 μm color range of 0.2–1.4 and 60 μm flux densities between 0.1 Jy and 1300 Jy are presented. The far-infrared lines detected in this sample include the seven fine structure lines ([C II] 158 μm , [O I] 145 μm , [N II] 122 μm , [O III] 88 μm , [O I] 63 μm , [N III] 57 μm , [O III] 52 μm) and multiple OH (53 μm , 65 μm , 79 μm , 84 μm , 119 μm , 163 μm) and H₂O (59 μm , 67 μm , 75 μm , 101 μm , 108 μm) transitions. An unidentified line at 74.24 μm previously reported in NGC 7027 is detected in NGC 1068. Serendipitous detections of Milky Way [C II] 158 μm are also observed in twelve sky positions. This sample is the largest collection of far-infrared line observations ever assembled and includes 465 independent LWS observations yielding some 1300 line fluxes, 600 line flux upper limits, and 800 continuum fluxes.

The data presented here can be separated into two subsets, one where the source is resolved and one where it is unresolved by the 75'' LWS beam. The resolved subset contains 46 galaxies and the unresolved subset contains 181 galaxies. The statistical trends in the unresolved subset are examined, and the following results are compared to earlier studies (Malhotra et al. 1997, 2001; Leech et al. 1999; Luhman et al. 1998, 2003; Negishi et al. 2001):

1. The LWS continuum agrees with fluxes predicted from *IRAS* data and the spectral energy distribution models of Dale & Helou (2002) to within 25% at 52 μm , 57 μm , 63 μm , 88 μm , 122 μm , 145 μm , 158 μm , and 170 μm .
2. The [C II] 158 μm /*FIR* ratio peaks for normal, star-forming galaxies with 60 μm /100 μm ratios of 0.3–0.6 and *FIR/B* ratios of 0.1–1. The [C II]/*FIR* ratio in quiescent galaxies with 60 μm /100 μm ratios less than 0.3 and *FIR/B* ratios less than 0.1 is consistent with normal, star-forming galaxies. The [C II] 158 μm /*FIR* ratio decreases with increasing dust temperatures (60 μm /100 μm > 0.6) and infrared to blue ratio (*FIR/B* > 1).

3. The $[\text{O I}] 63 \mu\text{m}/\text{FIR}$ ratio shows no obvious correlation with $60 \mu\text{m}/100 \mu\text{m}$ and a decrease as a function of FIR/B .
4. The ratio $[\text{N II}] 122 \mu\text{m}/\text{FIR}$ shows a similar correlation as $[\text{C II}] 158 \mu\text{m}/\text{FIR}$, decreasing as the $60 \mu\text{m}/100 \mu\text{m}$ and FIR/B ratios increase. The $[\text{N II}] 122 \mu\text{m}/[\text{C II}] 158 \mu\text{m}$ shows no correlation with either the $60 \mu\text{m}/100 \mu\text{m}$ or FIR/B ratio, indicating that a large fraction of $[\text{C II}] 158 \mu\text{m}$ may arise from H II regions.
5. In contrast to $[\text{C II}] 158 \mu\text{m}/\text{FIR}$ and $[\text{N II}] 122 \mu\text{m}/\text{FIR}$, the $[\text{O III}] 88 \mu\text{m}/\text{FIR}$ ratio increases as the $60 \mu\text{m}/100 \mu\text{m}$ ratio increases. This increase might be due to the higher density of H II regions found in galaxies with warmer far-infrared colors. The $[\text{O III}] 88 \mu\text{m}/\text{FIR}$ ratio, however, decreases with increasing FIR/B ratio.
6. The $[\text{O I}] 63 \mu\text{m}/[\text{C II}] 158 \mu\text{m}$ ratio increases as the $60 \mu\text{m}/100 \mu\text{m}$ ratio increases, but shows no correlation with FIR/B . In warmer galaxies ($60 \mu\text{m}/100 \mu\text{m} > 0.8$), $[\text{O I}] 63 \mu\text{m}$ becomes more important than $[\text{C II}] 158 \mu\text{m}$ in cooling the interstellar medium.
7. The $([\text{O I}] 63 \mu\text{m} + [\text{C II}] 158 \mu\text{m})/\text{FIR}$ ratio is a measure of the gas heating efficiency in PDRs, and shows only a slight decrease with increasing $60 \mu\text{m}/100 \mu\text{m}$ ratio for spirals but no decrease for the unresolved galaxies as a whole. The $([\text{O I}] 63 \mu\text{m} + [\text{C II}] 158 \mu\text{m})/\text{FIR}$ ratio does, however, decrease with increasing FIR/B ratio for the unresolved subset of galaxies as a whole.
8. The $[\text{O III}] 88 \mu\text{m}/[\text{C II}] 158 \mu\text{m}$ ratio increases with increasing $60 \mu\text{m}/100 \mu\text{m}$ ratio. This is due to the dramatic falloff of $[\text{C II}] 158 \mu\text{m}$ emission in galaxies showing warmer far-infrared emission. The $[\text{O III}] 88 \mu\text{m}/[\text{C II}] 158 \mu\text{m}$ ratio decreases with increasing FIR/B ratio.
9. The $[\text{O III}] 88 \mu\text{m}/[\text{O I}] 63 \mu\text{m}$ ratio has no correlation with the $60 \mu\text{m}/100 \mu\text{m}$ ratio. The $[\text{O III}] 88 \mu\text{m}/[\text{O I}] 63 \mu\text{m}$ ratio decreases slightly with increasing FIR/B .

These data provide a framework through which the interstellar medium of these galaxies may be studied in the future.

We thank several people for their contributions: Harold Corwin for reclassifying the galaxies in this sample according to the RC3 catalog; Steve Lord, Tom Jarrett, and Alessandra Contursi for helpful discussions; Heather Maynard for her suggestions and support; Pat Patterson and Niles McElveney for assistance with the preparation of the manuscript; and an anonymous referee for many helpful suggestions. The data for this project are based on observations with the Infrared Space Observatory, an ESA project with instruments funded by ESA member states (especially the PI countries: France, Germany, the Netherlands,

and the United Kingdom) with the participation of ISAS and NASA. The *ISO* Spectral Analysis Package (ISAP) is a joint development by the LWS and SWS Instrument Teams and Data Centers. Contributing institutes are CESR, IAS, IPAC, MPE, RAL, and SRON. This research has made use of the NASA/IPAC Extragalactic Database that is operated by the Jet Propulsion Laboratory, California Institute of Technology, under contract with the National Aeronautics and Space Administration (NASA). This work has made use of data services of the InfraRed Science Archive (IRSA) at the Infrared Processing and Analysis Center/California Institute of Technology, funded by the National Aeronautics and Space Administration (NASA).

Appendix: The Extended Source Correction

The flux calibration of the LWS instrument is based on observations of Uranus, a point source in the LWS aperture. The telescope is diffraction limited at about $110\text{ }\mu\text{m}$, beyond which a fraction of the flux of an on-axis point source may be diffracted out of the standard aperture. Significant diffraction loss does not occur in sources that appear extended in the LWS beam. Therefore, an extended source correction must be applied to put these fluxes on a point source calibration scale. In order to apply this correction, the LWS beam of each detector and the telescope PSF must be well known. The extended source correction also assumes that the source is infinitely extended and uniformly bright. None of these galaxies are either, so applying the correction requires great caution. From tests done by the LWS instrument team, the extended source correction works well for sources larger than $3\text{--}4'$ (Gry et al. 2003) when compared to *IRAS* at $100\text{ }\mu\text{m}$.

The fluxes quoted in Tables 2, 4, and 5 are those which have been measured according to the point source flux calibration. The current understanding of the LWS beam is still not complete, and the extended source correction may change in the future as more work is done. Therefore, the extended source correction has not been applied to the line fluxes listed in this paper, but those galaxies that may require an extended source correction have been noted in Tables 2, 4, and 5. The most up-to-date effective apertures and corrections are listed in Table 7, taken from the ISO LWS Handbook Volume III (Gry et al. 2003).

REFERENCES

- Abel, N.P., Ferland, G.,J., Shaw, G., & van Hoof, P.A.M. 2005, ApJS, 161, 65
- Bennett, C.L. et al. 1994, ApJ, 434, 587
- Boreiko, R.T. & Betz, A.L. 1997, ApJS, 111, 409
- Boulanger, F., Beichman, C., Désert, F.X., Helou, G., Perault, M., & Ryter, C. 1988, ApJ, 332, 328
- Bradford, C.M. et al. 1999, in “The Universe as Seen by ISO”, ed. Cox, P. & Kessler, M.F., ESA SP-427 (Noordwijk, Netherlands), 861
- Carral, P., Hollenbach, D.J., Lord, S.D., Colgan, S.W.J., Haas, M.R., Rubin, R.H., & Erickson, E.F. 1994, ApJ, 423, 223
- Colbert J.W. et al. 1999, ApJ, 511, 721
- Clegg, P. et al. 1996, A&A, 315, L38
- Colgan, S.W.J., Haas, M.R., Erickson, E.F., Rubin, R.H., Simpson, J.P., & Russell, R.W. 1993, ApJ, 413, 237
- Contursi, A. et al. 2002, ApJ, 124, 751
- Crawford, M.K., Genzel, R., Townes, C.H., & Watson, D.M. 1985, ApJ, 291, 755
- Dale, D.A. et al. 2000, ApJ, 120, 583
- Dale, D.A., Helou, G., Contursi, A., Silbermann, N.A., & Kolhatkar, S. 2001, ApJ, 549, 215
- Dale, D.A. & Helou, G. 2002, ApJ, 576, 159
- Dale, D.A., Helou, G., Brauher, J.R., Cutri, R.M., Malhotra, S., & Beichman, C.A. 2004, 604, 565
- Dopita, M.A., Fischera, J., Sutherland, R.S., Kewley, L.J., Leitherer, C., Tuffs, R.J., Popescu, C.C., van Breugel, W., & Groves, B.A. 2006, ApJS, 167, 177
- Duffy, P.B., Erickson, E.F., Haas, M.R., & Houck, J.R. 1987, ApJ, 315, 68
- Fischer, J. et al. 1996, A&A, 315, L97
- Fischer, J. et al. 1999, Astrophysics & Space Science, 266, 91

- Fullmer, L. & Lonsdale, C.J. 1989, Cataloged Galaxies and Quasars Observed in the *IRAS* Survey, Version 2 (Pasadena:JPL)
- Goicoechea, J.R., Martín-Pintado, J., & Cernicharo, J. 2005, ApJ, 619, 291
- González-Alfonso, E., Smith, H.A., Fischer, J., & Cernicharo, J. 2004, ApJ, 613, 247
- González-Alfonso, E., Smith, H.A., Ashby, M.L.N., Fischer, J., Spinoglio, L., & Grundy, T.W. 2008, ApJ, 675, 303
- Groves, B., Dopita, M., Sutherland, R., Kewley, L., Fischera, J., Leitherer, C., Brandl, B., & van Breugal, W. 2008,
apjs, in press
- Gry, C. et al. 2003, The ISO Handbook, Volume III – LWS – The Long Wavelength Spectrometer, Version 2.1 (European Space Agency)
- Hartmann, D. & Burton, W.B. 1997, Atlas of Galactic Neutral Hydrogen (Cambridge: Cambridge University Press)
- Heiles, C. 1994, ApJ, 436, 720
- Helou, G. 1986, ApJ, 311, L33
- Helou, G., Khan, I.R., Malek, L., & Boehmer, L. 1988, ApJS, 68, 151
- Hollenbach, D.J., Takahashi, T., & Tielens, A.G.G.M. 1991, ApJ, 377, 192
- Hollenbach, D.J. & Tielens, A.G.G.M. 1997, ARA&A, 35, 179
- Hunter, D.A. et al. 2001, ApJ, 553, 121
- Hutchinson, M.G., Chan, S.J., & Sidher, S.D. 2001, in “The Calibrations Legacy of the *ISO* Mission”, ed. Metcalfe, L. & Kessler, M.F., ESA SP-481
- Kaufman, M.J., Wolfire, M.G., Hollenbach, D.J., & Luhman, M.L. 1999, ApJ, 527, 795
Kegel, W.H., Hertenstein, T., & Quirrenbach, A. 1999, A&A, 351, 472
- Kessler, M.F. et al. 1996, A&A, 315, L27
- Kessler, M.F., Mueller, T.G., Leech, K., Arviset, C., Garcia-Lario, P., Metcalfe, L., Pollock, A., Prusti, T., & Salama, A. 2003, The ISO Handbook, Volume I – Mission & Satellite Overview, Version 2.0 (European Space Agency)

- Le Petit, F., Nehmé, C., Le Bourlot, J., & Roueff, E. 2006,
apjs, 164, 506
- Leech, K.J., Vlk, Heinrichsen, I., Hippelein, H., Metcalfe, L., Pierini, D., Popescu, C.C.,
Tuffs, R.J., & Xu, C. 1999, MNRAS, 310, 317
- Liu, X.-W. et al. 1996, A&A, 315, L257
- Lord, S.D. Hollenbach, D.J., Haas, M.R., Rubin, R.H., Colgan, S.W.J., & Erickson, E.F.
1996, ApJ, 465, 703
- Luhman, M.L., Satyapal. S., Fischer, J., Wolfire, M.G., Cox, P., Lord, S.D., Smith, H.A.,
Stacey, G.J., & Unger, S.J. 1998, ApJ, 504, L11
- Luhman, M.L., Satyapal. S., Fischer, J., Wolfire, M.G., Sturm, E., Dudley, C.C., Lutz, D.
& Genzel, R. 2003, ApJ, 594, 758
- Madden, S.C., Geis, N., Genzel, R., Herrmann, F., Jackson, J., Poglitsch, A., Stacey, G.J.,
& Townes, C.H. 1993, ApJ, 407, 579
- Madden, S.C., Poglitsch, A., Geis, N., Stacey, G.J., & Townes, C.H. 1997, ApJ, 483, 200
- Malhotra, S. et al. 1997, ApJ, 491, L27
- Malhotra, S. et al. 2000, ApJ, 543, 634
- Malhotra, S. et al. 2001, ApJ, 561, 766
- Maloney, P.R., Hollenbach, D.J., & Tielens, A.G.G.M. 1996, ApJ, 466, 561
- Meijerink, R., Spaans, M., & Israel, F.P. 2007, A&A, 461, 793
- Nakagawa, T., Doi, Y., Yui, Y.Y., Okuda, H., Mochizuki, K., Shibai, H., Nishimura, T., &
Low, F.J. 1995, ApJ, 455, L35
- Negishi, T., Onaka, T., Chan, K.-W., & Roellig, T.L., 2001, A&A, 375, 566
- Oliva, E., Moorwood, A.F.M., Drapatz, S., Lutz, D., & Sturm, E. 1999, A&A, 343, 943
- Petuchowski, S.J. & Bennett, C.L. 1993, ApJ, 405, 591
- Pierini, D., Leech, K.J., Tuffs, R.J., & Vlk, H.J. 1999, MNRAS, 303, L29
- Reach, W.T., Wall, W.F., & Odegard, N. 1998, ApJ, 507, 507

- Rubin, R.H. 1985, ApJS, 57, 349
- Rubin, R.H., Simpson, J.P., Lord, S.D., Colgan, S.W.J., Erickson, E.F., & Haas, M.R. 1994, ApJ, 420, 772
- Sauty, S., Gerin, M., & Casoli, F. 1998, A&A, 339, 19
- Sauvage, M., Tuff, R.J., & Popescu, C.C. 2005, Space Science Reviews, Vol. 119, Issue 1-4, 313
- Shibai, H., Okuda, H., Nakagawa, T., Matsuhara, H., Maihara, T., Mizutani, K., Kobayashi, Y., & Hiromoto, N. 1991, ApJ, 374, 522
- Skinner, C.J., Smith, H.A., Sturm, E., Barlow, M.J., Cohen, R.J., & Stacey, G.J. 1997, Nature, 386, 472
- Spinoglio, L. & Malkan, M.A. 1992, ApJ, 399, 504
- Spinoglio, L., Malkan, M.A., Smith, H.A., González-Alfonso, E., & Fischer, J. 2005, ApJ, 623, 123
- Sturm, E. et al. 1998, Astronomical Data Analysis Software and Systems VII, A.S.P. Conference Series, Vol. 145, eds. R. Albrecht, R.N. Hook, & H.A. Bushouse, p. 161
- Stacey, G.J., Geis, N., Genzel, R., Lugten, J.B., Poglitsch, A., Sternberg, A., & Townes, C.H. 1991, ApJ, 373, 423
- Stickel, M., Lemke, D., Klaas, U., Beichman, C.A., Rowan-Robinson, M., Efstathiou, A., Bogun, S., Kessler, M.F., & Richter, G. 2000, A&A, 359, 865
- Swinyard, B.M., Burgdorf, M.J., Clegg, P.E., Davis, G.R., Griffin, M.J., Gry, C., Leeks, S.J., Lim, T.L., Pezzuto, S., & Tommasi, E. 1998, SPIE, 3354, 888
- Tielens, A.G.G.M. & Hollenbach, D.J. 1985, ApJ, 291, 722
- Unger, S.J. et al. 2000, A&A, 355, 885
- Varberg, T.D. & Evenson, K.M. 1992, ApJ, 385, 763
- Verma, A., Charmandaris, V., Klaas, U., Lutz, D., & Haas, M. 2005, Space Science Reviews, Vol. 119, Issue 1-4, 355
- Wolfire, M.G., Tielens, A.G.G.M., & Hollenbach, D.J. 1990, ApJ, 358, 116
- Wright, E.L. et al. 1991, ApJ, 381, 200

Table 1. Galaxies and Properties

Galaxy	R.A. (J2000.0)	Dec. (J2000.0)	cz (km s $^{-1}$)	T^b	$2a^c$ '	$2b^c$ '	12 μ m (Jy)	25 μ m (Jy)	60 μ m (Jy)	100 μ m (Jy)	60/100
IC 10 ^a	00 20 24.55	+59 17 30.5	-344	10	6.3	5.1	4.88	13.95	112.9	179.2	0.63
ESO 350-IG38	00 36 52.53	-33 33 18.6	6156	-2			0.41	2.49	6.47	5.01	1.29
Cartwheel	00 37 40.80	-33 42 58.0	9050	10	1.1	0.9	0.08	0.11	0.73	1.57	0.46
NGC 0185	00 38 57.69	+48 20 12.2	-202	-5	11.7	10.0	0.04	<0.03	0.35	1.46	0.24
NGC 0247 ^a	00 47 08.30	-20 45 37.6	160	7	21.4	6.9	<0.12	<0.16	7.93	27.32	0.29
NGC 0253 ^a	00 47 34.37	-25 17 32.0	245	5	27.5	6.8	55.84	155.7	998.7	1862.	0.54
NGC 0278	00 52 04.58	+47 33 02.0	640	3	2.1	2.0	1.63	2.57	25.05	46.39	0.54
UGC 00545	00 53 34.90	+12 41 36.0	18330	-1	0.5	0.5	0.51	1.21	2.24	2.63	0.85
MCG+12-02-001	00 54 04.01	+73 05 12.6	4706	99			0.76	3.71	22.37	26.68	0.84
NGC 0300 ^a	00 54 53.72	-37 40 56.9	144	7	21.9	15.5	0.53	0.64	23.08	74.45	0.31
IC 1613 ^a	01 05 02.00	+02 08 03.0	-234	10	16.2	14.5	0.08	0.11	0.68	1.78	0.38
NGC 0449	01 16 07.23	+33 05 22.3	4780	-1	0.8	0.5	0.34	0.89	2.53	3.05	0.83
UGC 00852	01 19 38.30	+17 33 53.0	8817	5	1.1	0.4	0.14	0.13	0.77	4.02	0.19
NGC 0520	01 24 34.90	+03 47 30.0	2266	99	1.9	0.7	0.76	2.84	31.1	47.12	0.66
M 33 ^a	01 33 50.90	+30 39 37.0	-179	6	70.8	41.7	32.69	40.26	419.7	1256.	0.33
NGC 0625	01 35 04.20	-41 26 15.0	405	9	5.8	1.9	0.20	0.94	5.09	9.07	0.56
NGC 0628 ^a	01 36 41.70	+15 46 59.0	657	5	10.5	9.5	2.07	1.90	20.86	65.64	0.32
NGC 0660	01 43 01.70	+13 38 34.0	850	1	8.3	3.2	2.31	7.05	67.27	104.9	0.64
Mrk 573	01 43 57.80	+02 21 00.0	5174	-1	1.3	1.3	0.23	0.79	1.11	1.36	0.82
III Zw 35	01 44 30.50	+17 06 08.0	8225	11			0.09	1.08	13.33	14.13	0.94
NGC 0685	01 47 43.10	-52 45 40.0	1356	5	3.7	3.3	0.13	0.15	1.60	7.14	0.22
NGC 0693	01 50 31.00	+06 08 42.0	1567	90	2.1	1.0	0.29	0.55	6.73	11.81	0.57
NGC 0695	01 51 14.20	+22 34 57.0	9735	10	0.8	0.7	0.48	0.86	7.87	13.57	0.58
UGC 01449	01 58 06.70	+03 05 15.0	5589	9	1.2	0.7	0.31	0.56	4.96	8.41	0.59
NGC 0821	02 08 21.20	+10 59 41.0	1735	-5	2.6	1.6					
NGC 0814	02 10 37.70	-15 46 24.0	1616	-2	1.3	0.5	0.19	1.01	4.41	3.59	1.23
Arp 273	02 21 32.78	+39 21 29.9	7563				<0.17	0.24	1.87	3.85	0.49
NGC 0891 ^a	02 22 33.04	+42 20 47.7	528	3	13.5	2.5	5.66	7.78	61.1	198.6	0.31
NGC 0925 ^a	02 27 17.00	+33 34 43.0	553	7	10.5	5.9	0.26	0.66	7.65	26.68	0.29
NGC 0986	02 33 34.10	-39 02 41.0	2005	2	3.9	3.0	1.41	3.65	25.14	51.31	0.49
NGC 1022	02 38 32.70	-06 40 40.0	1453	1	2.4	2.0	0.75	3.29	19.83	27.16	0.73
NGC 1052	02 41 04.80	-08 15 20.8	1470	-5	3.0	2.1	0.20	0.49	0.93	1.5	0.62
Maffei 2 ^a	02 41 54.90	+59 36 14.9	-17	4	5.8	1.6					
NGC 1068	02 42 40.70	-00 00 47.9	1136	3	7.1	6.0	39.7	85.04	176.2	224.	0.79
UGC 02238	02 46 17.40	+13 05 44.0	6436	99	1.4	1.3	0.34	0.53	8.40	15.56	0.54
NGC 1097 ^a	02 46 18.89	-30 16 21.0	1275	3	9.3	6.3	2.88	7.70	46.73	116.3	0.40
NGC 1155	02 58 12.90	-10 21 00.0	4549	-2	0.8	0.7	0.21	0.47	2.89	4.98	0.58
NGC 1156	02 59 42.60	+25 14 17.0	375	10	3.3	2.5	0.17	0.55	5.24	10.48	0.50
NGC 1222	03 08 56.80	-02 57 18.0	2452	-3	1.1	0.9	0.51	2.29	13.07	15.38	0.85
UGC 02519	03 09 19.70	+80 07 52.0	2377	6	1.2	0.7	0.25	0.34	2.98	7.45	0.40
NGC 1266	03 16 00.80	-02 25 38.0	2194	-2	1.5	1.0	0.14	1.23	13.32	16.44	0.81
NGC 1313 ^a	03 18 15.40	-66 29 51.0	475	7	9.1	6.9	1.70	3.75	45.69	97.21	0.47
NGC 1275	03 19 48.16	+41 30 42.1	5264	99	2.2	1.7	1.06	3.53	7.14	6.98	1.02
NGC 1316 ^a	03 22 41.51	-37 12 33.4	1760	-2	12.0	8.5	0.32	0.24	2.97	7.33	0.41
NGC 1317	03 22 44.40	-37 06 13.0	1941	1	2.8	2.4	0.26	0.31	3.52	10.35	0.34

Table 1—Continued

Galaxy	R.A. (J2000.0)	Dec. (J2000.0)	<i>cz</i> (km s ⁻¹)	<i>T</i> ^b	2 <i>a</i> ^c '	2 <i>b</i> ^c '	12 μm (Jy)	25 μm (Jy)	60 μm (Jy)	100 μm (Jy)	60/100
NGC 1326	03 23 56.40	−36 27 52.0	1360	−1	3.9	2.9	0.38	0.86	8.17	13.85	0.59
NGC 1365 ^a	03 33 35.57	−36 08 22.9	1636	3	11.2	6.2	3.37	10.82	97.79	174.6	0.56
IC 1953	03 33 41.60	−21 28 41.0	1867	7	2.8	2.1	0.16	0.93	8.47	11.29	0.75
NGC 1377	03 36 38.90	−20 54 06.0	1792	−2	1.8	0.9	0.44	1.81	7.25	5.75	1.26
NGC 1385	03 37 28.20	−24 30 04.0	1493	6	3.4	2.0	1.19	2.02	17.3	37.61	0.46
IC 342 ^a	03 46 49.71	+68 05 44.7	31	6	21.4	20.9	23.66	45.20	256.0	661.7	0.39
UGC 02855	03 48 22.60	+70 07 57.0	1202	6	4.4	2.0	2.93	4.86	42.39	90.19	0.47
NGC 1482	03 54 39.50	−20 30 07.0	1916	−1	2.5	1.4	1.54	4.67	33.45	46.46	0.72
IC 356	04 07 46.80	+69 48 45.0	895	2	5.2	3.9	0.23	0.16	3.84	24.61	0.16
NGC 1546	04 14 37.20	−56 03 35.0	1276	1	3.0	1.7	0.62	0.79	7.21	22.53	0.32
NGC 1569	04 30 49.00	+64 50 53.0	−104	10	3.6	1.8	1.23	8.98	54.25	55.36	0.98
3C 120	04 33 11.10	+05 21 15.6	9896	−2	0.8	0.6	0.28	0.63	1.28	2.78	0.46
NGC 1614	04 34 00.03	−08 34 43.7	4778	5	1.3	1.1	1.44	7.28	32.31	32.69	0.99
NGC 1672 ^a	04 45 42.10	−59 14 57.0	1350	3	6.6	5.5	1.67	4.03	32.96	69.89	0.47
NGC 1741	05 01 38.30	−04 15 25.0	4107	99	0.6	0.3	0.10	0.57	3.91	5.83	0.67
IRAS 05189-2524	05 21 01.42	−25 21 45.9	12760	11	0.46	0.44	0.72	3.44	13.67	11.36	1.20
UGCA 116	05 55 42.60	+03 23 31.0	789	11	0.6	0.2	0.41	1.92	6.62	5.20	1.27
UGC 03426	06 15 36.74	+71 02 14.3	4050	−2	1.8	1.6	0.71	2.89	3.77	3.36	1.12
NGC 2146	06 18 39.70	+78 21 23.0	893	2	6.0	3.4	6.22	17.58	131.0	184.2	0.71
IC 450	06 52 12.32	+74 25 37.4	5537	−0.5	0.8	0.5	0.22	0.68	1.18	1.65	0.72
NGC 2388	07 28 53.50	+33 49 05.0	4134	3	1.0	0.6	0.51	2.07	17.01	25.39	0.67
NGC 2415	07 36 56.50	+35 14 32.0	3784	10	0.9	0.9	0.42	0.91	8.56	12.89	0.66
DDO 50 ^a	08 19 12.66	+70 43 06.4	157	10	7.9	6.3	0.12	0.17	1.51	2.62	0.58
M 81 ^a	09 55 33.20	+69 03 55.0	−34	2	26.9	14.1	5.86	5.42	44.73	174.0	0.26
M 82 ^a	09 55 54.03	+69 40 57.1	203	90	11.2	4.3	66.61	285.0	1271.	1351.	0.94
IC 2554	10 08 50.42	−67 01 47.5	1474	4	3.1	1.3	0.98	2.71	17.25	34.13	0.51
ESO 317-G023	10 24 42.40	−39 18 21.0	2892	1	1.9	0.8	0.34	0.88	13.5	23.68	0.57
NGC 3256	10 27 51.41	−43 54 20.6	2738	99	3.8	2.1	3.23	16.03	88.3	115.3	0.77
NGC 3344 ^a	10 43 31.10	+24 55 20.0	586	4	7.1	6.5	0.34	0.48	5.51	22.54	0.24
NGC 3359 ^a	10 46 37.65	+63 13 22.2	1014	5	7.2	4.4	0.16	0.28	4.06	14.66	0.28
NGC 3368 ^a	10 46 45.70	+11 49 12.0	897	2	7.6	5.2	0.53	0.54	8.26	25.93	0.32
IRASF10565+2448	10 59 18.10	+24 32 34.0	12921	99	0.4	0.3	0.21	1.13	12.08	15.29	0.79
NGC 3557	11 09 57.40	−37 32 17.0	3067	−5	4.1	3.0	0.35		0.24	0.71	0.34
NGC 3556 ^a	11 11 31.79	+55 40 14.7	699	6	8.7	2.2	2.25	4.09	32.19	80.77	0.40
NGC 3583	11 14 10.80	+48 19 03.0	2136	3	2.8	1.8	0.63	0.78	7.08	18.63	0.38
NGC 3620	11 16 04.30	−76 12 54.0	1680	2	2.8	1.1	1.29	4.71	46.8	66.86	0.70
NGC 3623 ^a	11 18 55.20	+13 05 35.0	807	1	9.8	2.9	0.20	0.40	2.42	14.35	0.17
NGC 3683	11 27 32.00	+56 52 43.0	1716	6	1.9	0.7	1.06	1.53	13.61	29.59	0.46
NGC 3690	11 28 32.20	+58 33 51.0	3121	9			3.8	23.19	103.7	107.4	0.97
NGC 3705	11 30 06.70	+09 16 36.0	1018	2	4.9	2.0	0.38	0.44	3.72	11.27	0.33
NGC 3885	11 46 46.50	−27 55 22.0	1802	0	2.4	1.0	0.46	1.41	11.66	16.42	0.71
NGC 3949	11 53 41.40	+47 51 32.0	807	4	2.9	1.7	0.82	1.37	11.28	25.64	0.44
NGC 4027	11 59 30.58	−19 15 48.3	1671	8	3.2	2.4	0.65	1.04	11.61	27.64	0.42
NGC 4038 ^a	12 01 52.82	−18 51 54.3	1642	9	5.2	3.1					
NGC 4039 ^a	12 01 53.82	−18 53 06.3	1641	9	3.1	1.6					

Table 1—Continued

Galaxy	R.A. (J2000.0)	Dec. (J2000.0)	cz (km s $^{-1}$)	T^b	$2a^c$ '	$2b^c$ '	12 μ m (Jy)	25 μ m (Jy)	60 μ m (Jy)	100 μ m (Jy)	60/100
NGC 4041	12 02 12.20	+62 08 14.0	1234	4	2.7	2.5	0.87	1.42	13.34	32.88	0.41
NGC 4051 ^a	12 03 09.50	+44 31 54.2	725	4	5.2	3.9	0.85	1.59	7.13	23.92	0.30
NGC 4102	12 06 23.10	+52 42 39.0	837	3	3.0	1.7	1.72	7.05	48.1	70.74	0.68
NGC 4125	12 08 05.60	+65 10 29.0	1356	-5	5.8	3.2	0.08	<0.09	0.70	1.46	0.48
IRAS 12071-0444	12 09 45.10	-05 01 14.0	38480	-2	0.2	0.2	0.08	0.64	2.48	2.64	0.94
NGC 4151	12 10 32.60	+39 24 21.0	995	2	6.3	4.5	2.02	4.95	6.18	7.90	0.78
VCC 66	12 12 46.20	+10 51 49.1	378	8	5.1	1.8	0.14	0.29	2.0	8.09	0.25
NGC 4189	12 13 47.30	+13 25 29.0	2115	6	2.4	1.7	0.26	0.40	3.04	8.92	0.34
VCC 92 ^a	12 13 48.17	+14 53 42.4	-142	2	9.8	2.8	0.65	0.36	7.19	23.18	0.31
NGC 4194	12 14 09.60	+54 31 35.0	2506	10	1.8	1.1	0.83	4.53	23.81	25.06	0.95
PG 1211+143	12 14 17.60	+14 03 12.0	24253		0.6	0.4	0.25	0.27	0.34	0.61	0.56
NGC 4222	12 16 22.80	+13 18 28.0	230	7	3.3	0.5	<0.12	<0.13	0.98	3.19	0.31
NGC 4236 ^a	12 16 43.37	+69 27 56.4	0	8	21.9	7.2	0.11	0.57	3.98	10.02	0.40
NGC 4278	12 20 06.82	+29 16 50.7	649	-5	4.1	3.8	0.15	0.11	0.62	1.74	0.36
VCC 460	12 21 12.91	+18 22 57.7	893	0	5.6	2.6	0.18	0.50	4.58	10.44	0.44
NGC 4294	12 21 17.80	+11 30 32.0	359	6	3.2	1.2	0.1	0.19	2.72	9.40	0.29
NGC 4299	12 21 40.20	+11 30 10.0	232	8	1.7	1.6	0.1	0.24	2.63	8.08	0.33
NGC 4314	12 22 31.97	+29 53 44.3	963	1	4.2	3.7	0.16	0.36	3.78	7.14	0.53
NGC 4374	12 25 03.65	+12 53 14.2	1000	-5	6.5	5.6	0.23	0.26	0.52	0.98	0.53
VCC 857	12 25 56.07	+18 12 53.7	922	3	3.6	3.2	0.15	0.14	0.95	4.01	0.24
VCC 873	12 26 07.85	+13 06 45.7	232	3	3.9	1.1	0.53	0.56	5.31	17.39	0.31
I Zw 36	12 26 16.02	+48 29 36.6	281	8	0.8	0.6	0.08		0.58	0.91	0.64
NGC 4414	12 26 26.69	+31 13 24.0	716	5	3.6	2.0	1.91	2.30	26.81	66.07	0.41
NGC 4418	12 26 54.60	-00 52 40.0	2179	1	1.4	0.7	1.0	9.69	43.89	32.04	1.37
VCC 1003	12 27 26.34	+11 06 29.4	1106	-1	5.6	2.6	0.23	0.18	1.65	4.27	0.39
VCC 1043	12 27 45.46	+13 00 35.5	71	0	8.5	3.2	0.2	0.17	3.76	11.27	0.33
NGC 4449 ^a	12 28 12.00	+44 05 41.0	207	10	6.2	4.4	1.37		35.49	67.97	0.52
VCC 1110	12 28 29.30	+17 05 05.0	1954	2	5.2	3.9	0.11	0.15	1.23	7.43	0.17
VCC 1158	12 29 02.94	+13 11 08.2	1931	-1	3.5	1.4	0.07	0.15	0.13	0.34	0.38
VCC 1253	12 30 02.41	+13 38 10.7	1353	-1	3.8	3.5	0.19	0.15	0.58	1.08	0.54
NGC 4490	12 30 36.90	+41 38 23.0	565	7	6.3	3.1	1.86	4.20	45.9	76.5	0.60
NGC 4486	12 30 49.42	+12 23 28.0	1282	-4	8.3	6.6	0.23	0.24	0.50	0.58	0.86
VCC 1326	12 30 57.20	+11 28 59.0	497	1	1.7	0.9	0.11	0.35	2.68	3.42	0.78
VCC 1412	12 32 06.36	+11 10 41.9	1342	-3	3.5	1.7	0.14		0.24	0.79	0.30
NGC 4519	12 33 30.30	+08 39 17.0	1220	7	3.2	2.5	0.36	0.55	3.74	7.06	0.53
NGC 4522	12 33 39.80	+09 10 31.0	2337	6	3.7	1.0	0.12	0.21	1.29	4.19	0.31
NGC 4559 ^a	12 35 58.17	+27 57 33.4	816	6	10.7	4.4	0.49	0.73	9.69	27.05	0.36
NGC 4569 ^a	12 36 50.02	+13 09 47.9	-235	2	9.5	4.4	0.75	1.28	9.19	27.33	0.34
NGC 4589	12 37 25.00	+74 11 31.0	1980	-5	3.2	2.6	<0.11	<0.09	0.20	0.82	0.24
VCC 1727	12 37 44.12	+11 49 10.5	1519	3	5.9	4.7	0.34	0.37	4.74	18.09	0.26
VCC 1813	12 39 56.02	+10 10 33.0	1874	-1	4.0	3.0	0.12	0.17	0.49	1.39	0.35
VCC 1869	12 41 13.42	+10 09 20.4	1864	-2	3.2	2.7	0.09		0.06		
VCC 1972	12 43 32.32	+11 34 55.8	1422	5	2.9	2.3	0.49	0.61	5.32	15.42	0.35
NGC 4651	12 43 42.60	+16 23 36.0	805	5	4.0	2.6	0.41	0.42	5.44	15.57	0.35
VCC 1987	12 43 56.54	+13 07 33.2	1037	6	4.9	2.8	0.90	1.34	13.08	34.91	0.37

Table 1—Continued

Galaxy	R.A. (J2000.0)	Dec. (J2000.0)	cz (km s $^{-1}$)	T^b	$2a^c$ '	$2b^c$ '	12 μ m (Jy)	25 μ m (Jy)	60 μ m (Jy)	100 μ m (Jy)	60/100
NGC 4656 ^a	12 43 57.70	+32 10 05.0	646	9			0.10	0.30	5.90	11.46	0.51
NGC 4670	12 45 16.90	+27 07 30.0	1069	0	1.4	1.1	<0.16	0.28	2.63	4.47	0.59
NGC 4691	12 48 13.54	-03 19 58.2	1110	0	2.8	2.3	0.71	2.43	14.73	20.59	0.72
VCC 2070	12 48 23.49	+08 29 15.9	1002	2	4.0	2.5	0.12	0.13	0.30	2.03	0.15
NGC 4713	12 49 57.80	+05 18 39.0	652	7	2.7	1.7	0.24	0.17	4.60	10.95	0.42
Mrk 231	12 56 14.23	+56 52 25.2	12642	5	1.3	1.0	1.87	8.66	31.99	30.29	1.06
IC 3908	12 56 40.40	-07 33 40.0	1296	7	1.8	0.7	0.44	0.87	8.09	17.08	0.47
NGC 4818	12 56 48.80	-08 31 31.0	1065	1.7	4.3	1.5	0.83	3.85	20.01	25.18	0.79
NGC 4861	12 59 01.80	+34 51 40.0	847	9	4.0	1.5	0.4	0.41	1.92	2.60	0.74
NGC 4945 ^a	13 05 22.90	-49 28 06.0	560	6	20.0	3.8	23.65	43.28	588.1	1416.	0.42
NGC 5005 ^a	13 10 56.23	+37 03 33.1	946	4	5.8	2.8	0.95	1.20	19.65	54.26	0.36
UGCA 332	13 11 58.90	-12 03 49.0	2107	7	1.7	1.1			0.23		
IC 860	13 15 03.50	+24 37 08.0	3347	1	0.5	0.3	0.1	1.31	17.93	18.6	0.96
IC 883	13 20 35.30	+34 08 22.0	7000	99	1.5	1.1	0.25	1.41	17.01	24.41	0.70
Cen A ^a	13 25 27.62	-43 01 08.8	547	-2	25.7	20.0	23.03	30.74	217.6	501.2	0.43
IC 4249	13 27 06.50	-27 57 22.0	2023		1.3	0.4	<0.06	<0.15	0.55	0.74	0.74
ESO 173-G015	13 27 23.70	-57 29 21.0	3006		1.1	0.2	1.19	7.59	81.58	99.87	0.82
M 51 ^a	13 29 52.30	+47 11 54.0	463	4	11.2	6.9	11.02	17.47	108.7	292.1	0.37
M 83 ^a	13 37 00.23	-29 52 04.5	516	5	12.9	11.5	26.28	47.72	266.0	638.6	0.42
NGC 5248 ^a	13 37 32.00	+08 53 07.0	1153	4	6.2	4.5	1.15	1.73	18.38	44.54	0.41
Mrk 273	13 44 42.03	+55 53 13.2	11326	99	1.1	0.3	0.23	2.28	21.74	21.38	1.02
NGC 5322	13 49 15.50	+60 11 28.0	1781	-5	5.9	3.9	<0.09	<0.08	0.40	0.81	0.49
IC 4329A	13 49 19.39	-30 18 35.3	4813	-0.7	1.4	0.4	1.08	2.21	2.03	1.66	1.22
Mrk 463	13 56 02.90	+18 22 19.0	14895	10	0.6	0.4	0.51	1.57	2.18	1.92	1.14
NGC 5430	14 00 45.69	+59 19 48.2	2961	3	2.2	1.1	0.56	1.62	10.41	19.47	0.53
NGC 5433	14 02 36.00	+32 30 38.0	4354	5	1.6	0.4	0.27	0.70	6.62	11.57	0.57
NGC 5457 ^a	14 03 12.50	+54 20 55.0	241	6	28.8	26.9	6.2	11.78	92.7	237.7	0.39
Circinus	14 13 09.30	-65 20 21.0	436	3	6.9	3.0	19.59	67.93	245.6	409.	0.60
NGC 5643	14 32 40.70	-44 10 28.0	1199	5	4.6	4.0	1.09	3.64	19.49	38.16	0.51
NGC 5713	14 40 11.30	-00 17 27.0	1883	4	2.8	2.5	1.3	2.84	21.89	38.09	0.57
I Zw 92	14 40 38.10	+53 30 16.0	11332	-2			0.12	0.50	1.31	1.85	0.71
NGC 5772	14 51 38.90	+40 35 57.0	4900	3	2.1	1.3	<0.10	<0.08	0.34	1.66	0.20
NGC 5786	14 58 56.70	-42 00 45.0	2998	4	2.3	1.1	0.36	0.76	5.26	14.98	0.35
NGC 5866	15 06 29.49	+55 45 43.9	672	-1	4.7	1.9	0.36	0.34	5.21	17.11	0.30
CGCG1510.8+0725	15 13 13.30	+07 13 27.0	3897	0	0.4	0.2	0.05	0.83	20.84	31.52	0.66
IRAS 15206+3342	15 22 38.00	+33 31 36.0	37297		0.2	0.16	0.08	0.34	1.76	1.88	0.94
IRAS 15250+3609	15 26 59.40	+35 58 38.0	16535	10	0.6	0.5	0.13	1.31	7.39	5.94	1.24
NGC 5937	15 30 46.02	-02 49 44.9	2807	3	1.9	1.1	0.64	1.13	9.76	20.35	0.48
NGC 5953	15 34 32.33	+15 11 41.8	1965	1	1.6	1.3	0.53	1.16	10.04	18.97	0.53
Arp 220	15 34 57.34	+23 30 11.9	5434	90	1.5	1.2	0.48	7.90	103.8	112.4	0.92
NGC 5962	15 36 31.70	+16 36 32.0	1958	5	3.0	2.1	0.74	1.03	8.89	22.11	0.40
IC 4545	15 41 27.80	-81 37 33.0	2696	5	1.9	0.9	0.12	0.12	1.18	5.38	0.22
Mrk 297	16 05 12.90	+20 32 32.0	4716	5			0.27	0.82	6.15	10.19	0.60
IC 4595	16 20 44.20	-70 08 35.0	3410	5	2.7	0.5	0.71	0.73	7.05	18.04	0.39
NGC 6217	16 32 39.83	+78 11 54.4	1362	4	3.0	2.5	0.50	1.61	10.83	19.33	0.56

Table 1—Continued

Galaxy	R.A. (J2000.0)	Dec. (J2000.0)	<i>cz</i> (km s ⁻¹)	<i>T</i> ^b	2 <i>a</i> ^c '	2 <i>b</i> ^c '	12 μm (Jy)	25 μm (Jy)	60 μm (Jy)	100 μm (Jy)	60/100
NGC 6156	16 34 52.71	−60 37 00.8	3300	4.8	1.6	1.4	1.00	2.47	16.11	33.35	0.48
CGCG 025-007	16 51 25.10	−02 48 18.0		−1	1.0	0.6	0.13	0.05	0.71	2.77	0.26
NGC 6221	16 52 46.67	−59 12 59.0	1482	5	3.5	2.5	1.89	5.95	40.68	81.6	0.50
NGC 6240	16 52 58.85	+02 24 08.8	7339	90	2.1	1.1	0.55	3.41	22.68	27.78	0.82
NGC 6286	16 58 31.40	+58 56 13.0	5501	−1	1.3	1.2	0.42	0.56	8.22	22.13	0.37
IRAS 17208-0014	17 23 21.90	−00 17 01.0	12834	−2	0.4	0.3	0.19	1.65	31.14	34.9	0.89
IC 4662	17 47 06.40	−64 38 25.0	308	10	2.8	1.6	0.30	1.27	8.81	11.9	0.74
NGC 6503 ^a	17 49 27.10	+70 08 43.0	62	6	7.1	2.4	0.44	0.50	7.57	25.94	0.29
Ark 535	17 58 07.10	+21 16 19.0	6000	−3	0.4	0.3	0.06	0.08	0.67	2.47	0.27
3C 368	18 05 06.30	+11 01 35.2	z=1.13		1.4		0.06	0.09	0.14	1.14	0.12
NGC 6574	18 11 51.30	+14 58 52.0		2282	4	1.4	1.1	0.80	1.60	13.22	27.96
HB89 1821+643	18 21 57.31	+64 20 36.4	89038				0.23	0.59	1.21	2.06	0.59
NGC 6764	19 08 16.43	+50 56 00.1	2416	3.5	2.3	1.3	0.36	1.29	6.32	11.56	0.55
NGC 6744 ^a	19 09 45.31	−63 51 21.5	841	4	20.0	12.9	0.17	0.22	28.84	96.13	0.30
NGC 6753	19 11 23.30	−57 02 56.0	3124	3	2.5	2.1	0.95	0.98	9.77	28.26	0.35
IRAS 19254-7245	19 31 21.40	−72 39 18.0	18500	−2			0.22	1.24	5.48	5.78	0.95
IRAS 19297-0406	19 32 21.20	−03 59 56.0	25701		0.2	0.2	0.11	0.68	7.14	8.55	0.84
NGC 6810	19 43 34.16	−58 39 20.6	2031	2	3.2	0.9	1.10	3.49	17.79	34.5	0.52
NGC 6824	19 43 41.03	+56 06 38.9	3386	3	1.7	1.2	0.50	0.63	5.48	15.53	0.35
NGC 6821	19 44 24.10	−06 50 02.0	1525	7	1.2	1.0	0.14	0.31	3.63	5.71	0.64
NGC 6822 ^a	19 44 56.14	−14 48 05.5	−57	10	15.5	13.5	0.84	6.63	58.86	130.3	0.45
Cygnus A	19 59 28.30	+40 44 02.0	16811	−2			0.20	1.06	2.32	<8.3	0.28
IRAS 20100-4156	20 13 29.50	−41 47 35.0	38848	−2	0.3	0.2	0.10	0.46	5.26	5.11	1.03
IC 5020	20 30 38.10	−33 29 05.0	3071	4	3.0	2.1	0.18	0.15	1.07	4.36	0.25
NGC 6946 ^a	20 34 52.30	+60 09 14.0	48	6	11.5	9.8	15.17	23.34	167.7	362.7	0.46
Mrk 509	20 44 09.08	−10 43 22.0	10312	−6	0.5	0.5	0.31	0.70	1.36	1.52	0.89
NGC 6958	20 48 42.20	−37 59 42.0	2713	−4	2.1	1.7	0.16	0.20	0.97	1.91	0.51
IC 5063	20 52 02.00	−57 04 09.0	3402	−0.8	2.1	1.4	1.06	3.91	5.33	4.16	1.28
IRAS 20551-4250	20 58 26.89	−42 39 06.2	12840	−2	1.1	0.4	0.28	1.90	12.78	9.94	1.29
NGC 7217	22 07 52.30	+31 21 32.0	952	2	3.9	3.2	0.37	0.30	4.96	18.45	0.27
NGC 7218	22 10 11.70	−16 39 36.0	1662	6	2.5	1.1	0.28	0.56	4.67	11.18	0.42
NGC 7314	22 35 45.76	−26 03 02.7	1422	4	4.6	2.1	0.26	0.57	3.73	14.15	0.26
NGC 7331 ^a	22 37 04.99	+34 25 07.6	816	3	10.5	3.7	3.36	4.20	35.29	115.1	0.31
IRAS 22491-1808	22 51 49.20	−17 52 23.0	23312	3	0.3	0.2	0.09	0.54	5.25	4.73	1.11
NGC 7418	22 56 36.00	−37 01 47.0	1446	6	3.5	2.6	0.63	0.69	5.38	16.13	0.33
IC 1459	22 57 10.61	−36 27 44.0	1691	−5	5.2	3.8	0.11	0.20	0.49	0.94	0.52
NGC 7469	23 03 15.59	+08 52 29.3	4892	1	1.5	1.1	1.34	5.78	25.87	34.9	0.74
IRAS 23128-5919	23 15 47.01	−59 03 16.9	13371	−2	0.9	0.7	0.24	1.59	10.8	10.99	0.98
NGC 7552	23 16 11.00	−42 34 59.0	1585	2	3.4	2.7	2.94	12.16	72.03	101.5	0.71
NGC 7582	23 18 23.19	−42 22 11.1	1575	2	5.0	2.1	1.62	6.43	49.1	72.92	0.67
IC 5325	23 28 43.10	−41 19 58.0	1503	4	2.8	2.5	0.48	0.70	5.15	14.35	0.36
III Zw 107	23 30 09.90	+25 31 58.0	5734	−2			0.08	0.36	1.59	1.81	0.88
NGC 7714	23 36 14.01	+02 09 22.3	2798	3	1.9	1.4	0.46	2.85	10.36	11.51	0.90
IRASF23365+3604	23 39 01.30	+36 21 10.0	19331	1	0.5	0.3	0.13	0.88	7.44	8.83	0.84
NGC 7771	23 51 24.80	+20 06 42.0	4277	1	2.5	1.0	0.77	1.77	19.67	40.12	0.49

Table 1—Continued

Galaxy	R.A. (J2000.0)	Dec. (J2000.0)	cz (km s $^{-1}$)	T^b	$2a^c$ '	$2b^c$ '	12 μ m (Jy)	25 μ m (Jy)	60 μ m (Jy)	100 μ m (Jy)	60/100
Mrk 331	23 51 26.80	+20 35 10.0	5541	1	0.7	0.4	0.55	2.39	18.04	23.61	0.76
NGC 7793 ^a	23 57 49.41	-32 35 23.6	227	7	9.3	6.3	1.54	2.09	19.62	56.34	0.35

Note. — Units of right ascension are hours, minutes, and seconds, and units of declination are degrees, arcminutes, and arcseconds.

^aGalaxy is considered an extended source in this paper.

^bOptical morphology classified by Harold Corwin using the RC3 numerology.

^cThe major and minor diameters at the B -band 25 mag arcsec $^{-2}$ level.

^dIRAS fluxes of the unresolved sample are taken from the IRAS Point Source Catalog. IRAS fluxes of the resolved sample are integrated flux densities from high resolution processed maps.

Table 2. Far-Infrared Continuum Flux Densities

Galaxy	170 μm (Jy)	158 μm (Jy)	145 μm (Jy)	122 μm (Jy)	88 μm (Jy)	63 μm (Jy)	57 μm (Jy)	52 μm (Jy)
NGC 0185	2.0±0.5	1.5±0.2	1.6±0.2	2.8±0.3				
UGC 00545		4.8±0.5				5.8±0.6		
MCG +12-02-001	27.8±2.1	28.9±3.1	28.7±2.3	30.1±2.7	37.4±4.4	30.2±2.8	24.8±2.2	21.8±2.0
IC 1613		1.6±0.2	1.7±0.2			2.2±0.3		
NGC 0449		4.4±0.6	2.9±0.3	2.4±0.3		5.2±0.5	2.4±1.3	
UGC 00852	6.3±4.2	1.3±1.0	3.7±0.7	4.3±0.7				
NGC 0520	29.6±2.8	33.0±4.3	39.4±4.2	48.7±3.7	57.7±7.6	44.4±4.6	37.9±3.4	30.7±2.8
NGC 0625	8.8±1.6		3.5±0.6	5.9±1.0	4.0±0.6		5.5±0.8	
NGC 0660	75.6±7.6	92.0±9.2	91.5±9.2	106.3±10.6	110.0±11.2	80.3±8.0	70.1±7.1	60.4±6.1
Mrk 573		1.1±0.2	1.8±0.3	2.0±0.2	3.7±0.5	8.4±0.9		
III Zw 35	12.5±1.2	5.3±0.6	8.2±0.8	10.4±1.0	9.9±1.3	18.4±1.7	16.2±1.5	8.5±1.0
NGC 0685			3.0±0.5					
NGC 0693		10.7±2.3	7.6±1.0	11.0±0.9		14.5±1.5		
NGC 0695	15.5±1.4		18.5±1.5	14.9±1.3	19.3±2.4	12.6±1.2		
UGC 01449	7.4±1.2	6.9±1.6	6.9±0.7	8.1±0.7		8.2±0.9		
NGC 0814	1.3±0.2	4.1±1.0		4.2±0.3		14.6±1.5		
NGC 0986	28.2±2.5	39.8±5.8	37.0±3.4	46.4±3.0	44.1±5.5	26.1±2.7	25.6±2.2	23.0±2.1
NGC 1022	22.5±2.0	24.0±3.3	21.0±2.4	26.0±2.4	36.7±4.3	27.1±2.5	24.6±2.3	23.3±2.0
UGC 02238	18.8±1.8	23.8±2.9	18.4±1.9	17.2±1.4	24.4±2.4	17.3±1.8	7.4±1.4	
NGC 1155		2.6±0.5	2.4±0.3	2.2±0.2		4.1±0.4		
NGC 1156	5.3±0.5	17.0±2.1	7.4±0.7	8.2±0.7		2.1±0.2		
NGC 1222	8.0±0.9	10.8±2.2	11.4±1.1	12.9±1.1		20.4±2.0	20.2±1.8	
UGC 02519	5.5±0.9	8.1±1.8	7.9±0.8	7.7±0.7		6.3±0.6		
NGC 1266	10.1±1.0	14.8±4.8	13.3±1.3	16.7±1.3	21.6±2.7	18.5±1.8	15.5±1.4	
NGC 1275	4.5±0.6	7.8±0.9	7.5±0.8	6.4±0.5	7.3±1.0	12.1±1.2	10.7±1.0	11.5±1.2
NGC 1317	2.6±0.3	7.5±1.5				5.1±0.5		
NGC 1326	10.3±1.0			13.6±1.0		13.0±1.2		
IC 1953	2.0±0.3	8.4±1.0		7.3±0.6	13.2±1.6	11.5±1.2		
NGC 1377		5.8±0.8		4.2±0.4	11.3±1.3	13.6±1.3		
NGC 1385	20.2±1.7	23.3±4.3	26.8±3.0	27.9±2.2	28.9±3.5	23.7±2.2	19.9±1.6	
UGC 02855	66.8±5.7	67.3±8.9	57.6±4.6	64.2±4.9	59.4±7.6	37.8±3.7	22.2±1.9	17.7±1.6
NGC 1482	55.7±4.8		50.5±4.1	52.7±4.5	61.7±7.4	40.7±4.1	37.3±3.2	30.4±2.6
NGC 1546	13.7±1.3	16.6±3.8	22.7±2.1	23.1±1.9	18.6±2.5	9.4±0.9	4.5±0.7	
NGC 1569	27.1±2.2	31.0±5.5	30.9±3.3	31.8±2.6	53.2±6.1	51.9±4.8	44.1±3.8	42.7±3.7
3C 120	9.9±1.0	8.0±1.0	5.1±0.5	4.0±0.3	4.0±0.5	2.4±0.3		
NGC 1614	12.5±1.2	16.3±2.2	20.3±1.9	25.0±2.1	49.2±4.9	43.1±4.4	30.7±3.0	25.6±2.6
NGC 1672	40.2±3.6	47.9±5.5	44.8±5.1	54.1±4.4	60.5±7.5	40.5±3.9	30.6±2.6	
IRAS 05189-2524	4.2±0.5	6.6±0.9	5.0±0.5	6.9±0.6				
UGCA 116	7.9±1.6	11.7±1.4	10.7±1.1	10.5±0.9	9.7±1.2	10.4±1.0	8.5±0.9	4.9±0.6
UGC 03426	2.7±0.4	2.2±0.3			5.7±0.7	8.3±0.8		
NGC 2146	124.9±3.5	138.3±4.2	139.4±1.8	192.1±1.7	250.1±6.2	183.4±3.2	160.6±2.8	134.7±3.2
IC 450		5.4±0.7			4.7±0.5	3.7±0.4		
NGC 2388	17.3±1.5	26.2±3.2	22.9±2.5	24.7±2.1	33.9±4.3	20.9±2.1	20.5±1.7	
IC 2554	24.6±3.6	26.2±4.2	25.3±4.2	30.1±6.0	37.3±6.0	22.3±3.0	19.8±2.7	15.6±2.2
ESO 317-G023	17.5±3.0	26.7±5.3	23.7±5.8	23.5±3.6	27.5±4.4	20.8±3.0	14.2±1.9	

Table 2—Continued

Galaxy	170 μm (Jy)	158 μm (Jy)	145 μm (Jy)	122 μm (Jy)	88 μm (Jy)	63 μm (Jy)	57 μm (Jy)	52 μm (Jy)
NGC 3256	43.9±7.9	92.6±19.1	101.2±29.7	130.5±27.8	165.3±29.0	130.2±19.0	97.9±13.1	91.3±12.2
IRAS F10565+2448	11.5±1.3	10.1±1.6	8.4±1.0	9.3±0.7	23.2±2.2	14.0±1.5		
NGC 3583	19.6±2.1	18.7±2.7		17.2±1.6		12.0±1.1		
NGC 3620	53.8±8.0	66.0±11.1	55.4±9.8	71.7±12.7	83.6±15.1	56.3±7.8	56.8±8.2	45.4±6.5
NGC 3683	18.8±2.1	23.8±3.4	22.0±2.6	25.8±2.0	34.4±4.4	15.7±1.6	9.0±0.9	
NGC 3690	60.7±6.3	58.6±7.5	65.7±5.3	86.4±7.9	140.6±19.9	150.8±14.6	142.3±13.1	128.8±12.3
NGC 3705	8.7±0.8	15.5±2.6		9.5±1.1		3.8±0.4		
NGC 3885	7.9±1.2	13.8±3.4	10.1±1.8	12.7±2.6	23.7±4.0	15.0±1.8	7.5±1.1	
NGC 3949	18.6±1.9	13.3±2.4	12.9±1.7	17.6±1.6	17.3±2.3	11.6±1.1		10.6±0.9
NGC 4027	14.4±2.6	18.9±4.3		15.4±2.9	20.8±3.6	12.8±1.8	11.2±1.4	
NGC 4041	21.3±1.8	24.9±3.4	25.7±2.5	26.0±2.2	34.6±4.6	17.4±1.8	14.6±1.3	11.6±1.1
NGC 4102	50.5±4.7	53.9±6.8	49.6±5.7	63.3±7.1	84.2±10.9	58.4±5.5	52.3±5.0	35.9±3.5
IRAS 12071-0444		2.4±1.6						
NGC 4151	3.0±1.0	3.1±1.0	2.8±0.7	4.4±0.5	3.7±1.0	8.9±2.2	8.1±1.7	8.8±2.4
VCC 66	5.5±0.9	6.4±1.0				2.0±0.4		
NGC 4189	6.5±3.4	11.4±1.4		6.5±0.5			4.6±2.5	
VCC 92	13.3±1.3	14.2±2.1				5.9±0.6		
NGC 4194	10.3±1.0	17.8±2.3	14.5±1.3	17.6±1.8	28.7±3.8	31.6±3.1	23.1±1.9	
PG 1211+143						4.7±1.6		
NGC 4222		6.7±0.9						
VCC 460	7.3±0.7	9.8±1.2		8.8±0.8		9.5±0.9		
NGC 4294	8.4±6.7	10.0±2.8		4.2±0.7		6.1±3.1		
NGC 4299	6.8±4.7	7.6±1.3		3.6±0.4				
NGC 4374	2.8±0.4	2.6±0.4				6.7±0.8		
VCC 857	3.3±0.4	5.2±0.6						
VCC 873	13.3±1.5	17.1±2.5		14.5±1.2		6.7±0.7		
NGC 4414	55.9±5.5	54.6±7.9	58.7±6.0	67.3±5.5	59.9±8.0	30.0±3.1	24.7±2.1	21.7±1.8
NGC 4418	14.2±2.3	20.2±3.6	14.3±2.3	23.7±4.1	46.2±7.0	55.3±7.8	41.4±6.3	50.2±7.6
VCC 1003	6.3±0.6	4.2±0.6		5.2±0.5				
VCC 1043	11.4±1.0	10.8±1.5		10.1±0.9		3.6±0.4		
VCC 1158		1.5±0.2						
VCC 1253		0.8±0.1						
NGC 4490	28.2±3.1	31.2±4.7	21.7±3.3	26.2±2.2	32.9±4.5	22.0±2.2	22.3±2.2	15.3±1.5
VCC 1326	1.6±0.3	3.3±0.5		2.9±0.3				
VCC 1412	2.4±0.3	2.2±0.3						
NGC 4519	5.0±0.5	7.4±1.1	5.1±0.7	3.7±0.4				
NGC 4522	7.9±3.5	9.7±1.2		4.8±0.6				
VCC 1727	8.0±1.3	10.6±1.9						
VCC 1813		2.7±0.5						
VCC 1972	16.6±2.5	19.6±3.3		13.3±2.4		7.2±1.1		
VCC 1987	22.7±2.4	25.4±3.5						
NGC 4691	14.3±1.7	21.9±3.4	17.0±2.6	19.2±1.6	23.2±3.7	26.7±2.4	19.9±2.0	
VCC 2070		3.8±0.6						
NGC 4713	4.0±0.4	11.0±1.5		6.9±0.7		4.9±0.5		
MRK 231	15.3±1.6	16.1±2.2	16.0±1.7	19.5±1.7	34.1±4.4	42.9±4.0	37.2±3.6	32.4±3.2

Table 2—Continued

Galaxy	170 μm (Jy)	158 μm (Jy)	145 μm (Jy)	122 μm (Jy)	88 μm (Jy)	63 μm (Jy)	57 μm (Jy)	52 μm (Jy)
IC 3908	15.5±2.4	19.8±3.4	18.0±3.1	16.6±2.9	25.8±4.1	15.5±2.3		
IC 860	5.4±0.9	14.3±2.5	12.8±2.3	11.0±2.0	24.8±3.8	22.2±3.2	21.8±3.1	
IC 883	13.7±1.5	14.7±2.2	16.0±1.8	17.3±1.6	34.1±4.3	22.3±2.3		
ESO 173-G015	63.8±5.8	76.4±5.4	85.6±4.1	104.9±4.6	122.5±6.9	105.7±4.5	95.7±6.0	80.1±6.4
Mrk 273	8.3±1.0	8.4±1.0	12.5±1.3	15.4±1.3	22.6±2.3	24.9±2.5	22.3±2.0	
IC 4329A		2.4±0.3			3.5±0.4	7.4±0.7		
Mrk 463		1.0±0.2			5.4±0.5	2.0±0.2		
NGC 5430	8.1±1.5	10.0±1.9	10.2±1.7	15.7±2.9		9.8±1.4		
NGC 5433	9.7±1.0	11.6±1.9	10.1±1.0	10.4±0.8		3.3±0.4		
Circinus	230.7±5.1	259.8±6.4	291.1±3.9	365.5±3.5	452.0±12.3	360.8±6.6	329.0±7.9	293.1±8.8
NGC 5643	34.4±3.3	34.3±1.4	29.1±1.1	25.1±0.8		17.9±1.4	17.8±2.3	18.3±2.5
NGC 5713	41.3±7.1	34.9±6.0	29.9±4.8	35.7±6.5	40.3±7.4	33.3±5.0	29.1±3.8	23.2±3.0
I Zw 92					1.5±1.1	3.3±1.2		
NGC 5786	15.6±2.2	19.8±3.4	11.9±2.2	12.5±2.1		7.4±1.2		
NGC 5866	4.4±0.7	18.1±3.0	14.1±2.7	16.4±3.0		7.2±1.0		
CGCG 1510.8+0725	16.4±1.4	23.9±2.8	21.5±1.9	28.0±2.4	40.0±4.0	28.6±2.9	28.6±2.4	19.5±1.7
IRAS 15250+3609	3.0±1.5	4.4±1.6						
NGC 5937	11.6±1.1	17.9±2.1	18.0±1.7	20.4±1.8	23.2±3.0	8.1±0.8	11.6±1.0	9.8±1.0
NGC 5953	15.5±1.4	17.9±2.1	17.2±1.8	17.0±1.3	21.2±2.6	16.9±1.7	15.5±1.4	15.7±1.5
Arp 220	77.1±6.7	84.5±8.5	100.2±10.1	118.4±9.5	151.4±18.7	148.1±15.0	134.2±11.8	120.9±10.8
NGC 5962	21.5±3.1	25.6±4.1	17.7±3.4	19.5±3.7		9.1±1.3	4.6±0.9	
IC 4545	10.5±5.2	11.3±1.3				1.9±1.4		
IC 4595	19.0±3.3	20.2±5.2	16.9±2.8	15.7±2.8		7.4±1.1		
NGC 6217	18.2±2.1	22.6±2.8		14.0±1.2		14.0±1.4		
UGC 10445		3.8±0.7						
NGC 6156	34.7±2.9	37.4±3.2	35.4±2.8	35.6±2.3	31.7±4.0	20.0±2.0	18.2±1.5	17.8±1.6
CGCG 025-007	3.3±2.6	3.1±1.2		4.3±0.4				
NGC 6221	55.4±10.0	62.7±10.3	54.2±10.7	70.0±12.4		51.7±7.1		
NGC 6240	11.5±2.1	16.8±2.8	17.9±3.1	20.8±3.7	25.8±4.0	23.5±3.4	27.5±4.0	16.5±2.5
NGC 6286	20.9±2.2	24.9±3.4	21.9±2.1	18.9±1.8	21.6±2.7	11.5±1.0	10.1±1.2	
IRAS 17208-0014	26.4±3.2	24.3±2.9	27.0±2.5	31.5±2.6	48.5±4.9	41.9±3.9	31.6±2.7	40.7±4.9
IC 4662	4.1±0.4	6.6±1.8	7.1±1.0	6.8±0.6	10.7±1.3	12.4±1.3	8.5±1.0	
NGC 6503	42.7±3.4	48.6±1.5						
Ark 535		1.9±1.0		2.6±0.3				
3C 368	4.1±0.5					1.8±0.2		
NGC 6574	27.8±2.7	30.6±1.5	31.3±0.8	30.1±0.8	27.3±2.1	18.7±1.5	17.8±2.2	17.6±2.5
HB89 1821+643						1.5±0.2		
NGC 6764	9.2±1.7	10.2±1.7	8.1±1.4	7.8±1.5	9.3±1.6	8.7±1.1	12.0±1.7	11.4±1.7
IRAS 19254-7245	6.1±1.1	8.2±1.2	2.0±0.3	5.2±0.9		7.6±1.2	8.7±1.2	8.1±1.5
IRAS 19297-0406	10.9±1.6	12.3±0.6				9.1±2.4		
NGC 6810	29.0±2.6	33.3±1.2	30.9±0.7	32.8±0.9	32.8±3.5	21.5±1.4	17.5±2.6	14.9±2.9
NGC 6824	15.1±1.9	16.7±1.6	17.8±1.5	17.5±1.2	12.5±2.3	7.6±1.3	5.2±0.7	4.1±0.6
Cygnus A	7.2±1.3					5.8±0.9		
IC 5020	10.7±3.3	7.2±1.0		5.4±0.6				
Mrk 509	1.0±0.3	2.4±0.4			3.7±0.5	8.4±0.8		

Table 2—Continued

Galaxy	170 μm (Jy)	158 μm (Jy)	145 μm (Jy)	122 μm (Jy)	88 μm (Jy)	63 μm (Jy)	57 μm (Jy)	52 μm (Jy)
NGC 6958		2.7±0.4	1.8±0.2	1.7±0.2		1.8±0.2		
IC 5063		2.3±2.0	1.9±0.5	3.8±0.7		6.4±1.9		7.8±3.0
IRAS 20551-4250	4.63±1.3	5.4±0.8	6.0±0.7	7.7±0.7		22.6±2.4	18.3±1.8	20.4±1.9
NGC 7217	37.3±5.3							
NGC 7218	9.9±1.8	11.3±2.9	7.6±1.3	10.1±1.8		8.0±1.1	3.5±0.8	
IRAS 22491-1808	6.1±1.1	3.3±1.0						
NGC 7418	23.1±3.4	20.8±3.6		8.9±1.6			6.4±1.1	
IC 1459	2.4±0.4	1.7±0.2						
NGC 7469	28.9±4.4	25.8±3.9	26.0±4.7	33.0±6.1		35.7±4.8	32.4±4.3	29.3±3.9
IRAS 23128-5919	5.7±0.8	6.1±1.3	4.6±0.5	6.0±0.7		15.2±1.6	9.0±1.1	10.9±1.0
NGC 7552	75.4±13.7	84.4±13.6	91.5±15.2	103.7±18.8	128.6±22.1	95.4±12.9	79.0±11.8	63.7±9.6
NGC 7582	61.1±6.3	53.7±7.8	60.0±6.4	69.1±6.7	88.6±10.9	63.9±6.2	53.1±5.1	42.8±4.1
IC 5325		20.6±7.0	17.2±3.1	13.9±2.5		8.3±1.3		
NGC 7714	8.4±2.0	7.9±1.3	6.3±1.0	8.9±1.6	13.5±2.6	13.8±2.3	17.1±2.3	14.2±2.1
IRAS F23365+3604	9.2±1.1	7.1±0.9	5.6±0.6			12.0±1.2		
NGC 7771	39.0±3.3	39.9±6.5	38.4±4.3	40.3±3.3	42.3±5.2	20.9±2.1	15.9±1.3	16.3±1.5
Mrk 331	12.4±1.2	24.7±2.9	19.8±1.9	20.2±1.7	33.0±3.9	23.0±2.2	13.9±1.3	11.2±1.0

Table 3. Detected Far-Infrared Lines

Line	Wavelength (μm)	Transition
[OIII]	51.82	$^3P_2 \rightarrow ^3P_1$
OH ^a	52.93/53.06	$^2\pi_{3/2} J = 11/2 \rightarrow ^2\pi_{3/2} J = 9/2$
	53.26/53.35	$^2\pi_{1/2} J = 3/2 \rightarrow ^2\pi_{3/2} J = 3/2$
[NIII]	57.32	$^2P_{3/2} \rightarrow ^2P_{1/2}$
H ₂ O	58.70	o-H ₂ O 4 ₃₂ – 3 ₂₁
[OI]	63.18	$^3P_1 \rightarrow ^3P_2$
OH ^a	65.13/65.28	$^2\pi_{3/2} J = 9/2 \rightarrow ^2\pi_{3/2} J = 7/2$
H ₂ O ^a	66.44	o-H ₂ O 3 ₃₀ – 2 ₂₁
	67.09	p-H ₂ O 3 ₃₁ – 2 ₂₀
Unidentified Line	74.24	
H ₂ O	75.38	o-H ₂ O 3 ₂₁ – 2 ₁₂
OH ^a	79.12/79.18	$^2\pi_{1/2} J = 1/2 \rightarrow ^2\pi_{3/2} J = 3/2$
OH ^a	84.42/84.60	$^2\pi_{3/2} J = 7/2 \rightarrow ^2\pi_{3/2} J = 5/2$
[OIII]	88.36	$^3P_1 \rightarrow ^3P_0$
H ₂ O ^a	100.91	o-H ₂ O 5 ₁₄ – 4 ₂₃
	100.98	p-H ₂ O 2 ₂₀ – 1 ₁₁
H ₂ O	108.07	o-H ₂ O 2 ₂₁ – 1 ₁₀
OH ^a	119.23/119.44	$^2\pi_{3/2} J = 5/2 \rightarrow ^2\pi_{3/2} J = 3/2$
[NII]	121.89	$^3P_2 \rightarrow ^3P_1$
[OI]	145.53	$^3P_0 \rightarrow ^3P_1$
[CII]	157.74	$^2P_{3/2} \rightarrow ^2P_{1/2}$
OH ^a	163.12/163.40	$^2\pi_{1/2} J = 3/2 \rightarrow ^2\pi_{1/2} J = 1/2$
CO ^a	162.81	$J = 16 \rightarrow 15$

^aLine detected cannot be accurately identified due to the resolution of the LWS. The line is one or a blend of the listed transitions.

Table 4. Far-Infrared Emission Line Fluxes

Galaxy	TDT ^a	AOT ^b	R.A. (J2000.0)	Dec. (J2000.0)	[CII] 158 μ m	[OI] 145 μ m	[NII] 122 μ m	[OIII] 88 μ m	[OI] 63 μ m	[NIII] 57 μ m	[OIII] 52 μ m
IC 10	45700606 ^c	L02	00 19 37.6	+59 23 31	2.15 \pm 0.05				0.53 \pm 0.06		
IC 10	45700607 ^c	L02	00 21 11.5	+59 11 30	1.29 \pm 0.05						
IC 10	45700608 ^c	L02	00 20 14.0	+59 18 38	3.64 \pm 0.14		0.38 \pm 0.08	10.56 \pm 0.35	3.33 \pm 0.34		
IC 10	45700609 ^c	L02	00 20 25.3	+59 17 17	7.63 \pm 0.21	0.24 \pm 0.04	0.46 \pm 0.11	15.97 \pm 0.57	6.57 \pm 0.20	<3.51	11.86 \pm 0.94
IC 10	45700610 ^c	L02	00 19 58.3	+59 17 02	2.01 \pm 0.07				1.32 \pm 0.07		
ESO 350-IG38	54900720	L02	00 36 52.8	-33 33 23	0.48 \pm 0.04			2.67 \pm 0.30	0.81 \pm 0.09		
Cartwheel	37101917	L02	00 37 40.1	-33 43 26	0.15 \pm 0.02		<0.06			<0.18	
NGC 0185	78500682	L01	00 38 56.9	+48 20 10	0.37 \pm 0.10						
NGC 0247	57001101 ^c	L02	00 47 06.5	-20 41 07	<0.21						
NGC 0247	57001101 ^c	L02	00 47 06.9	-20 42 06	0.16 \pm 0.03						
NGC 0247	57001101 ^c	L02	00 47 07.3	-20 43 06	0.53 \pm 0.08						
NGC 0247	57001101 ^c	L02	00 47 07.8	-20 44 05	0.43 \pm 0.04						
NGC 0247	57001101 ^c	L02	00 47 08.2	-20 45 05	0.47 \pm 0.06						
NGC 0247	57001101 ^c	L02	00 47 08.7	-20 46 05	0.51 \pm 0.03						
NGC 0247	57001101 ^c	L02	00 47 09.1	-20 47 04	0.41 \pm 0.05						
NGC 0247	57001101 ^c	L02	00 47 09.6	-20 48 04	0.49 \pm 0.12						
NGC 0247	57001101 ^c	L02	00 47 10.0	-20 49 04	0.29 \pm 0.04						
NGC 0247	57001101 ^c	L02	00 47 10.4	-20 50 04	0.15 \pm 0.04						
NGC 0253	24701103 ^c	L01	00 47 33.3	-25 17 18	48.93 \pm 0.86	2.94 \pm 0.52	7.28 \pm 0.77	8.38 \pm 1.27	38.83 \pm 1.47		
NGC 0253	24701145 ^c	L02	00 47 28.2	-25 18 15	11.41 \pm 0.17	<0.89	2.18 \pm 0.24	<2.27	4.26 \pm 0.25		
NGC 0253	24701145 ^c	L02	00 47 38.3	-25 16 20	12.11 \pm 0.33	<0.61	1.94 \pm 0.39	<1.69	5.07 \pm 0.38		
NGC 0253	56901708 ^c	L01	00 47 33.3	-25 17 18	50.53 \pm 0.66		8.23 \pm 0.71		38.43 \pm 0.92		
NGC 0253	79900107 ^c	L02	00 47 33.2	-25 17 16		3.82 \pm 0.28	9.11 \pm 0.72				
NGC 0253	79900210 ^c	L02	00 47 33.2	-25 17 16					42.49 \pm 1.27		
NGC 0253	79900309 ^c	L02	00 47 33.2	-25 17 17				9.06 \pm 0.87			
NGC 0278	59702260	L02	00 52 04.6	+47 33 01	7.28 \pm 0.12	<0.21	0.46 \pm 0.06	1.71 \pm 0.18	3.47 \pm 0.16	<1.07	1.19 \pm 0.33
UGC 00545	57701507	L02	00 53 34.9	+12 41 36	<0.13				<0.33		
UGC 00545	57701507	L02	00 53 34.9	+12 44 36	<0.16				<0.40		
MCG+12-02-001	47300813	L01	00 54 03.8	+73 05 03	3.11 \pm 0.11			2.34 \pm 0.24	2.84 \pm 0.27		
NGC 0300	54901001 ^c	L02	00 54 28.5	-37 39 01	0.20 \pm 0.02						
NGC 0300	54901001 ^c	L02	00 54 34.8	-37 39 30	0.40 \pm 0.04						
NGC 0300	54901001 ^c	L02	00 54 41.1	-37 39 59	0.57 \pm 0.02						
NGC 0300	54901001 ^c	L02	00 54 47.4	-37 40 28	0.70 \pm 0.03						
NGC 0300	54901001 ^c	L02	00 54 53.7	-37 40 56	0.48 \pm 0.04						

Table 4—Continued

Galaxy	TDT ^a	AOT ^b	R.A. (J2000.0)	Dec. (J2000.0)	[CII] 158 μ m	[OI] 145 μ m	[NII] 122 μ m	[OIII] 88 μ m	[OI] 63 μ m	[NIII] 57 μ m	[OIII] 52 μ m
NGC 0300	54901051 ^c	L01	00 54 28.5	-37 39 01	<0.24				<1.14		
NGC 0300	54901051 ^c	L01	00 54 34.8	-37 39 30	0.44 \pm 0.07				<0.91		
NGC 0300	54901051 ^c	L01	00 54 41.1	-37 39 59	0.53 \pm 0.05				<1.12		
NGC 0300	54901051 ^c	L01	00 54 47.4	-37 40 28	0.68 \pm 0.07				<1.02		
NGC 0300	54901051 ^c	L01	00 54 53.7	-37 40 57	0.57 \pm 0.07				<1.20		
NGC 0300	54901103 ^c	L02	00 54 57.6	-37 42 40	0.28 \pm 0.04						
NGC 0300	54901103 ^c	L02	00 55 03.8	-37 43 08	0.85 \pm 0.03						
NGC 0300	54901103 ^c	L02	00 55 10.1	-37 43 37	0.23 \pm 0.05						
NGC 0300	54901103 ^c	L02	00 55 16.4	-37 44 06	0.27 \pm 0.03						
NGC 0300	54901153 ^c	L01	00 54 57.6	-37 42 40	<0.44				<0.89		
NGC 0300	54901153 ^c	L01	00 55 03.8	-37 43 08	0.76 \pm 0.10				<0.85		
NGC 0300	54901153 ^c	L01	00 55 10.1	-37 43 37	0.21 \pm 0.07				<1.13		
NGC 0300	54901153 ^c	L01	00 55 16.4	-37 44 06	0.31 \pm 0.09				<1.09		
NGC 0300	54901202 ^c	L02	00 54 60.0	-37 41 25	0.41 \pm 0.04						
NGC 0300	54901202 ^c	L02	00 55 06.2	-37 41 53	0.54 \pm 0.02						
NGC 0300	54901202 ^c	L02	00 55 12.5	-37 42 22	0.26 \pm 0.05						
NGC 0300	54901202 ^c	L02	00 55 18.8	-37 42 51	0.16 \pm 0.04						
NGC 0300	54901252 ^c	L01	00 54 60.0	-37 41 25	<0.46				<0.88		
NGC 0300	54901252 ^c	L01	00 55 06.2	-37 41 54	0.47 \pm 0.07				<1.14		
NGC 0300	54901252 ^c	L01	00 55 12.5	-37 42 22	0.38 \pm 0.05				<0.98		
NGC 0300	54901252 ^c	L01	00 55 18.8	-37 42 51	0.19 \pm 0.06				<0.83		
NGC 0300	54901913 ^c	L02	00 54 33.4	-37 36 32	0.15 \pm 0.02						
NGC 0300	54901913 ^c	L02	00 54 39.7	-37 37 01	0.12 \pm 0.02						
NGC 0300	54901913 ^c	L02	00 54 46.0	-37 37 30	0.34 \pm 0.03						
NGC 0300	54901913 ^c	L02	00 54 52.3	-37 37 58	0.55 \pm 0.04						
NGC 0300	54901913 ^c	L02	00 54 58.6	-37 38 27	0.25 \pm 0.04						
NGC 0300	54901963 ^c	L01	00 54 33.4	-37 36 32	<0.23				<0.93		
NGC 0300	54901963 ^c	L01	00 54 39.7	-37 37 01	<0.18				<1.07		
NGC 0300	54901963 ^c	L01	00 54 46.0	-37 37 30	0.29 \pm 0.07				<1.32		
NGC 0300	54901963 ^c	L01	00 54 52.3	-37 37 58	0.57 \pm 0.06				<1.26		
NGC 0300	54901963 ^c	L01	00 54 58.6	-37 38 27	<0.25				<1.33		
NGC 0300	54902004 ^c	L02	00 54 31.0	-37 37 47	0.36 \pm 0.03						
NGC 0300	54902004 ^c	L02	00 54 37.3	-37 38 15	0.24 \pm 0.02						
NGC 0300	54902004 ^c	L02	00 54 43.6	-37 38 44	0.54 \pm 0.02						

Table 4—Continued

Galaxy	TDT ^a	AOT ^b	R.A. (J2000.0)	Dec. (J2000.0)	[CII] 158 μ m	[OI] 145 μ m	[NII] 122 μ m	[OIII] 88 μ m	[OI] 63 μ m	[NIII] 57 μ m	[OIII] 52 μ m
NGC 0300	54902004 ^c	L02	00 54 49.9	-37 39 13	0.53±0.03						
NGC 0300	54902004 ^c	L02	00 54 56.2	-37 39 42	0.37±0.05						
NGC 0300	54902054 ^c	L01	00 54 31.0	-37 37 47	0.54±0.11				<0.93		
NGC 0300	54902054 ^c	L01	00 54 37.3	-37 38 15	<0.30				<0.99		
NGC 0300	54902054 ^c	L01	00 54 43.6	-37 38 44	<0.27				<1.09		
NGC 0300	54902054 ^c	L01	00 54 49.9	-37 39 13	0.57±0.06				<1.04		
NGC 0300	54902054 ^c	L01	00 54 56.2	-37 39 42	0.35±0.07				<1.24		
NGC 0300	54902106 ^c	L02	00 54 23.7	-37 41 31	0.14±0.03						
NGC 0300	54902106 ^c	L02	00 54 30.0	-37 41 59	0.30±0.05						
NGC 0300	54902106 ^c	L02	00 54 36.3	-37 42 28	0.31±0.04						
NGC 0300	54902106 ^c	L02	00 54 42.6	-37 42 57	0.87±0.04						
NGC 0300	54902106 ^c	L02	00 54 48.9	-37 43 26	0.27±0.04						
NGC 0300	54902156 ^c	L01	00 54 23.7	-37 41 31	<0.42				<0.98		
NGC 0300	54902156 ^c	L01	00 54 30.0	-37 41 59	0.35±0.07				<0.93		
NGC 0300	54902156 ^c	L01	00 54 36.3	-37 42 28	<0.31				<0.96		
NGC 0300	54902156 ^c	L01	00 54 42.6	-37 42 57	0.85±0.07				<1.15		
NGC 0300	54902156 ^c	L01	00 54 48.9	-37 43 26	0.26±0.06				<0.92		
NGC 0300	54902205 ^c	L02	00 54 26.1	-37 40 16	0.38±0.08						
NGC 0300	54902205 ^c	L02	00 54 32.4	-37 40 45	0.26±0.03						
NGC 0300	54902205 ^c	L02	00 54 38.7	-37 41 14	0.55±0.05						
NGC 0300	54902205 ^c	L02	00 54 45.0	-37 41 42	0.29±0.04						
NGC 0300	54902205 ^c	L02	00 54 51.3	-37 42 11	0.36±0.03						
NGC 0300	54902255 ^c	L01	00 54 26.1	-37 40 16	0.36±0.08				<1.10		
NGC 0300	54902255 ^c	L01	00 54 32.4	-37 40 45	<0.27				<0.88		
NGC 0300	54902255 ^c	L01	00 54 38.7	-37 41 14	0.49±0.06				<0.92		
NGC 0300	54902255 ^c	L01	00 54 45.0	-37 41 42	0.27±0.05				<1.53		
NGC 0300	54902255 ^c	L01	00 54 51.3	-37 42 11	0.40±0.05				<0.81		
NGC 0300	54902308 ^c	L02	00 54 55.2	-37 43 54	0.44±0.05						
NGC 0300	54902308 ^c	L02	00 55 01.4	-37 44 23	0.34±0.04						
NGC 0300	54902308 ^c	L02	00 55 07.7	-37 44 52	0.23±0.03						
NGC 0300	54902308 ^c	L02	00 55 14.0	-37 45 21	0.10±0.02						
NGC 0300	54902358 ^c	L01	00 54 55.2	-37 43 54	0.35±0.08				<1.02		
NGC 0300	54902358 ^c	L01	00 55 01.4	-37 44 23	0.33±0.07				<1.09		
NGC 0300	54902358 ^c	L01	00 55 07.7	-37 44 52	0.26±0.06				<0.93		

Table 4—Continued

Galaxy	TDT ^a	AOT ^b	R.A. (J2000.0)	Dec. (J2000.0)	[CII] 158 μ m	[OI] 145 μ m	[NII] 122 μ m	[OIII] 88 μ m	[OI] 63 μ m	[NIII] 57 μ m	[OIII] 52 μ m
NGC 0300	54902358 ^c	L01	00 55 14.0	-37 45 21	<0.21						<1.01
NGC 0300	57200707 ^c	L02	00 55 02.5	-37 40 10	0.44±0.03						
NGC 0300	57200707 ^c	L02	00 55 08.7	-37 40 39	0.47±0.02						
NGC 0300	57200707 ^c	L02	00 55 15.0	-37 41 08	0.53±0.03						
NGC 0300	57200707 ^c	L02	00 55 21.3	-37 41 36	0.19±0.02						
NGC 0300	57200757 ^c	L01	00 55 02.5	-37 40 10	0.45±0.07						<1.17
NGC 0300	57200757 ^c	L01	00 55 08.7	-37 40 39	0.38±0.06						<1.07
NGC 0300	57200757 ^c	L01	00 55 15.0	-37 41 08	0.53±0.07						<1.18
NGC 0300	57200757 ^c	L01	00 55 21.3	-37 41 36	<0.19						<1.23
NGC 0300	73701114 ^c	L02	00 55 04.9	-37 38 56	0.27±0.03						
NGC 0300	73701114 ^c	L02	00 55 11.1	-37 39 24	0.27±0.03						
NGC 0300	73701114 ^c	L02	00 55 17.4	-37 39 53	0.21±0.03						
NGC 0300	73701114 ^c	L02	00 55 23.7	-37 40 21	0.17±0.02						
NGC 0300	73701164 ^c	L01	00 55 04.9	-37 38 56	<0.46						<1.08
NGC 0300	73701164 ^c	L01	00 55 11.1	-37 39 24	<0.38						<1.06
NGC 0300	73701164 ^c	L01	00 55 17.4	-37 39 53	<0.29						<0.94
NGC 0300	73701164 ^c	L01	00 55 23.7	-37 40 21	<0.23						<1.09
IC 1613	57500280 ^c	L02	01 04 50.6	+02 09 20	<0.21	<0.10					<0.39
IC 1613	57500280 ^c	L02	01 05 02.6	+02 09 20	0.41±0.05	<0.15					<0.50
IC 1613	57500280 ^c	L02	01 05 14.6	+02 09 20	<0.13	<0.09					<0.45
IC 1613	57500281 ^c	L02	01 05 02.6	+02 12 20	<0.12	<0.11					<0.67
IC 1613	57500281 ^c	L02	01 05 02.6	+02 09 20	0.38±0.04	<0.06					<0.58
IC 1613	57500281 ^c	L02	01 05 02.6	+02 06 20	<0.11	<0.10					<0.56
NGC 0449	80700656	L02	01 16 07.2	+33 05 22	0.21±0.05						0.57±0.09
NGC 0449	80700656	L02	01 16 07.2	+33 08 22	<0.14						<0.47
UGC 00852	58703445	L02	01 19 38.5	+17 33 57	0.34±0.05						
NGC 0520	77702295	L01	01 24 35.0	+03 47 42	2.83±0.07	0.18±0.04	0.47±0.17	1.56±0.21	1.92±0.23	<1.68	<2.08
M 33	45100970 ^c	L02	01 33 33.9	+30 41 30	4.31±0.11		0.33±0.10	10.99±0.19	2.48±0.26		
M 33	59901083 ^c	L01	01 33 33.2	+30 41 47	4.07±0.08			10.70±0.30	1.30±0.16		
M 33	78600403 ^c	L02	01 33 23.5	+30 24 40	<0.48						
M 33	78600403 ^c	L02	01 33 25.0	+30 25 26	0.81±0.11						
M 33	78600403 ^c	L02	01 33 26.5	+30 26 12	0.54±0.12						
M 33	78600403 ^c	L02	01 33 28.0	+30 26 58	0.32±0.09						
M 33	78600403 ^c	L02	01 33 29.5	+30 27 44	0.32±0.10						

Table 4—Continued

Galaxy	TDT ^a	AOT ^b	R.A. (J2000.0)	Dec. (J2000.0)	[CII] 158 μ m	[OI] 145 μ m	[NII] 122 μ m	[OIII] 88 μ m	[OI] 63 μ m	[NIII] 57 μ m	[OIII] 52 μ m
M 33	78600403 ^c	L02	01 33 31.0	+30 28 30	0.32±0.10						
M 33	78600403 ^c	L02	01 33 32.5	+30 29 16	0.38±0.08						
M 33	78600403 ^c	L02	01 33 34.1	+30 30 02	0.71±0.10						
M 33	78600403 ^c	L02	01 33 35.6	+30 30 48	1.21±0.09						
M 33	78600403 ^c	L02	01 33 37.1	+30 31 34	1.98±0.09						
M 33	78600403 ^c	L02	01 33 38.6	+30 32 20	2.26±0.09						
M 33	78600403 ^c	L02	01 33 40.1	+30 33 06	2.00±0.08						
M 33	78600403 ^c	L02	01 33 41.6	+30 33 52	1.26±0.12						
M 33	78600403 ^c	L02	01 33 43.2	+30 34 38	1.30±0.07						
M 33	78600403 ^c	L02	01 33 44.7	+30 35 24	1.92±0.08						
M 33	78600403 ^c	L02	01 33 46.2	+30 36 10	2.46±0.10						
M 33	78600403 ^c	L02	01 33 47.7	+30 36 56	2.07±0.16						
M 33	78600403 ^c	L02	01 33 49.3	+30 37 42	1.80±0.14						
M 33	78600403 ^c	L02	01 33 50.8	+30 38 28	2.39±0.07						
M 33	80800367 ^c	L02	01 33 50.9	+30 39 36	4.14±0.13		0.56±0.11	1.60±0.43	2.00±0.21		
M 33	81200172 ^c	L01	01 33 33.8	+30 41 31	4.69±0.08			11.51±0.66	1.91±0.34		6.74±1.43
NGC 0625	37301411	L02	01 35 07.2	-41 26 08	1.00±0.08	<0.05	<0.04				
NGC 0628	60802731 ^c	L02	01 36 36.7	+15 44 28					<0.34		
NGC 0628	60802731 ^c	L02	01 36 38.5	+15 45 22					0.74±0.10		
NGC 0628	60802731 ^c	L02	01 36 40.2	+15 46 17					<0.44		
NGC 0628	60802731 ^c	L02	01 36 42.0	+15 47 11					<0.72		
NGC 0628	60802731 ^c	L02	01 36 43.7	+15 48 05					<0.58		
NGC 0628	60802731 ^c	L02	01 36 45.5	+15 49 00					<0.84		
NGC 0628	60802731 ^c	L02	01 36 47.2	+15 49 54					<0.70		
NGC 0628	60802802 ^c	L02	01 36 33.2	+15 42 39	<0.21						
NGC 0628	60802802 ^c	L02	01 36 35.0	+15 43 33	<0.23						
NGC 0628	60802802 ^c	L02	01 36 36.7	+15 44 28	0.76±0.08						
NGC 0628	60802802 ^c	L02	01 36 38.5	+15 45 22	0.78±0.09						
NGC 0628	60802802 ^c	L02	01 36 40.2	+15 46 16	0.98±0.06						
NGC 0628	60802802 ^c	L02	01 36 42.0	+15 47 11	1.13±0.02						
NGC 0628	60802802 ^c	L02	01 36 43.7	+15 48 05	1.27±0.06						
NGC 0628	60802802 ^c	L02	01 36 45.5	+15 49 00	0.79±0.08						
NGC 0628	60802802 ^c	L02	01 36 47.2	+15 49 54	0.29±0.04						
NGC 0628	60802802 ^c	L02	01 36 49.0	+15 50 48	0.16±0.03						

Table 4—Continued

Galaxy	TDT ^a	AOT ^b	R.A. (J2000.0)	Dec. (J2000.0)	[CII] 158 μ m	[OI] 145 μ m	[NII] 122 μ m	[OIII] 88 μ m	[OI] 63 μ m	[NIII] 57 μ m	[OIII] 52 μ m
NGC 0628	60802802 ^c	L02	01 36 50.8	+15 51 43	<0.16						
NGC 0660	63300505	L01	01 43 02.3	+13 38 44	7.67±0.19						4.33±0.28
Mrk 573	58601390	L02	01 43 57.7	+02 20 59	0.18±0.02						0.49±0.11 0.36±0.08
III Zw 35	63300601	L02	01 44 30.7	+17 06 09	0.21±0.03						
III Zw 35	63300601	L02	01 44 30.7	+17 09 09	<0.08						
III Zw 35	63300602	L01	01 44 30.7	+17 06 09	<0.30						<0.92
III Zw 35	63300602	L01	01 44 30.7	+17 09 09	<0.20						<0.92
NGC 0685	37301213	L02	01 47 43.1	-52 45 34	0.61±0.04	<0.03					
NGC 0693	59502312	L02	01 50 30.9	+06 08 41	1.65±0.06		<0.10				0.81±0.06
NGC 0695	63300744	L02	01 51 14.2	+22 34 56	2.04±0.08		0.15±0.03	0.79±0.06			1.18±0.09
UGC 01449	58600877	L02	01 58 05.6	+03 05 05	1.48±0.08		<0.11				0.86±0.06
NGC 0821	81200691	L01	02 08 21.5	+10 59 42	<0.10	<0.09	<0.10	<0.49			<0.35 <1.07
NGC 0814	59800305	L02	02 10 37.7	-15 46 24	0.36±0.04						0.34±0.10
Arp 273	80802606	L02	02 21 31.7	+39 22 29	0.16±0.02		<0.08				<0.31
NGC 0891	61100157 ^c	L02	02 22 40.1	+42 23 59	2.39±0.13		<0.54	<1.58			<1.47
NGC 0891	61100157 ^c	L02	02 22 38.4	+42 23 13	5.03±0.08		<0.57	<1.76			1.87±0.29
NGC 0891	61100157 ^c	L02	02 22 36.6	+42 22 27	8.10±0.24		0.84±0.10	1.71±0.39			3.15±0.40
NGC 0891	61100157 ^c	L02	02 22 34.9	+42 21 41	7.37±0.12		0.83±0.19	<1.85			2.44±0.22
NGC 0891	61100256 ^c	L01	02 22 33.0	+42 20 55	7.79±0.12		1.11±0.12	1.52±0.45			1.85±0.34
NGC 0891	61100358 ^c	L02	02 22 31.2	+42 20 09	7.29±0.15		1.07±0.13	1.22±0.34			2.01±0.25
NGC 0891	61100358 ^c	L02	02 22 29.4	+42 19 23	5.41±0.09		<0.87	<1.90			1.30±0.31
NGC 0891	61100358 ^c	L02	02 22 27.7	+42 18 37	3.54±0.09		0.39±0.13	<1.87			1.49±0.38
NGC 0891	61100358 ^c	L02	02 22 25.9	+42 17 51	2.16±0.10		<0.32	<1.28			1.08±0.21
NGC 0891	61401060 ^c	L02	02 22 26.4	+42 21 26	0.74±0.08		<0.31	<1.07			<0.75
NGC 0891	61401060 ^c	L02	02 22 29.7	+42 21 11	2.91±0.08		0.70±0.20	<1.86			0.91±0.26
NGC 0891	61401060 ^c	L02	02 22 33.0	+42 20 55	7.60±0.18		1.09±0.22	1.79±0.44			2.37±0.38
NGC 0891	61401060 ^c	L02	02 22 36.3	+42 20 39	2.90±0.13		0.71±0.11	<1.28			1.78±0.34
NGC 0891	61401060 ^c	L02	02 22 39.7	+42 20 24	0.85±0.16		<0.29	<1.18			<1.15
NGC 0891	61401144 ^c	L01	02 22 33.2	+42 20 58	7.67±0.11		1.51±0.21	2.64±0.71			1.94±0.36
NGC 0891	61401144 ^c	L01	02 22 33.2	+42 23 58	0.74±0.07						<1.15
NGC 0891	80802059 ^c	L02	02 22 24.1	+42 17 05	1.27±0.14		<0.38	<1.81			<1.03
NGC 0891	80802059 ^c	L02	02 22 22.4	+42 16 20	0.53±0.09		<0.31	<1.04			<0.45
NGC 0891	80802059 ^c	L02	02 22 20.6	+42 15 34	<0.38		<0.32	<1.27			<0.67
NGC 0891	80802059 ^c	L02	02 22 18.8	+42 14 48	<0.28		<0.30	<1.42			<0.69

Table 4—Continued

Galaxy	TDT ^a	AOT ^b	R.A. (J2000.0)	Dec. (J2000.0)	[CII] 158 μ m	[OI] 145 μ m	[NII] 122 μ m	[OIII] 88 μ m	[OI] 63 μ m	[NIII] 57 μ m	[OIII] 52 μ m
NGC 0925	65600603 ^c	L02	02 26 57.0	+33 36 39	0.12±0.04						
NGC 0925	65600603 ^c	L02	02 27 01.3	+33 36 14	0.24±0.03						
NGC 0925	65600603 ^c	L02	02 27 05.6	+33 35 49	0.54±0.06						
NGC 0925	65600603 ^c	L02	02 27 10.0	+33 35 24	0.66±0.04						
NGC 0925	65600603 ^c	L02	02 27 14.4	+33 34 59	1.05±0.06						
NGC 0925	65600603 ^c	L02	02 27 18.7	+33 34 33	1.06±0.07						
NGC 0925	65600603 ^c	L02	02 27 23.1	+33 34 08	0.71±0.05						
NGC 0925	65600603 ^c	L02	02 27 27.4	+33 33 43	0.37±0.05						
NGC 0925	65600603 ^c	L02	02 27 31.8	+33 33 18	0.27±0.07						
NGC 0925	65600603 ^c	L02	02 27 36.1	+33 32 52	<0.25						
NGC 0986	74300187	L02	02 33 34.2	-39 02 46	3.04±0.11	<0.25	0.52±0.09	<0.81	1.27±0.13	<1.40	<0.98
NGC 1022	78401017	L02	02 38 32.5	-06 40 38	1.87±0.06		<0.27	<0.52	2.01±0.18		
NGC 1052	83300510	L02	02 41 04.8	-08 15 20	0.15±0.01						
Maffei 2	85800682 ^c	L01	02 41 54.4	+59 36 17	8.81±0.33	0.44±0.07	1.76±0.21	2.05±0.22	5.52±0.42	<1.40	<1.64
NGC 1068	60500401	L01	02 42 40.7	-00 00 48	21.54±0.17	0.68±0.08	3.63±0.30	9.92±0.31	17.36±0.43	6.07±0.44	13.13±0.78
NGC 1068	60501183	L01	02 42 40.7	-00 00 48	21.23±0.17	0.76±0.14	3.54±0.29	9.95±0.33	17.18±0.29	5.68±0.40	11.68±0.52
NGC 1068	82000704	L02	02 42 40.6	-00 00 48	21.74±0.33						
NGC 1068	82001106	L02	02 42 40.6	-00 00 48	22.34±0.37						
NGC 1068	82001404	L02	02 42 40.8	-00 00 48		1.04±0.12			5.11±0.38		
UGC 02238	63301029	L02	02 46 17.4	+13 05 44	2.35±0.09	0.07±0.01	0.13±0.04	0.69±0.09	0.76±0.21		
NGC 1097	81300966 ^c	L02	02 46 18.7	-30 16 32	6.61±0.10						
NGC 1097	81900163 ^c	L01	02 46 18.7	-30 16 32	6.93±0.16		1.52±0.15		3.47±0.40		
NGC 1097	81900264 ^c	L02	02 46 18.7	-30 16 32	7.13±0.18						
NGC 1097	81901067 ^c	L02	02 46 18.7	-30 16 32	6.50±0.11						
NGC 1097	81901165 ^c	L02	02 46 18.7	-30 16 32	6.57±0.17						
NGC 1097	81901262 ^c	L01	02 46 18.7	-30 16 32	6.45±0.15		1.68±0.19		3.35±0.29		
NGC 1097	82000161 ^c	L01	02 46 18.7	-30 16 32	6.93±0.20		1.12±0.24		4.09±0.50		
NGC 1155	60501624	L02	02 58 12.3	-10 20 57	0.38±0.04				0.36±0.07		
NGC 1156	65300184	L02	02 59 42.5	+25 14 14	1.56±0.14		<0.08		0.82±0.05		
NGC 1222	82400836	L02	03 08 56.8	-02 57 17	2.42±0.09		0.13±0.04		2.73±0.16		
UGC 02519	70100901	L02	03 09 19.1	+80 07 55	1.64±0.06				0.75±0.06		
NGC 1266	78801467	L02	03 16 00.8	-02 25 37	0.50±0.10		<0.19	<0.30	0.52±0.06		
NGC 1313	51901937 ^c	L02	03 14 56.5	-66 09 39	0.07±0.02						
NGC 1313	51901938 ^c	L02	03 18 26.9	-66 28 36	2.37±0.07		<0.22		1.13±0.13		

Table 4—Continued

Galaxy	TDT ^a	AOT ^b	R.A. (J2000.0)	Dec. (J2000.0)	[CII] 158 μ m	[OI] 145 μ m	[NII] 122 μ m	[OIII] 88 μ m	[OI] 63 μ m	[NIII] 57 μ m	[OIII] 52 μ m
NGC 1313	51901939 ^c	L02	03 18 09.0	-66 29 59	2.06±0.14		<0.15	1.64±0.13	1.33±0.15		
NGC 1313	51901940 ^c	L02	03 18 04.2	-66 32 29	0.79±0.08		<0.20		0.44±0.12		
NGC 1313	85900201 ^c	L02	03 16 59.1	-66 29 57	<0.38						
NGC 1313	85900201 ^c	L02	03 17 09.3	-66 29 15	<0.43						
NGC 1313	85900201 ^c	L02	03 17 19.5	-66 28 31	0.45±0.07						
NGC 1313	85900201 ^c	L02	03 17 29.7	-66 27 48	0.34±0.07						
NGC 1313	85900201 ^c	L02	03 17 40.0	-66 27 05	0.50±0.10						
NGC 1313	85900201 ^c	L02	03 17 50.2	-66 26 22	0.48±0.12						
NGC 1313	85900201 ^c	L02	03 18 00.4	-66 25 38	0.34±0.11						
NGC 1313	85900201 ^c	L02	03 18 10.6	-66 24 55	0.40±0.11						
NGC 1313	85900201 ^c	L02	03 18 20.8	-66 24 11	0.29±0.07						
NGC 1313	85900201 ^c	L02	03 18 31.0	-66 23 28	0.35±0.08						
NGC 1313	85900201 ^c	L02	03 18 41.1	-66 22 44	<0.38						
NGC 1313	85900201 ^c	L02	03 17 06.4	-66 30 59	0.30±0.07						
NGC 1313	85900201 ^c	L02	03 17 16.6	-66 30 15	0.44±0.11						
NGC 1313	85900201 ^c	L02	03 17 26.9	-66 29 32	0.53±0.13						
NGC 1313	85900201 ^c	L02	03 17 37.1	-66 28 49	0.43±0.08						
NGC 1313	85900201 ^c	L02	03 17 47.3	-66 28 06	0.36±0.10						
NGC 1313	85900201 ^c	L02	03 17 57.5	-66 27 22	0.48±0.06						
NGC 1313	85900201 ^c	L02	03 18 07.8	-66 26 39	0.41±0.06						
NGC 1313	85900201 ^c	L02	03 18 18.0	-66 25 55	0.32±0.09						
NGC 1313	85900201 ^c	L02	03 18 28.1	-66 25 12	0.37±0.08						
NGC 1313	85900201 ^c	L02	03 18 38.3	-66 24 29	0.45±0.09						
NGC 1313	85900201 ^c	L02	03 18 48.4	-66 23 45	0.34±0.12						
NGC 1313	85900201 ^c	L02	03 17 13.5	-66 32 00	0.38±0.08						
NGC 1313	85900201 ^c	L02	03 17 23.7	-66 31 17	0.40±0.04						
NGC 1313	85900201 ^c	L02	03 17 34.0	-66 30 34	0.38±0.09						
NGC 1313	85900201 ^c	L02	03 17 44.2	-66 29 51	0.63±0.12						
NGC 1313	85900201 ^c	L02	03 17 54.4	-66 29 07	0.80±0.12						
NGC 1313	85900201 ^c	L02	03 18 04.7	-66 28 24	0.68±0.08						
NGC 1313	85900201 ^c	L02	03 18 14.9	-66 27 41	0.53±0.06						
NGC 1313	85900201 ^c	L02	03 18 25.1	-66 26 57	0.48±0.07						
NGC 1313	85900201 ^c	L02	03 18 35.3	-66 26 14	0.28±0.05						
NGC 1313	85900201 ^c	L02	03 18 45.4	-66 25 30	0.26±0.04						

Table 4—Continued

Galaxy	TDT ^a	AOT ^b	R.A. (J2000.0)	Dec. (J2000.0)	[CII] 158 μ m	[OI] 145 μ m	[NII] 122 μ m	[OIII] 88 μ m	[OI] 63 μ m	[NIII] 57 μ m	[OIII] 52 μ m
NGC 1313	85900201 ^c	L02	03 18 55.6	-66 24 47	0.26±0.05						
NGC 1313	85900201 ^c	L02	03 17 20.8	-66 33 01	0.43±0.09						
NGC 1313	85900201 ^c	L02	03 17 31.1	-66 32 18	0.30±0.10						
NGC 1313	85900201 ^c	L02	03 17 41.3	-66 31 35	0.66±0.08						
NGC 1313	85900201 ^c	L02	03 17 51.6	-66 30 51	0.62±0.10						
NGC 1313	85900201 ^c	L02	03 18 01.8	-66 30 08	2.26±0.10						
NGC 1313	85900201 ^c	L02	03 18 12.0	-66 29 25	1.98±0.12						
NGC 1313	85900201 ^c	L02	03 18 22.2	-66 28 41	2.23±0.10						
NGC 1313	85900201 ^c	L02	03 18 32.5	-66 27 58	1.08±0.08						
NGC 1313	85900201 ^c	L02	03 18 42.6	-66 27 14	0.43±0.08						
NGC 1313	85900201 ^c	L02	03 18 52.8	-66 26 31	0.38±0.10						
NGC 1313	85900201 ^c	L02	03 19 02.9	-66 25 47	0.42±0.08						
NGC 1313	85900201 ^c	L02	03 17 27.9	-66 34 02	0.27±0.06						
NGC 1313	85900201 ^c	L02	03 17 38.2	-66 33 20	0.27±0.07						
NGC 1313	85900201 ^c	L02	03 17 48.4	-66 32 36	0.56±0.16						
NGC 1313	85900201 ^c	L02	03 17 58.7	-66 31 53	0.57±0.08						
NGC 1313	85900201 ^c	L02	03 18 08.9	-66 31 10	1.18±0.06						
NGC 1313	85900201 ^c	L02	03 18 19.2	-66 30 26	1.24±0.13						
NGC 1313	85900201 ^c	L02	03 18 29.4	-66 29 43	1.01±0.07						
NGC 1313	85900201 ^c	L02	03 18 39.6	-66 28 59	1.57±0.08						
NGC 1313	85900201 ^c	L02	03 18 49.8	-66 28 16	0.47±0.08						
NGC 1313	85900201 ^c	L02	03 18 60.0	-66 27 32	0.49±0.07						
NGC 1313	85900201 ^c	L02	03 19 10.2	-66 26 49	0.37±0.08						
NGC 1313	85900201 ^c	L02	03 17 35.3	-66 35 04	0.24±0.07						
NGC 1313	85900201 ^c	L02	03 17 45.6	-66 34 20	0.26±0.07						
NGC 1313	85900201 ^c	L02	03 17 55.8	-66 33 37	0.36±0.08						
NGC 1313	85900201 ^c	L02	03 18 06.1	-66 32 54	0.79±0.07						
NGC 1313	85900201 ^c	L02	03 18 16.3	-66 32 10	0.50±0.07						
NGC 1313	85900201 ^c	L02	03 18 26.6	-66 31 27	0.58±0.05						
NGC 1313	85900201 ^c	L02	03 18 36.8	-66 30 43	0.68±0.08						
NGC 1313	85900201 ^c	L02	03 18 47.0	-66 30 00	0.61±0.07						
NGC 1313	85900201 ^c	L02	03 18 57.2	-66 29 16	0.45±0.08						
NGC 1313	85900201 ^c	L02	03 19 07.4	-66 28 33	0.41±0.04						
NGC 1313	85900201 ^c	L02	03 19 17.5	-66 27 49	0.40±0.06						

Table 4—Continued

Galaxy	TDT ^a	AOT ^b	R.A. (J2000.0)	Dec. (J2000.0)	[CII] 158 μ m	[OI] 145 μ m	[NII] 122 μ m	[OIII] 88 μ m	[OI] 63 μ m	[NIII] 57 μ m	[OIII] 52 μ m
NGC 1313	85900201 ^c	L02	03 17 42.5	-66 36 05	0.23±0.06						
NGC 1313	85900201 ^c	L02	03 17 52.7	-66 35 22	0.38±0.06						
NGC 1313	85900201 ^c	L02	03 18 03.0	-66 34 39	0.36±0.09						
NGC 1313	85900201 ^c	L02	03 18 13.2	-66 33 56	0.43±0.07						
NGC 1313	85900201 ^c	L02	03 18 23.5	-66 33 12	0.56±0.09						
NGC 1313	85900201 ^c	L02	03 18 33.7	-66 32 29	0.31±0.05						
NGC 1313	85900201 ^c	L02	03 18 43.9	-66 31 45	0.42±0.06						
NGC 1313	85900201 ^c	L02	03 18 54.2	-66 31 02	0.43±0.06						
NGC 1313	85900201 ^c	L02	03 19 04.4	-66 30 18	0.46±0.09						
NGC 1313	85900201 ^c	L02	03 19 14.6	-66 29 34	0.31±0.02						
NGC 1313	85900201 ^c	L02	03 19 24.7	-66 28 51	0.41±0.09						
NGC 1313	85900201 ^c	L02	03 17 49.8	-66 37 06	0.28±0.08						
NGC 1313	85900201 ^c	L02	03 18 00.1	-66 36 23	<0.50						
NGC 1313	85900201 ^c	L02	03 18 10.4	-66 35 40	0.23±0.05						
NGC 1313	85900201 ^c	L02	03 18 20.6	-66 34 56	<0.30						
NGC 1313	85900201 ^c	L02	03 18 30.9	-66 34 13	0.51±0.09						
NGC 1313	85900201 ^c	L02	03 18 41.1	-66 33 29	0.36±0.05						
NGC 1313	85900201 ^c	L02	03 18 51.4	-66 32 46	0.53±0.10						
NGC 1313	85900201 ^c	L02	03 19 01.6	-66 32 02	0.44±0.07						
NGC 1313	85900201 ^c	L02	03 19 11.8	-66 31 18	0.30±0.06						
NGC 1313	85900201 ^c	L02	03 19 22.0	-66 30 35	0.25±0.08						
NGC 1313	85900201 ^c	L02	03 19 32.1	-66 29 51	0.36±0.08						
NGC 1275	64500914	L02	03 19 48.1	+41 30 42	1.10±0.10				2.59±0.20		<0.89
NGC 1275	64500914	L02	03 19 48.1	+41 33 41	<0.21				<1.07		<1.34
NGC 1275	84002595	L01	03 19 48.6	+41 30 38	1.16±0.07				2.32±0.19		
NGC 1316	80300783 ^c	L02	03 22 41.5	-37 12 33	0.50±0.03						
NGC 1316	80300884 ^c	L02	03 22 41.5	-37 12 33				<0.37			
NGC 1316	80300985 ^c	L02	03 22 41.5	-37 12 33				<0.36			
NGC 1316	80301088 ^c	L02	03 22 41.5	-37 12 33				<0.34			
NGC 1316	80301187 ^c	L02	03 22 41.5	-37 12 33				0.35±0.06			
NGC 1316	80301286 ^c	L02	03 22 41.5	-37 12 33				0.42±0.13			
NGC 1317	75001075	L02	03 22 44.7	-37 06 09	0.91±0.05				0.37±0.04		
NGC 1326	75001155	L02	03 23 56.4	-36 27 49	1.33±0.11			<0.10	0.79±0.06		
NGC 1365	76501123 ^c	L02	03 31 56.9	-35 48 17	<0.19						

Table 4—Continued

Galaxy	TDT ^a	AOT ^b	R.A. (J2000.0)	Dec. (J2000.0)	[CII] 158 μ m	[OI] 145 μ m	[NII] 122 μ m	[OIII] 88 μ m	[OI] 63 μ m	[NIII] 57 μ m	[OIII] 52 μ m
NGC 1365	76501124 ^c	L01	03 33 36.5	-36 08 19	10.41±0.25	0.64±0.09	2.07±0.24	2.52±0.45	5.71±0.41	<2.21	<3.08
NGC 1365	76501127 ^c	L02	03 33 28.5	-36 06 24	0.39±0.03					<0.36	
NGC 1365	76501128 ^c	L02	03 33 10.6	-36 04 29	<0.19					<0.37	
NGC 1365	85201943 ^c	L02	03 33 36.4	-36 08 25	11.04±0.24		1.95±0.25	2.63±0.51	5.44±0.28	2.13±0.40	
NGC 1365	85201943 ^c	L02	03 33 36.4	-36 05 25	0.45±0.08						
IC 1953	81902108	L02	03 33 41.6	-21 28 41	0.58±0.04		<0.14	<0.43	<0.28		
NGC 1377	81901601	L02	03 36 39.0	-20 54 03	<0.20		<0.12	<0.22	<0.28		
NGC 1385	79600839	L02	03 37 28.2	-24 30 04	5.55±0.20	0.11±0.01	0.23±0.05	2.43±0.12	2.41±0.15	<0.73	
IC 342	64600302 ^c	L01	03 46 31.9	+68 04 54	2.39±0.16					<1.75	
IC 342	64600302 ^c	L01	03 46 31.8	+68 05 44	1.97±0.09					<1.82	
IC 342	64600302 ^c	L01	03 46 31.8	+68 06 34	2.03±0.14					<1.47	
IC 342	64600302 ^c	L01	03 46 40.9	+68 04 54	3.81±0.12					<2.28	
IC 342	64600302 ^c	L01	03 46 40.8	+68 05 44	6.94±0.22					3.35±0.47	
IC 342	64600302 ^c	L01	03 46 40.7	+68 06 34	2.81±0.18					<1.61	
IC 342	64600302 ^c	L01	03 46 49.8	+68 04 54	4.77±0.15					<2.77	
IC 342	64600302 ^c	L01	03 46 49.7	+68 05 44	13.45±0.28					9.05±1.12	
IC 342	64600302 ^c	L01	03 46 49.6	+68 06 34	6.35±0.18					4.14±0.43	
IC 342	64600302 ^c	L01	03 46 58.7	+68 04 55	2.77±0.11					<1.50	
IC 342	64600302 ^c	L01	03 46 58.7	+68 05 45	3.62±0.17					<2.42	
IC 342	64600302 ^c	L01	03 46 58.6	+68 06 35	3.22±0.13					<1.99	
IC 342	64600302 ^c	L01	03 47 07.6	+68 04 55	1.91±0.10					<1.80	
IC 342	64600302 ^c	L01	03 47 07.6	+68 05 45	2.04±0.08					<1.54	
IC 342	64600302 ^c	L01	03 47 07.5	+68 06 35	2.41±0.10					<1.63	
UGC 02855	62902696	L02	03 48 22.9	+70 07 59	4.73±0.09	0.29±0.04	0.43±0.09	0.91±0.24	2.64±0.20	<1.78	<1.95
NGC 1482	79600984	L02	03 54 39.5	-20 30 06	6.39±0.17	<0.23	0.43±0.06	1.46±0.22	3.35±0.16	0.82±0.23	<1.01
IC 356	63701906	L02	04 07 35.5	+69 48 46	0.60±0.07						
IC 356	63701906	L02	04 07 47.0	+69 48 47	0.68±0.11						
IC 356	63701906	L02	04 07 58.6	+69 48 47	0.61±0.10						
NGC 1546	68900655	L02	04 14 36.6	-56 03 38	3.18±0.18		0.35±0.05			0.80±0.07	
NGC 1569	64600489	L02	04 30 49.1	+64 50 52	5.99±0.16	0.13±0.03	<0.32	27.68±0.72	6.59±0.42	<2.06	18.53±0.84
3C 120	80901988	L02	04 33 11.1	+05 21 15	0.38±0.02			1.06±0.08	0.32±0.06		
NGC 1614	85501010	L01	04 33 59.8	-08 34 29	2.26±0.10		0.29±0.06		3.43±0.16		2.36±0.61
NGC 1672	74400622 ^c	L02	04 45 42.1	-59 14 56	5.37±0.11						
NGC 1741	68801706	L02	05 01 37.7	-04 15 32		0.03±0.01					

Table 4—Continued

Galaxy	TDT ^a	AOT ^b	R.A. (J2000.0)	Dec. (J2000.0)	[CII] 158 μ m	[OI] 145 μ m	[NII] 122 μ m	[OIII] 88 μ m	[OI] 63 μ m	[NIII] 57 μ m	[OIII] 52 μ m
NGC 1741	68801805	L02	05 01 37.7	-04 15 32		<0.03					
NGC 1741	85801023	L02	05 01 37.7	-04 13 32	<0.39					<0.24	
NGC 1741	85801124	L02	05 01 37.7	-04 15 32				1.45 \pm 0.14			
IRAS 05189-2524	87001501	L02	05 21 01.4	-25 21 45	0.14 \pm 0.02						
UGCA 116	66701399	L01	05 55 42.6	+03 23 31	2.04 \pm 0.09			6.15 \pm 0.43	1.32 \pm 0.34		4.63 \pm 1.16
UGCA 116	85801807	L02	05 55 42.7	+03 23 29	1.62 \pm 0.10						
UGC 03426	70500987	L02	06 15 36.4	+71 02 15	0.41 \pm 0.02			1.31 \pm 0.08	1.76 \pm 0.09		
NGC 2146	67900165	L01	06 18 38.7	+78 21 23	25.37 \pm 0.32	0.99 \pm 0.14	1.12 \pm 0.32	15.77 \pm 0.65	18.03 \pm 0.99	5.51 \pm 0.59	15.14 \pm 2.01
IC 450	70501077	L02	06 52 12.4	+74 25 37	0.19 \pm 0.02			<0.27	0.47 \pm 0.12		
NGC 2388	71802360	L02	07 28 53.5	+33 49 05	1.74 \pm 0.08		0.36 \pm 0.07	0.38 \pm 0.06	1.02 \pm 0.11	<0.79	
NGC 2415	71703876	L01	07 36 56.3	+35 14 30	2.44 \pm 0.09	<0.19	<0.31	1.72 \pm 0.14	1.90 \pm 0.24	<3.61	<4.17
DDO 50	71001701 ^c	L02	08 19 18.4	+70 43 07	0.16 \pm 0.02						
DDO 50	71001805 ^c	L02	08 19 04.3	+70 41 15	<0.17						
DDO 50	71001806 ^c	L02	08 19 27.3	+70 42 36	0.10 \pm 0.03						
M 81	18000405 ^c	L01	09 55 33.3	+69 03 55	0.71 \pm 0.08				<1.25		
M 82	18000501 ^c	L01	09 55 52.4	+69 40 46	130.77 \pm 0.92	12.39 \pm 0.68	17.91 \pm 0.91	86.11 \pm 1.41	177.03 \pm 1.90	34.80 \pm 2.03	96.78 \pm 2.62
M 82	19400310 ^c	L02	09 55 36.0	+69 42 49	2.02 \pm 0.05		<0.33		1.44 \pm 0.30		
M 82	19400310 ^c	L02	09 55 41.4	+69 42 08	6.39 \pm 0.09		0.67 \pm 0.09		2.63 \pm 0.18		
M 82	19400310 ^c	L02	09 55 46.9	+69 41 27	32.39 \pm 0.94		8.60 \pm 1.11		54.58 \pm 1.93		
M 82	19400310 ^c	L02	09 55 52.3	+69 40 46	122.26 \pm 1.17		15.97 \pm 1.58		174.94 \pm 4.26		
M 82	19400310 ^c	L02	09 55 57.8	+69 40 04	25.56 \pm 1.05		10.9		34.44 \pm 1.96		
M 82	19400310 ^c	L02	09 56 03.2	+69 39 23	7.07 \pm 0.12		<1.28		2.84 \pm 0.23		
M 82	19400310 ^c	L02	09 56 08.6	+69 38 42	1.23 \pm 0.04		<0.36		1.18 \pm 0.20		
M 82	19400415 ^c	L02	09 55 28.6	+69 39 20	1.57 \pm 0.08		0.09 \pm 0.02		1.45 \pm 0.13		
M 82	19400415 ^c	L02	09 55 36.5	+69 39 49	6.22 \pm 0.18		<0.70		4.43 \pm 0.33		
M 82	19400415 ^c	L02	09 55 44.4	+69 40 17	42.27 \pm 0.88		6.22 \pm 0.90		96.42 \pm 2.85		
M 82	19400415 ^c	L02	09 55 52.3	+69 40 45	117.21 \pm 0.86		15.28 \pm 1.61		176.97 \pm 3.74		
M 82	19400415 ^c	L02	09 56 00.2	+69 41 14	24.83 \pm 0.28		<8.18		26.52 \pm 0.74		
M 82	19400415 ^c	L02	09 56 08.2	+69 41 42	5.59 \pm 0.12		0.70 \pm 0.15		1.69 \pm 0.30		
M 82	19400415 ^c	L02	09 56 16.1	+69 42 10	1.02 \pm 0.04		<0.34		1.06 \pm 0.35		
M 82	19400538 ^c	L01	09 55 52.3	+69 40 45	125.53 \pm 0.87	12.84 \pm 0.70	16.73 \pm 0.77	85.95 \pm 1.45	178.96 \pm 1.73	34.67 \pm 1.98	97.86 \pm 2.99
M 82	65800502 ^c	L01	09 55 52.2	+69 40 46	140.97 \pm 0.90	13.91 \pm 0.33	19.75 \pm 0.87	103.22 \pm 4.42	189.22 \pm 1.93	37.49 \pm 2.29	97.89 \pm 11.1
M 82	65800611 ^c	L01	09 55 52.2	+69 40 46	132.49 \pm 0.79	14.32 \pm 0.43	19.64 \pm 0.62	105.88 \pm 6.65	188.76 \pm 1.94	39.33 \pm 2.12	89.21 \pm 10.0
M 82	65800710 ^c	L02	09 55 52.2	+69 40 46	15.69 \pm 0.73	20.77 \pm 0.87			35.41 \pm 2.28		

Table 4—Continued

Galaxy	TDT ^a	AOT ^b	R.A. (J2000.0)	Dec. (J2000.0)	[CII] 158 μ m	[OI] 145 μ m	[NII] 122 μ m	[OIII] 88 μ m	[OI] 63 μ m	[NIII] 57 μ m	[OIII] 52 μ m
M 82	65800803 ^c	L02	09 55 52.2	+69 40 46							107.01 \pm 2.91
IC 2554	27100926	L01	10 08 50.5	-67 01 53	3.53 \pm 0.06			1.34 \pm 0.20	2.55 \pm 0.26		
ESO 317-G023	25200164	L02	10 24 42.5	-39 18 20	1.24 \pm 0.12	0.06 \pm 0.02	0.29 \pm 0.07	0.32 \pm 0.06	0.62 \pm 0.08	<0.68	
NGC 3256	25200456	L01	10 27 51.2	-43 54 13	12.99 \pm 0.16	0.54 \pm 0.12	1.23 \pm 0.25	6.25 \pm 0.64	12.92 \pm 0.41		5.94 \pm 1.70
NGC 3256	25200456	L01	10 27 51.2	-43 51 13							
NGC 3344	16900707 ^c	L02	10 43 30.7	+24 54 24	1.07 \pm 0.06						
NGC 3344	16900707 ^c	L02	10 43 30.7	+24 55 24	1.11 \pm 0.06						
NGC 3344	16900707 ^c	L02	10 43 30.7	+24 56 24	0.80 \pm 0.05						
NGC 3359	16200409 ^c	L02	10 46 35.4	+63 14 50	0.43 \pm 0.06						
NGC 3359	16200409 ^c	L02	10 46 36.9	+63 13 51	0.90 \pm 0.05						
NGC 3359	16200409 ^c	L02	10 46 38.4	+63 12 52	0.80 \pm 0.04						
NGC 3359	16200409 ^c	L02	10 46 39.9	+63 11 53	0.21 \pm 0.04						
NGC 3368	17400510 ^c	L02	10 46 45.1	+11 47 42	0.26 \pm 0.04						
NGC 3368	17400510 ^c	L02	10 46 45.5	+11 48 41	0.35 \pm 0.04						
NGC 3368	17400510 ^c	L02	10 46 45.8	+11 49 41	0.40 \pm 0.02						
NGC 3368	17400510 ^c	L02	10 46 46.2	+11 50 41	0.21 \pm 0.03						
NGC 3368	17400518 ^c	L02	10 47 45.6	+11 49 10	<0.12						
IRAS F10565+2448	20200453	L02	10 59 18.1	+24 32 34	0.47 \pm 0.09			<0.16	<0.26	0.76 \pm 0.08	
NGC 3557	25400927	L02	11 09 58.4	-37 32 17	<0.17		<0.05	<0.10	<0.55	<0.71	<1.21
NGC 3556	20400612 ^c	L02	11 11 21.3	+55 39 59	1.99 \pm 0.08						<2.09
NGC 3556	20400612 ^c	L02	11 11 28.2	+55 40 09	3.79 \pm 0.11						
NGC 3556	20400612 ^c	L02	11 11 35.2	+55 40 19	2.73 \pm 0.08						
NGC 3556	20400612 ^c	L02	11 11 42.3	+55 40 29	2.24 \pm 0.06						
NGC 3556	20400650 ^c	L02	11 11 21.3	+55 39 59					1.15 \pm 0.12		
NGC 3556	20400650 ^c	L02	11 11 28.2	+55 40 09					2.75 \pm 0.16		
NGC 3556	20400650 ^c	L02	11 11 35.2	+55 40 19					1.62 \pm 0.09		
NGC 3556	20400650 ^c	L02	11 11 42.3	+55 40 29					1.35 \pm 0.08		
NGC 3583	19500252	L02	11 14 10.8	+48 19 03	1.85 \pm 0.11		0.21 \pm 0.06			0.93 \pm 0.05	
NGC 3620	27600981	L02	11 16 04.4	-76 12 53	2.17 \pm 0.18	0.22 \pm 0.05	<0.29	<1.10	1.94 \pm 0.19	<1.91	<2.20
NGC 3623	18400913 ^c	L02	11 18 55.1	+13 07 41	0.28 \pm 0.05						
NGC 3623	18400913 ^c	L02	11 18 55.5	+13 06 41	0.22 \pm 0.02						
NGC 3623	18400913 ^c	L02	11 18 55.9	+13 05 42	0.50 \pm 0.03						
NGC 3623	18400913 ^c	L02	11 18 56.3	+13 04 42	0.39 \pm 0.04						
NGC 3623	18400913 ^c	L02	11 18 56.8	+13 03 42	0.29 \pm 0.05						

Table 4—Continued

Galaxy	TDT ^a	AOT ^b	R.A. (J2000.0)	Dec. (J2000.0)	[CII] 158 μ m	[OI] 145 μ m	[NII] 122 μ m	[OIII] 88 μ m	[OI] 63 μ m	[NIII] 57 μ m	[OIII] 52 μ m
NGC 3683	19401033	L02	11 27 32.0	+56 52 43	3.43±0.27		<0.24	1.39±0.09	1.84±0.08	0.63±0.21	
NGC 3690	18000704	L01	11 28 32.4	+58 33 43	8.22±0.12	0.36±0.04	0.42±0.09	8.38±0.43	8.32±0.27	1.91±0.38	7.48±0.88
NGC 3705	18400670	L02	11 30 06.8	+09 16 36	0.98±0.05		<0.07				
NGC 3885	25200720	L02	11 46 46.5	-27 55 22	1.50±0.05		0.22±0.04	0.41±0.10	1.20±0.12		
NGC 3949	19500325	L02	11 53 41.4	+47 51 31	2.76±0.07	0.06±0.01	<0.21	1.67±0.12	1.79±0.07		
NGC 4027	24200362	L02	11 59 30.6	-19 15 48	2.92±0.10		<0.20	1.31±0.10	1.62±0.04	0.61±0.20	
NGC 4038	25301107 ^c	L01	12 01 53.0	-18 52 05	5.02±0.13	0.22±0.03	0.27±0.06	2.87±0.30	3.82±0.33		3.02±0.56
NGC 4039	24002548 ^c	L01	12 01 54.3	-18 53 02	7.03±0.21			7.11±0.49	6.09±0.60		
NGC 4041	22202506	L01	12 02 12.0	+62 08 10	3.48±0.05		0.58±0.09		1.97±0.16		
NGC 4051	17400919 ^c	L02	12 03 05.1	+44 32 48	1.14±0.05						
NGC 4051	17400919 ^c	L02	12 03 09.1	+44 32 06	0.94±0.08						
NGC 4051	17400919 ^c	L02	12 03 13.0	+44 31 23	1.16±0.08						
NGC 4102	19500584	L02	12 06 23.4	+52 42 41	2.88±0.12	0.26±0.05	<0.31	0.75±0.21	3.49±0.31	<2.13	<1.31
NGC 4125	22400435	L01	12 08 04.4	+65 10 36	<0.16		<0.09	<0.38	<0.60	<1.05	<0.99
IRAS 12071-0444	24600521	L02	12 09 45.3	-05 m1 13	<0.10						
NGC 4151	35300163	L01	12 10 32.6	+39 24 20	0.74±0.06				3.76±0.29		
NGC 4151	35400167	L01	12 10 32.6	+39 24 20	0.62±0.05				3.94±0.27		
NGC 4151	35400268	L01	12 10 32.6	+39 24 20	0.74±0.08				3.38±0.57		
NGC 4151	35700169	L01	12 10 32.6	+39 24 20	0.71±0.08				3.26±0.30		
NGC 4151	35800185	L01	12 10 32.6	+39 24 20	0.78±0.06				3.70±0.30		
VCC 66	23901366	L02	12 12 46.9	+10 52 06	0.78±0.03						
NGC 4189	23800501	L02	12 13 47.2	+13 25 26	0.94±0.06		0.07±0.01				
VCC 92	23501001 ^c	L02	12 13 48.3	+14 54 07	0.93±0.05						
NGC 4194	19401369	L02	12 14 10.1	+54 31 40	2.17±0.08	0.13±0.03	<0.19	2.06±0.14	2.80±0.17	0.65±0.22	
NGC 4222	23800507	L02	12 16 22.7	+13 18 24	0.47±0.03						
PG 1211+143	23800176	L01	12 14 17.6	+14 03 12	<0.25				0.84		
NGC 4236	17700222 ^c	L02	12 16 31.3	+69 31 16	<0.28						
NGC 4236	17700222 ^c	L02	12 16 34.7	+69 30 19	0.16±0.04						
NGC 4236	17700222 ^c	L02	12 16 38.1	+69 29 22	0.21±0.04						
NGC 4236	17700222 ^c	L02	12 16 41.6	+69 28 25	0.25±0.05						
NGC 4236	17700222 ^c	L02	12 16 45.0	+69 27 27	<0.25						
NGC 4236	17700222 ^c	L02	12 16 48.5	+69 26 30	0.24±0.04						
NGC 4236	17700222 ^c	L02	12 16 51.9	+69 25 33	<0.14						
NGC 4236	17700222 ^c	L02	12 16 55.4	+69 24 35	0.27±0.05						

Table 4—Continued

Galaxy	TDT ^a	AOT ^b	R.A. (J2000.0)	Dec. (J2000.0)	[CII] 158 μ m	[OI] 145 μ m	[NII] 122 μ m	[OIII] 88 μ m	[OI] 63 μ m	[NIII] 57 μ m	[OIII] 52 μ m
NGC 4278	22900838	L01	12 20 06.6	+29 16 57	0.25±0.03						
VCC 460	23401707	L02	12 21 13.2	+18 23 03	0.28±0.02						
NGC 4294	23800903	L02	12 21 17.7	+11 30 36	0.94±0.08		<0.08				
NGC 4299	23800905	L02	12 21 40.5	+11 30 04	0.93±0.09		<0.07				
NGC 4314	22901024	L02	12 22 29.6	+29 54 35	<0.19						
NGC 4314	22901024	L02	12 22 31.9	+29 53 43	0.66±0.04						
NGC 4314	22901024	L02	12 22 34.2	+29 52 51	0.10±0.02						
NGC 4374	23502543	L01	12 25 03.1	+12 53 11	<0.14				<0.56		
VCC 857	23401706	L02	12 25 55.9	+18 12 47	0.16±0.02						
VCC 873	23100325	L02	12 26 06.8	+13 06 47	1.90±0.05						
VCC 873	23100326	L02	12 26 06.8	+13 06 47	1.86±0.05						
I Zw 36	19401278	L02	12 25 59.0	+48 29 37	<0.09	<0.06				<0.39	
I Zw 36	19401278	L02	12 26 17.1	+48 29 36	<0.09	<0.06				<0.54	
I Zw 36	19401278	L02	12 26 35.2	+48 29 36	<0.08	<0.06				<0.44	
I Zw 36	19401279	L02	12 26 17.2	+48 32 36	<0.09	<0.05				<0.55	
I Zw 36	19401279	L02	12 26 17.1	+48 29 36	<0.12	<0.07				<0.43	
I Zw 36	19401279	L02	12 26 17.1	+48 26 36	<0.05	<0.06				<0.66	
NGC 4414	22901605	L01	12 26 27.1	+31 13 21	7.53±0.09		0.98±0.11			3.31±0.24	
NGC 4414	22901606	L01	12 26 50.3	+31 13 21	<0.15		<0.16			<0.82	
NGC 4418	24100401	L02	12 26 54.6	-00 52 40	0.17±0.03	<0.14	<0.28	<0.52	<0.67	<1.86	1.29±0.46
VCC 1003	23100640	L02	12 27 26.2	+11 06 30	0.15±0.02						
VCC 1043	23100330	L02	12 27 45.7	+13 00 30	0.77±0.02						
NGC 4449	23400120	L01	12 28 11.1	+44 06 47	2.78±0.08			4.18±0.69		1.33±0.13	
VCC 1110	23401705	L02	12 28 29.5	+17 05 06	0.25±0.02						
VCC 1158	23100329	L02	12 29 03.0	+13 11 07	<0.11						
VCC 1253	23100328	L02	12 30 02.9	+13 38 07	<0.08						
NGC 4490	20501578	L02	12 30 36.9	+41 38 23	4.32±0.11	<0.16	0.23±0.07	5.46±0.34	3.29±0.16	<2.68	4.41±0.50
NGC 4486	23800817	L02	12 30 49.5	+12 23 28	0.15±0.05				0.58±0.08		
NGC 4486	23800817	L02	12 30 49.5	+12 26 28	<0.15				<0.21		
VCC 1326	23100638	L02	12 30 57.1	+11 29 02	0.15±0.03						
VCC 1412	23100639	L02	12 32 05.5	+11 10 38	<0.09						
NGC 4519	23600324	L02	12 33 30.4	+08 39 15	0.84±0.05		<0.05				
NGC 4522	23900709	L02	12 33 39.8	+09 10 29	0.89±0.06						
NGC 4559	18402027 ^c	L02	12 35 51.8	+27 59 42	0.36±0.02						

Table 4—Continued

Galaxy	TDT ^a	AOT ^b	R.A. (J2000.0)	Dec. (J2000.0)	[CII] 158 μ m	[OI] 145 μ m	[NII] 122 μ m	[OIII] 88 μ m	[OI] 63 μ m	[NIII] 57 μ m	[OIII] 52 μ m
NGC 4559	18402027 ^c	L02	12 35 54.0	+27 58 50	0.73±0.04						
NGC 4559	18402027 ^c	L02	12 35 56.3	+27 57 58	1.32±0.05						
NGC 4559	18402027 ^c	L02	12 35 58.5	+27 57 06	1.48±0.05						
NGC 4559	18402027 ^c	L02	12 36 00.8	+27 56 14	0.78±0.06						
NGC 4559	18402027 ^c	L02	12 36 03.1	+27 55 22	0.16±0.04						
NGC 4559	18402052 ^c	L02	12 35 51.8	+27 59 42				0.52±0.05			
NGC 4559	18402052 ^c	L02	12 35 54.0	+27 58 50				0.31±0.09			
NGC 4559	18402052 ^c	L02	12 35 56.3	+27 57 58				0.99±0.17			
NGC 4559	18402052 ^c	L02	12 35 58.5	+27 57 06				0.78±0.06			
NGC 4559	18402052 ^c	L02	12 36 00.8	+27 56 14				0.42±0.09			
NGC 4559	18402052 ^c	L02	12 36 03.1	+27 55 22				<0.28			
NGC 4569	23100323 ^c	L02	12 36 49.9	+13 09 53	1.53±0.04						
NGC 4569	23902579 ^c	L02	12 36 49.8	+13 09 46	1.52±0.08			1.23±0.23			<1.69
NGC 4569	23902579 ^c	L02	12 36 49.8	+13 12 45	<0.28				<0.67		<1.96
NGC 4589	22401253	L01	12 37 24.0	+74 11 30	<0.13			<0.42			<1.46
VCC 1727	24101145	L02	12 37 43.5	+11 49 06	0.74±0.03						<1.03
VCC 1813	24101147	L02	12 39 56.3	+10 10 37	<0.09						
VCC 1869	24101148	L02	12 41 13.6	+10 09 14	<0.09						
VCC 1972	24101146	L02	12 43 32.4	+11 34 46	1.96±0.05						
NGC 4651	56400639	L02	12 43 38.5	+16 23 29					0.44		
NGC 4651	56400639	L02	12 43 42.6	+16 23 39					0.90		
NGC 4651	56400639	L02	12 43 46.7	+16 23 50					0.53		
NGC 4651	56400717	L02	12 43 34.4	+16 23 19	<0.29						
NGC 4651	56400717	L02	12 43 38.4	+16 23 29	0.76±0.09						
NGC 4651	56400717	L02	12 43 42.5	+16 23 39	2.03±0.08						
NGC 4651	56400717	L02	12 43 46.6	+16 23 50	0.50±0.06						
NGC 4651	56400717	L02	12 43 50.8	+16 24 00	<0.30						
VCC 1987	22601512	L02	12 43 57.2	+13 07 35	3.00±0.06						
NGC 4656	22901831 ^c	L02	12 43 50.9	+32 08 04	<0.26						
NGC 4656	22901831 ^c	L02	12 43 53.5	+32 08 54	<0.17						
NGC 4656	22901831 ^c	L02	12 43 56.1	+32 09 44	0.58±0.06						
NGC 4656	22901831 ^c	L02	12 43 58.7	+32 10 34	0.52±0.06						
NGC 4656	22901831 ^c	L02	12 44 01.2	+32 11 24	0.33±0.06						
NGC 4656	22901831 ^c	L02	12 44 03.8	+32 12 15	0.44±0.06						

Table 4—Continued

Galaxy	TDT ^a	AOT ^b	R.A. (J2000.0)	Dec. (J2000.0)	[CII] 158 μ m	[OI] 145 μ m	[NII] 122 μ m	[OIII] 88 μ m	[OI] 63 μ m	[NIII] 57 μ m	[OIII] 52 μ m
NGC 4656	22901831 ^c	L02	12 44 06.4	+32 13 05	0.24±0.04						
NGC 4670	58000205	L01	12 45 17.1	+27 07 31	0.94±0.08	<0.17	<0.24	2.00±0.41	<1.13	<2.67	<4.81
NGC 4691	23101063	L02	12 48 13.5	-03 19 59	2.46±0.10		<0.34	1.34±0.07	1.66±0.10	<0.93	
VCC 2070	24101451	L02	12 48 23.3	+08 29 14	0.13±0.02						
NGC 4713	22500755	L02	12 49 58.0	+05 18 38	1.40±0.06		<0.07		0.94±0.04		
Mrk 231	02700457	L01	12 56 14.6	+56 52 24	<0.59					<3.05	
Mrk 231	03100357	L01	12 56 14.6	+56 52 24	<0.66					<3.23	
Mrk 231	05100540	L01	12 56 14.6	+56 52 24	0.23±0.05				0.62±0.17		
Mrk 231	18001306	L01	12 56 14.2	+56 52 24	0.27±0.06					<0.75	
Mrk 231	60300241	L01	12 56 14.2	+56 52 24	0.44±0.03					<0.45	
IC 3908	25202247	L02	12 56 40.4	-07 33 39	2.24±0.07	0.08±0.01	<0.24	0.73±0.07	1.26±0.08		
NGC 4818	25700436	L02	12 56 48.7	-08 30 56	0.83±0.10						
NGC 4818	25700436	L02	12 56 48.9	-08 31 55	1.14±0.05						
NGC 4818	25700454	L02	12 57 48.8	-08 31 24	<0.15						
NGC 4818	25700454	L02	12 56 48.7	-08 30 56					1.62±0.15		
NGC 4818	25700454	L02	12 56 48.9	-08 31 55					1.30±0.18		
NGC 4818	25700471	L02	12 57 48.8	-08 31 24					<0.20		
NGC 4861	24500610	L02	12 59 01.7	+34 51 39	<0.19		<0.24		<0.50		<1.84
NGC 4945	08101705 ^c	L01	13 05 26.2	-49 28 15	37.77±0.95					20.82±1.26	
NGC 4945	28000440 ^c	L01	13 05 26.5	-49 27 54	32.12±0.87		4.25±0.75	7.89±1.16	19.62±1.26		
NGC 4945	28000446 ^c	L02	13 05 26.5	-49 27 54	32.12±0.94	<3.34	5.30±1.01	<6.21	17.67±1.48		
NGC 4945	28000449 ^c	L02	13 05 36.9	-49 25 45	8.33±0.16	<0.36	<0.70	1.69±0.36	4.28±0.20		
NGC 4945	28000450 ^c	L02	13 05 12.3	-49 30 54	10.38±0.18	0.45±0.10	<0.94	3.28±0.22	5.47±0.21		
NGC 5005	23902737 ^c	L02	13 10 51.7	+37 03 07	1.58±0.05						
NGC 5005	23902737 ^c	L02	13 10 56.2	+37 03 32	2.45±0.06						
NGC 5005	23902737 ^c	L02	13 11 00.8	+37 03 57	1.40±0.08						
NGC 5005	23902756 ^c	L02	13 10 51.7	+37 03 07					1.03±0.05		
NGC 5005	23902756 ^c	L02	13 10 56.2	+37 03 32					2.18±0.22		
NGC 5005	23902756 ^c	L02	13 11 00.8	+37 03 57					0.57±0.08		
UGCA 332	25700705	L02	13 11 58.4	-12 03 50	0.07±0.01						
IC 860	24300656	L02	13 15 03.5	+24 37 07	<0.20		<0.22	<0.30	<0.27	<0.33	
IC 883	21501370	L02	13 20 35.3	+34 08 21	0.96±0.04		<0.20	0.58±0.09	1.30±0.09		
Cen A	28001742 ^c	L02	13 25 30.2	-43 01 20						<1.90	3.66±0.48
Cen A	45400109 ^c	L01	13 25 27.6	-43 01 08	27.70±0.34			6.93±1.22	21.44±1.56		

Table 4—Continued

Galaxy	TDT ^a	AOT ^b	R.A. (J2000.0)	Dec. (J2000.0)	[CII] 158 μm	[OI] 145 μm	[NII] 122 μm	[OIII] 88 μm	[OI] 63 μm	[NIII] 57 μm	[OIII] 52 μm
Cen A	45400151 ^c	L02	13 25 22.8	-43 00 42	22.23 \pm 0.38	0.95 \pm 0.11	2.57 \pm 0.36	6.24 \pm 0.51	9.43 \pm 0.42		
Cen A	45400151 ^c	L02	13 25 37.6	-43 01 58	9.07 \pm 0.20	0.21 \pm 0.06	<0.60	2.36 \pm 0.44	5.65 \pm 0.39		
Cen A	63400212 ^c	L02	13 25 57.1	-43 01 54	0.57 \pm 0.02		0.03 \pm 0.01				
Cen A	63400464 ^c	L01	13 25 27.6	-43 01 08	30.61 \pm 0.26	1.10 \pm 0.14	1.36 \pm 0.21	6.41 \pm 0.48	20.33 \pm 0.52		4.99 \pm 0.94
IC 4249	25201902	L02	13 27 06.7	-27 57 21	<0.14						
ESO 173-G015	30601434	L01	13 27 24.4	-57 29 23	5.05 \pm 0.34			3.55 \pm 0.27	4.06 \pm 0.25		
M 51	35100317 ^c	L01	13 29 44.3	+47 10 23	3.41 \pm 0.06		0.37 \pm 0.07			1.89 \pm 0.24	
M 51	35100450 ^c	L02	13 29 42.9	+47 11 41	2.17 \pm 0.13		<0.36	<0.88	0.68 \pm 0.15		
M 51	35100450 ^c	L02	13 29 44.4	+47 10 12	3.34 \pm 0.13		0.43 \pm 0.10	<0.83	1.09 \pm 0.20		
M 51	35100450 ^c	L02	13 29 45.9	+47 08 44	0.94 \pm 0.11		<0.28	<0.99	<0.56		
M 51	35100651 ^c	L01	13 29 53.2	+47 11 48	9.77 \pm 0.27		2.20 \pm 0.19	1.32 \pm 0.28	4.54 \pm 0.70		
M 51	35100749 ^c	L02	13 30 03.8	+47 15 23	9.63 \pm 0.08		<0.21	<1.25	<0.77		
M 51	35100749 ^c	L02	13 30 01.7	+47 14 41	1.37 \pm 0.11		<0.33	<1.56	<0.84		
M 51	35100749 ^c	L02	13 29 59.6	+47 13 58	4.44 \pm 0.15		0.40 \pm 0.09	<1.37	1.60 \pm 0.29		
M 51	35100749 ^c	L02	13 29 57.4	+47 13 15	3.71 \pm 0.15		<0.41	<0.89	1.83 \pm 0.26		
M 51	35100749 ^c	L02	13 29 55.3	+47 12 32	5.29 \pm 0.18		1.02 \pm 0.24	<1.21	1.43 \pm 0.19		
M 51	35400552 ^c	L02	13 29 59.4	+47 15 55	0.84 \pm 0.07		<0.26	<0.60	<0.50		
M 51	54100212 ^c	L01	13 29 45.0	+47 09 17	2.37 \pm 0.06					<0.64	
M 51	54100310 ^c	L01	13 29 52.3	+47 11 54	9.32 \pm 0.16		1.55 \pm 0.26			5.18 \pm 0.26	
M 83	25601006 ^c	L01	13 37 06.1	-29 50 42	6.00 \pm 0.11		0.51 \pm 0.07	0.97 \pm 0.16	2.44 \pm 0.14		
M 83	25601102 ^c	L01	13 36 51.2	-29 51 47	6.54 \pm 0.12		0.37 \pm 0.08	1.58 \pm 0.25	3.20 \pm 0.48		
M 83	44700555 ^c	L02	13 37 00.3	-29 51 51						<2.93	<4.24
M 83	44700574 ^c	L01	13 37 00.3	-29 51 51	18.14 \pm 0.35		2.51 \pm 0.27	3.36 \pm 0.41	12.24 \pm 0.79		
M 83	45400254 ^c	L02	13 37 12.5	-29 50 16	3.68 \pm 0.25		<0.34	1.55 \pm 0.32	1.56 \pm 0.27		
M 83	45400254 ^c	L02	13 37 15.0	-29 50 47	2.75 \pm 0.09		<0.34	<2.15	<1.93		
M 83	45400254 ^c	L02	13 37 17.4	-29 51 19	1.50 \pm 0.08		<0.34	<1.71	<0.96		
M 83	45400254 ^c	L02	13 37 10.1	-29 50 47	5.59 \pm 0.30		0.67 \pm 0.11	<2.12	2.15 \pm 0.40		
M 83	45400254 ^c	L02	13 37 12.5	-29 51 19	3.59 \pm 0.14		0.35 \pm 0.09	<1.69	1.47 \pm 0.31		
M 83	45400254 ^c	L02	13 37 15.0	-29 51 51	1.98 \pm 0.10		<0.36	<1.45	<1.25		
M 83	45400254 ^c	L02	13 37 07.6	-29 51 19	7.40 \pm 0.09		1.05 \pm 0.14	1.79 \pm 0.49	3.75 \pm 0.40		
M 83	45400254 ^c	L02	13 37 10.1	-29 51 51	5.11 \pm 0.18		0.55 \pm 0.15	<1.63	2.57 \pm 0.70		
M 83	45400254 ^c	L02	13 37 12.5	-29 52 23	2.18 \pm 0.12		<0.36	<1.79	<0.77		
M 83	45400254 ^c	L02	13 37 05.2	-29 51 51	4.19 \pm 0.20		0.90 \pm 0.18	<1.14	3.55 \pm 0.43		
M 83	45400254 ^c	L02	13 37 07.6	-29 52 23	4.82 \pm 0.12		0.57 \pm 0.10	<1.50	1.78 \pm 0.19		

Table 4—Continued

Galaxy	TDT ^a	AOT ^b	R.A. (J2000.0)	Dec. (J2000.0)	[CII] 158 μm	[OI] 145 μm	[NII] 122 μm	[OIII] 88 μm	[OI] 63 μm	[NIII] 57 μm	[OIII] 52 μm
M 83	45400254 ^c	L02	13 37 10.1	-29 52 55	3.15±0.15		<0.41	<1.70	1.91±0.30		
M 83	45400254 ^c	L02	13 37 02.7	-29 52 23	6.74±0.19		1.78±0.25	<1.85	10.35±0.77		
M 83	45400254 ^c	L02	13 37 05.2	-29 52 54	3.27±0.13		0.39±0.12	<1.76	1.62±0.34		
M 83	45400254 ^c	L02	13 37 07.6	-29 53 26	3.27±0.12		<0.39	<1.69	1.65±0.44		
M 83	45400254 ^c	L02	13 37 00.3	-29 52 54	4.87±0.10		1.18±0.26	<2.26	2.42±0.28		
M 83	45400254 ^c	L02	13 37 02.7	-29 53 26	3.15±0.09		0.55±0.14	<1.17	1.40±0.25		
M 83	45400254 ^c	L02	13 37 05.2	-29 53 58	3.50±0.13		<0.47	<1.54	1.75±0.49		
M 83	45400254 ^c	L02	13 36 57.8	-29 53 26	4.30±0.09		0.48±0.08	<1.30	1.74±0.38		
M 83	45400254 ^c	L02	13 37 00.3	-29 53 58	3.37±0.12		<0.45	<1.26	<1.52		
M 83	45400254 ^c	L02	13 37 02.7	-29 54 30	3.04±0.14		<0.34	<1.55	1.45±0.35		
M 83	45400254 ^c	L02	13 36 55.4	-29 53 58	3.05±0.20		0.46±0.12	<1.60	1.90±0.31		
M 83	45400254 ^c	L02	13 36 57.8	-29 54 30	2.70±0.20		<0.36	<1.76	<1.02		
M 83	45400254 ^c	L02	13 37 00.3	-29 55 02	2.02±0.09		0.31±0.10	<2.23	1.16±0.17		
M 83	64200153 ^c	L02	13 37 02.7	-29 48 07	1.68±0.09		<0.31	<2.20	<1.69		
M 83	64200153 ^c	L02	13 37 05.2	-29 48 39	2.67±0.12		<0.37	<1.68	1.40±0.38		
M 83	64200153 ^c	L02	13 37 07.6	-29 49 10	4.73±0.12		<0.38	<2.09	1.42±0.45		
M 83	64200153 ^c	L02	13 37 10.1	-29 49 42	4.29±0.21		<0.61	<1.93	<2.06		
M 83	64200153 ^c	L02	13 37 00.3	-29 48 39	2.66±0.12		<0.47	<1.40	<1.47		
M 83	64200153 ^c	L02	13 37 02.7	-29 49 11	3.36±0.13		<0.42	<2.09	1.96±0.65		
M 83	64200153 ^c	L02	13 37 05.2	-29 49 42	5.10±0.17		<0.55	<1.76	2.35±0.52		
M 83	64200153 ^c	L02	13 37 07.6	-29 50 14	4.24±0.11		0.62±0.11	<1.98	1.64±0.33		
M 83	64200153 ^c	L02	13 36 57.8	-29 49 11	3.00±0.11		0.41±0.11	<1.70	<1.40		
M 83	64200153 ^c	L02	13 37 00.3	-29 49 42	3.29±0.14		<0.43	<1.53	<3.10		
M 83	64200153 ^c	L02	13 37 02.7	-29 50 14	4.54±0.12		0.51±0.16	<1.58	1.37±0.27		
M 83	64200153 ^c	L02	13 37 05.2	-29 50 46	6.05±0.18		1.02±0.27	<1.56	<1.98		
M 83	64200153 ^c	L02	13 36 55.4	-29 49 43	4.22±0.14		<0.44	<1.88	1.91±0.52		
M 83	64200153 ^c	L02	13 36 57.8	-29 50 14	4.95±0.13		<0.54	<1.19	<2.09		
M 83	64200153 ^c	L02	13 37 00.3	-29 50 46	4.72±0.13		0.71±0.16	<1.90	<1.81		
M 83	64200153 ^c	L02	13 37 02.7	-29 51 18	7.39±0.10		1.59±0.32	<2.43	3.90±0.39		
M 83	64200153 ^c	L02	13 36 53.0	-29 50 14	4.52±0.16		0.53±0.12	<2.16	2.19±0.19		
M 83	64200153 ^c	L02	13 36 55.4	-29 50 46	6.50±0.21		0.68±0.13	<2.43	1.86±0.47		
M 83	64200153 ^c	L02	13 36 57.8	-29 51 18	5.51±0.17		0.88±0.12	<2.26	5.93±0.52		
M 83	64200153 ^c	L02	13 37 00.3	-29 51 50	16.40±0.44		2.59±0.27	3.79±0.79	11.91±0.41		
M 83	64200153 ^c	L02	13 36 50.5	-29 50 46	5.11±0.12		<0.60	<2.03	2.30±0.65		

Table 4—Continued

Galaxy	TDT ^a	AOT ^b	R.A. (J2000.0)	Dec. (J2000.0)	[CII] 158 μ m	[OI] 145 μ m	[NII] 122 μ m	[OIII] 88 μ m	[OI] 63 μ m	[NIII] 57 μ m	[OIII] 52 μ m
M 83	64200153 ^c	L02	13 36 53.0	-29 51 18	8.61 \pm 0.39		1.06 \pm 0.14	<2.12	2.90 \pm 0.68		
M 83	64200153 ^c	L02	13 36 55.4	-29 51 50	5.53 \pm 0.13		0.62 \pm 0.17	<2.71	2.43 \pm 0.36		
M 83	64200153 ^c	L02	13 36 57.9	-29 52 22	8.57 \pm 0.24		1.66 \pm 0.23	1.62 \pm 0.32	7.58 \pm 0.65		
M 83	64200153 ^c	L02	13 36 48.1	-29 51 18	3.01 \pm 0.12		<0.44	<2.01	<1.96		
M 83	64200153 ^c	L02	13 36 50.5	-29 51 50	6.34 \pm 0.16		0.90 \pm 0.15	<1.74	2.48 \pm 0.31		
M 83	64200153 ^c	L02	13 36 53.0	-29 52 22	8.82 \pm 0.20		1.11 \pm 0.17	<1.79	3.88 \pm 0.40		
M 83	64200153 ^c	L02	13 36 55.4	-29 52 54	9.03 \pm 0.22		1.16 \pm 0.22	2.43 \pm 0.81	3.53 \pm 0.34		
M 83	64200153 ^c	L02	13 36 45.6	-29 51 50	2.64 \pm 0.10		<0.31	<1.06	<1.83		
M 83	64200153 ^c	L02	13 36 48.1	-29 52 22	4.36 \pm 0.13		<0.44	<1.74	1.47 \pm 0.33		
M 83	64200153 ^c	L02	13 36 50.5	-29 52 54	9.17 \pm 0.16		<0.87	<2.27	<1.73		
M 83	64200153 ^c	L02	13 36 53.0	-29 53 02	8.57 \pm 0.29		0.94 \pm 0.14	<3.30	3.85 \pm 0.44		
M 83	64200513 ^c	L01	13 37 00.8	-29 51 58	14.59 \pm 0.21		2.78 \pm 0.14	3.45 \pm 0.44	13.30 \pm 0.37		
M 83	64700115 ^c	L01	13 36 53.9	-29 55 07	1.87 \pm 0.07				<0.74		
NGC 5248	58301539 ^c	L02	13 37 26.3	+08 53 38	1.25 \pm 0.05						
NGC 5248	58301539 ^c	L02	13 37 30.1	+08 53 18	3.16 \pm 0.10						
NGC 5248	58301539 ^c	L02	13 37 33.9	+08 52 57	3.39 \pm 0.08						
NGC 5248	58301539 ^c	L02	13 37 37.7	+08 52 37	1.07 \pm 0.10						
NGC 5248	58301557 ^c	L02	13 37 26.3	+08 53 38					0.40 \pm 0.10		
NGC 5248	58301557 ^c	L02	13 37 30.1	+08 53 18					1.65 \pm 0.18		
NGC 5248	58301557 ^c	L02	13 37 33.9	+08 52 57					1.30 \pm 0.16		
NGC 5248	58301557 ^c	L02	13 37 37.7	+08 52 37					0.39 \pm 0.09		
NGC 5248	58301560 ^c	L02	13 38 32.0	+08 53 09	<0.18						
NGC 5248	58301573 ^c	L02	13 38 32.0	+08 53 09					<0.25		
Mrk 273	16001621	L02	13 44 42.1	+55 53 13	0.48 \pm 0.06				1.27 \pm 0.41	<1.58	
Mrk 273	16001621	L02	13 44 42.1	+55 56 13	<0.13				<0.57	<0.81	
Mrk 273	18402511	L02	13 44 42.1	+55 53 13	0.48 \pm 0.09						
Mrk 273	61400705	L01	13 44 41.6	+55 53 18	0.55 \pm 0.03		<0.14		0.48 \pm 0.16		
NGC 5322	20801069	L01	13 49 15.3	+60 11 31	<0.17	<0.06		<0.42	<0.381	<1.43	<1.75
IC 4329A	63003093	L02	13 49 19.2	-30 18 34	0.15 \pm 0.02			0.47 \pm 0.07	0.56 \pm 0.10		
Mrk 463	60200989	L02	13 56 02.9	+18 22 17	0.22 \pm 0.03			0.46 \pm 0.09	0.43 \pm 0.07		
NGC 5430	33700417	L01	14 00 45.5	+59 19 43	1.61 \pm 0.05		0.21 \pm 0.04		1.08 \pm 0.15		
NGC 5433	57100308	L02	14 02 36.0	+32 30 37	1.53 \pm 0.07				1.13 \pm 0.12		
NGC 5457	36801545 ^c	L02	14 02 29.4	+54 16 17				2.75 \pm 0.27		<2.19	<6.83
NGC 5457	36801546 ^c	L02	14 03 02.1	+54 14 35				1.70 \pm 0.32		<3.38	<5.69

Table 4—Continued

Galaxy	TDT ^a	AOT ^b	R.A. (J2000.0)	Dec. (J2000.0)	[CII] 158 μ m	[OI] 145 μ m	[NII] 122 μ m	[OIII] 88 μ m	[OI] 63 μ m	[NIII] 57 μ m	[OIII] 52 μ m
NGC 5457	36801548 ^c	L02	14 03 52.9	+54 21 58				1.90±0.20		<2.55	<7.00
NGC 5457	36801549 ^c	L02	14 04 28.8	+54 23 37				2.61±0.36		<3.00	<4.52
NGC 5457	53200328 ^c	L02	14 00 54.9	+54 40 57	<0.09						
NGC 5457	53200329 ^c	L02	14 03 13.0	+54 21 05	1.39±0.09		0.27±0.05	<0.50	0.69±0.11		
NGC 5457	53200330 ^c	L02	14 02 28.6	+54 16 37	1.52±0.07		<0.11	2.42±0.19	0.94±0.09		
NGC 5457	53200331 ^c	L02	14 03 41.1	+54 19 21	2.31±0.10		0.10±0.03	5.67±0.30	1.64±0.14		
NGC 5457	53200333 ^c	L02	14 04 00.2	+54 21 12	0.14±0.03						
NGC 5457	53200334 ^c	L02	14 04 09.8	+54 22 09	<0.08						
NGC 5457	53200336 ^c	L02	14 04 29.0	+54 24 01	0.38±0.04				0.32±0.07		
NGC 5457	53200372 ^c	L02	14 00 54.8	+54 40 57	<0.13						
Circinus	10401133	L01	14 13 09.7	-65 20 21	25.93±0.37	1.46±0.17		8.38±0.83	23.35±0.50		
NGC 5643	44700462	L02	14 32 40.7	-44 10 26	2.34±0.11				2.61±0.30		<2.02
NGC 5643	44700462	L02	14 32 40.7	-44 07 26	<0.20				<1.20		<2.58
NGC 5713	06301063	L02	14 40 11.5	-00 17 27	5.06±0.19		0.45±0.10	1.47±0.17	2.88±0.11	0.36±0.08	1.41±0.38
NGC 5713	28400956	L02	14 40 11.5	-00 17 27	4.68±0.13	0.25±0.06	0.29±0.08	1.73±0.16			
I Zw 92	54300486	L02	14 40 38.1	+53 30 15	0.16±0.01			0.21±0.05	0.45±0.05		
NGC 5772	26409097	L02	14 51 39.3	+40 34 23	<0.23						
NGC 5786	29900760	L02	14 58 56.7	-42 00 45	1.42±0.07		0.20±0.05				
NGC 5866	26902852	L02	15 06 29.4	+55 45 47	0.51±0.06		0.11±0.03			<0.18	
CGCG 1510.8+0725	28101063	L02	15 13 13.3	+07 13 35	0.33±0.05	<0.07	<0.28	<0.42	<0.25	0.64±0.23	
CGCG 1510.8+0725	60201001	L02	15 13 13.3	+07 13 35	0.29±0.04	<0.10				<0.31	
IRAS 15206+3342	66000222	L02	15 22 38.1	+33 31 33	0.25±0.02						
IRAS 15250+3609	30900660	L02	15 26 59.3	+35 58 37	<0.28						
NGC 5937	62802841	L01	15 30 46.1	-02 49 46	4.01±0.11			1.07±0.27	2.05±0.02		
NGC 5953	64000602	L01	15 34 32.5	+15 11 37	2.87±0.09						
Arp 220	27800202	L01	15 34 57.2	+23 30 11	0.91±0.05				0.50±0.15 ^d		
Arp 220	64000717	L02	15 34 57.2	+23 30 11	1.16±0.11						
Arp 220	64000718	L02	15 34 57.2	+23 30 11	1.33±0.14						
Arp 220	64000801	L01	15 34 57.2	+23 30 11	0.95±0.10						
Arp 220	64000916	L01	15 34 57.2	+23 30 11	1.20±0.14				0.53±0.18 ^d		
NGC 5962	27800776	L02	15 36 31.7	+16 36 31	2.78±0.13		0.26±0.05			0.94±0.10	
IC 4545	27600129	L02	15 41 27.7	-81 37 33	0.52±0.08						
Mrk 297	62702069	L01	16 05 13.1	+20 32 31	2.09±0.08	<0.18	<0.26	2.47±0.27	2.25±0.18	<2.80	<3.54
IC 4595	27601368	L02	16 20 44.3	-70 08 35	2.30±0.24		0.33±0.04			0.87±0.09	

Table 4—Continued

Galaxy	TDT ^a	AOT ^b	R.A. (J2000.0)	Dec. (J2000.0)	[CII] 158 μ m	[OI] 145 μ m	[NII] 122 μ m	[OIII] 88 μ m	[OI] 63 μ m	[NIII] 57 μ m	[OIII] 52 μ m
NGC 6217	52900625	L02	16 32 40.1	+78 10 57	0.52±0.07						
NGC 6217	52900625	L02	16 32 40.0	+78 11 56	1.88±0.03						
NGC 6217	52900625	L02	16 32 39.9	+78 12 56	0.57±0.05						
NGC 6217	71702644	L02	16 32 39.9	+78 10 57					0.57±0.06		
NGC 6217	71702644	L02	16 32 40.0	+78 11 56					1.43±0.13		
NGC 6217	71702644	L02	16 32 40.1	+78 12 57					<0.75		
NGC 6156	64402006	L01	16 34 51.8	-60 37 07	3.84±0.11			1.10±0.36	2.15±0.23		
CGCG 025-007	31800915	L02	16 51 23.1	-02 48 18	0.17±0.05						
NGC 6221	29401119	L02	16 52 45.9	-59 12 59	6.64±0.25						
NGC 6240	27801108	L01	16 52 58.8	+02 24 04	2.72±0.06	0.31±0.04			6.87±0.24		
NGC 6240	81000771	L02	16 52 58.8	+02 24 04					<0.47		
NGC 6240	81000872	L02	16 52 58.8	+02 24 04					<0.31		
NGC 6240	81000973	L02	16 52 58.8	+02 24 04					<0.44		
NGC 6240	81001074	L02	16 52 58.8	+02 24 04					<0.53		
NGC 6240	81600475	L02	16 52 58.8	+02 24 04					<0.45		
NGC 6240	81600577	L02	16 52 58.8	+02 24 04					<2.05		
NGC 6240	81600676	L02	16 52 58.8	+02 24 04					<0.46		
NGC 6240	81600779	L02	16 52 58.8	+02 24 04					<1.65		
NGC 6240	81600880	L02	16 52 58.8	+02 24 04					<1.57		
NGC 6240	81600981	L02	16 52 58.8	+02 24 04					<1.73		
NGC 6240	81601082	L02	16 52 58.8	+02 24 04					<2.06		
NGC 6240	81601178	L02	16 52 58.8	+02 24 04					<2.02		
NGC 6286	20700509	L02	16 58 31.4	+58 56 12	1.68±0.05	0.05±0.01	0.17±0.05	0.26±0.05	0.73±0.09		
IRAS 17208-0014	10901728	L02	17 23 22.0	-00 17 01	0.74±0.07				<1.26	<2.74	
IRAS 17208-0014	10901728	L02	17 23 22.0	-00 14 01	<0.12				1.25±0.34	<3.14	
IRAS 17208-0014	65000608	L01	17 23 21.9	-00 17 01	0.67±0.08		<0.30		<0.75		
IC 4662	29100701	L02	17 47 08.7	-64 38 36	1.12±0.07		<0.10	4.46±0.15	1.43±0.09		
IC 4662	64800901	L02	17 47 08.7	-64 38 36	1.39±0.06		<0.11	4.71±0.13	1.48±0.08		
NGC 6503	16201043 ^c	L02	17 49 17.6	+70 09 13	1.50±0.04						
NGC 6503	16201043 ^c	L02	17 49 27.4	+70 08 41	2.29±0.06						
NGC 6503	16201043 ^c	L02	17 49 37.4	+70 08 08	1.65±0.05						
NGC 6503	16201064 ^c	L02	17 51 27.4	+70 08 49	<0.19						
Ark 535	33601307	L02	17 58 07.0	+21 16 19	0.41±0.07						
3C 368	15900101	L02	18 05 06.3	+11 01 31				<0.04			

| 63 |

Table 4—Continued

Galaxy	TDT ^a	AOT ^b	R.A. (J2000.0)	Dec. (J2000.0)	[CII] 158 μ m	[OI] 145 μ m	[NII] 122 μ m	[OIII] 88 μ m	[OI] 63 μ m	[NIII] 57 μ m	[OIII] 52 μ m
3C 368	15900102	L02	18 04 54.1	+11 01 30					<0.04		
3C 368	15900203	L02	18 05 06.3	+11 01 31					<0.02		
3C 368	15900204	L02	18 05 18.5	+11 01 31					<0.03		
3C 368	31901205	L02	18 05 06.3	+11 01 30					<0.04		
3C 368	31901206	L02	18 05 06.3	+11 04 31					<0.02		
NGC 6574	70500604	L01	18 11 51.8	+14 58 55	4.47±0.20				2.31±0.41		
HB89 1821+643	17801811	L01	18 21 57.2	+64 20 36				<0.08	<0.67		
HB89 1821+643	63501211	L01	18 21 57.2	+64 20 36				<0.09	<0.74		
NGC 6764	03502201	L01	19 08 16.0	+50 55 59	1.25±0.13						
NGC 6764	30200964	L01	19 08 16.3	+50 55 59	1.03±0.05		<0.19		1.93±0.43		
NGC 6744	47401673 ^c	L02	19 06 42.5	-63 31 40	<0.13						
NGC 6744	47401676 ^c	L02	19 10 18.7	-63 55 02	0.21±0.02						
NGC 6744	47401676 ^c	L02	19 10 08.1	-63 53 51	0.44±0.04						
NGC 6744	47401676 ^c	L02	19 09 57.4	-63 52 40	0.70±0.02						
NGC 6744	47401676 ^c	L02	19 09 46.8	-63 51 29	0.39±0.03						
NGC 6744	47401676 ^c	L02	19 09 36.1	-63 50 18	0.57±0.04						
NGC 6744	47401676 ^c	L02	19 09 25.5	-63 49 07	0.34±0.03						
NGC 6744	47401676 ^c	L02	19 09 14.9	-63 47 55	<0.14						
NGC 6753	29901225	L02	19 11 23.3	-57 02 55	2.52±0.13		0.54±0.05	0.31±0.08	0.91±0.10		
IRAS 19254-7245	29902031	L02	19 31 21.8	-72 39 24	0.26±0.07				<0.66	<1.28	
IRAS 19254-7245	29902031	L02	19 31 21.4	-72 36 25	<0.24				<0.59	<1.37	
IRAS 19297-0406	85700411	L02	19 32 22.1	-04 00 02	0.24±0.02						
NGC 6810	84700610	L01	19 43 34.0	-58 39 20	3.83±0.13		0.55±0.08		1.57±0.22		
NGC 6824	54301102	L01	19 43 40.7	+56 06 34	1.80±0.04		0.24±0.04		0.81±0.16		
NGC 6821	31900732	L02	19 44 24.2	-06 50 02	0.98±0.10		<0.05				
NGC 6822	34300915 ^c	L02	19 44 52.9	-14 43 05	1.87±0.11	<0.05	<0.12		1.43±0.06		
NGC 6822	34300923 ^c	L02	19 44 59.7	-14 47 43	1.04±0.09	<0.05					
Cygnus A	34700703	L02	19 59 28.4	+40 44 01					0.76±0.05		
Cygnus A	35200702	L02	19 59 28.4	+40 44 01					0.92±0.05		
Cygnus A	35800701	L02	19 59 28.4	+40 44 01					0.75±0.05		
Cygnus A	58001306	L02	19 59 28.4	+40 44 01					0.90±0.04		
IRAS 20100-4156	85900713	L02	20 13 29.7	-41 47 34	0.08±0.02						
IC 5020	72701155	L02	20 30 38.0	-33 29 05	0.70±0.08						
NGC 6946	45100131 ^c	L02	20 32 10.4	+60 29 03	0.28±0.05						

Table 4—Continued

Galaxy	TDT ^a	AOT ^b	R.A. (J2000.0)	Dec. (J2000.0)	[CII] 158 μ m	[OI] 145 μ m	[NII] 122 μ m	[OIII] 88 μ m	[OI] 63 μ m	[NIII] 57 μ m	[OIII] 52 μ m
NGC 6946	45100132 ^c	L02	20 35 20.3	+60 10 11	2.59±0.23		<0.34	1.23±0.14	1.34±0.33		
NGC 6946	45100133 ^c	L02	20 35 11.6	+60 11 27	2.47±0.11		0.19±0.06	1.23±0.15	1.40±0.13		
NGC 6946	45100134 ^c	L02	20 35 02.9	+60 12 43	0.70±0.05				<0.44		
NGC 6946	45100135 ^c	L02	20 35 10.1	+60 09 06	4.69±0.13		0.46±0.07	1.18±0.09	2.11±0.23		
NGC 6946	45100136 ^c	L02	20 35 01.4	+60 10 22	4.16±0.15		0.58±0.11	0.97±0.15	1.91±0.12		
NGC 6946	45100137 ^c	L02	20 34 52.7	+60 11 38	1.60±0.06		0.12±0.02		0.56±0.09		
NGC 6946	45700138 ^c	L02	20 34 59.9	+60 08 01	3.63±0.10		<0.38	0.66±0.09	1.58±0.19		
NGC 6946	45700139 ^c	L01	20 34 51.2	+60 09 17	9.45±0.10	0.39±0.07	1.08±0.23	1.75±0.50	6.06±0.69	<3.41	<3.80
NGC 6946	45700140 ^c	L02	20 34 42.5	+60 10 33	2.33±0.06		0.17±0.04	0.44±0.10	1.13±0.14		
NGC 6946	45700141 ^c	L02	20 34 33.8	+60 11 49	2.29±0.09		0.11±0.03		1.10±0.09		
NGC 6946	45700142 ^c	L02	20 34 25.0	+60 13 05	0.38±0.03				0.21±0.04		
NGC 6946	45700143 ^c	L02	20 34 16.4	+60 14 22	0.12±0.03						
NGC 6946	45700151 ^c	L02	20 32 10.4	+60 29 02	0.32±0.03						
NGC 6946	45100153 ^c	L02	20 35 20.3	+60 10 11	2.40±0.06				1.23±0.12		
NGC 6946	45700155 ^c	L02	20 35 20.3	+60 10 11	2.67±0.14				1.32±0.28		
NGC 6946	45100244 ^c	L02	20 34 49.6	+60 06 56	2.73±0.07		0.18±0.03		1.61±0.12		
NGC 6946	45100245 ^c	L02	20 34 41.0	+60 08 12	3.05±0.10		0.37±0.10	0.50±0.10	2.06±0.14		
NGC 6946	45100246 ^c	L02	20 34 32.3	+60 09 28	1.91±0.06		0.18±0.03		1.17±0.09		
NGC 6946	45100247 ^c	L02	20 34 39.6	+60 05 51	0.77±0.04				0.57±0.07		
NGC 6946	45100248 ^c	L02	20 34 30.8	+60 07 07	0.80±0.04				0.39±0.07		
NGC 6946	45100249 ^c	L02	20 34 22.1	+60 08 23	0.92±0.04				0.45±0.08		
NGC 6946	45100250 ^c	L02	20 32 10.4	+60 29 02	0.33±0.07						
NGC 6946	45100254 ^c	L02	20 35 20.3	+60 10 11	2.46±0.08				1.11±0.22		
NGC 6946	84901120 ^c	L02	20 35 20.3	+60 10 11			0.17±0.02				
NGC 6946	84901121 ^c	L02	20 34 59.9	+60 08 01			0.30±0.04				
NGC 6946	84901122 ^c	L02	20 34 32.3	+60 09 28			0.17±0.05				
NGC 6946	86100405 ^c	L02	20 34 12.7	+60 08 29	0.11±0.09						
NGC 6946	86100405 ^c	L02	20 34 22.8	+60 09 34	1.43±0.11						
NGC 6946	86100405 ^c	L02	20 34 33.0	+60 10 38	2.91±0.19						
NGC 6946	86100405 ^c	L02	20 34 43.2	+60 11 43	1.21±0.19						
NGC 6946	86100405 ^c	L02	20 34 53.5	+60 12 48	1.34±0.08						
NGC 6946	86100405 ^c	L02	20 35 03.7	+60 13 53	<0.26						
NGC 6946	86100405 ^c	L02	20 34 21.4	+60 07 14	0.50±0.10						
NGC 6946	86100405 ^c	L02	20 34 31.6	+60 08 18	2.53±0.11						

Table 4—Continued

Galaxy	TDT ^a	AOT ^b	R.A. (J2000.0)	Dec. (J2000.0)	[CII] 158 μ m	[OI] 145 μ m	[NII] 122 μ m	[OIII] 88 μ m	[OI] 63 μ m	[NIII] 57 μ m	[OIII] 52 μ m
NGC 6946	86100405 ^c	L02	20 34 41.8	+60 09 23	3.23±0.13						
NGC 6946	86100405 ^c	L02	20 34 52.0	+60 10 28	4.37±0.12						
NGC 6946	86100405 ^c	L02	20 35 02.3	+60 11 33	2.53±0.09						
NGC 6946	86100405 ^c	L02	20 35 12.4	+60 12 37	0.30±0.15						
NGC 6946	86100405 ^c	L02	20 34 30.0	+60 05 57	0.29±0.09						
NGC 6946	86100405 ^c	L02	20 34 40.2	+60 07 01	1.50±0.08						
NGC 6946	86100405 ^c	L02	20 34 50.4	+60 08 06	4.62±0.26						
NGC 6946	86100405 ^c	L02	20 35 00.6	+60 09 11	4.58±0.12						
NGC 6946	86100405 ^c	L02	20 35 10.8	+60 10 15	3.70±0.13						
NGC 6946	86100405 ^c	L02	20 35 21.0	+60 11 20	1.00±0.05						
NGC 6946	86100405	L02	20 34 38.7	+60 04 41	0.86±0.09						
NGC 6946	86100405 ^c	L02	20 34 48.9	+60 05 46	1.14±0.12						
NGC 6946	86100405 ^c	L02	20 34 59.2	+60 06 51	1.22±0.19						
NGC 6946	86100405 ^c	L02	20 35 09.4	+60 07 55	1.80±0.07						
NGC 6946	86100405 ^c	L02	20 35 19.6	+60 09 00	1.94±0.10						
NGC 6946	86100405 ^c	L02	20 35 29.7	+60 10 05	1.13±0.11						
NGC 6946	86100502 ^c	L02	20 34 48.3	+60 04 35	0.21±0.07						
NGC 6946	86100502 ^c	L02	20 34 58.5	+60 05 40	0.38±0.13						
NGC 6946	86100502 ^c	L02	20 35 08.7	+60 06 44	1.08±0.10						
NGC 6946	86100502 ^c	L02	20 35 18.9	+60 07 49	0.58±0.10						
NGC 6946	86100502 ^c	L02	20 35 29.1	+60 08 54	0.33±0.06						
NGC 6946	86100503 ^c	L02	20 35 17.3	+60 05 28	0.11±0.10						
NGC 6946	86100503 ^c	L02	20 35 26.1	+60 04 13	<0.43						
NGC 6946	86100503 ^c	L02	20 35 34.9	+60 02 57	<0.35						
NGC 6946	86100504 ^c	L02	20 35 21.7	+60 12 32	<0.61						
NGC 6946	86100504 ^c	L02	20 35 31.9	+60 13 36	<0.35						
NGC 6946	86100504 ^c	L02	20 35 42.1	+60 14 41	<0.47						
NGC 6946	86100506 ^c	L02	20 34 00.3	+60 03 53	<0.54						
NGC 6946	86100506 ^c	L02	20 34 10.5	+60 04 57	<0.65						
NGC 6946	86100506 ^c	L02	20 34 20.7	+60 06 02	<0.49						
Mrk 509	17000925	L01	20 44 09.7	-10 43 24	0.29±0.05			0.31±0.08		<0.43	
NGC 6958	54200617	L02	20 48 42.8	-37 59 45	0.11±0.01					<0.24	
IC 5063	33301165	L02	20 52 02.2	-57 04 07	0.36±0.05				0.93±0.19		<1.69
IC 5063	33301165	L02	20 52 02.2	-57 01 07	<0.21					<0.61	<2.07

Table 4—Continued

Galaxy	TDT ^a	AOT ^b	R.A. (J2000.0)	Dec. (J2000.0)	[CII] 158 μ m	[OI] 145 μ m	[NII] 122 μ m	[OIII] 88 μ m	[OI] 63 μ m	[NIII] 57 μ m	[OIII] 52 μ m
IRAS 20551-4250	15500812	L02	20 58 26.7	-42 38 57	0.35±0.07				<0.96		<1.48
IRAS 20551-4250	15500812	L02	20 58 26.7	-42 35 57	<0.16				<1.10		<0.94
IRAS 20551-4250	72501106	L02	20 58 26.8	-42 39 06	0.41±0.03						
NGC 7217	18500444	L02	22 07 50.0	+31 21 35	0.62±0.07						
NGC 7217	18500444	L02	22 07 54.6	+31 21 30	0.66±0.06						
NGC 7217	18500465	L02	22 08 52.5	+31 21 35	<0.20						
NGC 7218	36902408	L02	22 10 11.7	-16 39 36	1.92±0.09		<0.11		0.88±0.05		
NGC 7314	35301177	L02	22 35 49.7	-26 04 17	0.26±0.06						
NGC 7314	35301177	L02	22 35 43.4	-26 01 38	0.22±0.05						
NGC 7331	55101020 ^c	L01	22 37 02.9	+34 23 28	2.18±0.06				<0.57		
NGC 7331	55101419 ^c	L01	22 37 01.8	+34 25 08	5.13±0.15				<1.26		
NGC 7331	60001501 ^c	L01	22 37 04.1	+34 24 56	6.91±0.10		1.11±0.08		3.40±0.20		
IRAS 22491-1808	18600619	L02	22 51 49.3	-17 52 24	<0.17						
NGC 7418	36902716	L02	22 56 35.9	-37 01 45	1.39±0.06		0.12±0.02				
IC 1459	20002076	L01	22 57 10.5	-36 27 44	0.15±0.04						
NGC 7469	37200648	L01	23 03 15.6	+08 52 26	2.13±0.08				2.52±0.29		
NGC 7469	37200648	L01	23 03 15.6	+08 55 26	<0.21				<1.57		
NGC 7469	73601214	L01	23 03 15.4	+08 52 25	2.27±0.03				2.48±0.12		
IRAS 23128-5919	15500239	L02	23 15 46.8	-59 03 14	0.49±0.12				<0.90		<1.68
IRAS 23128-5919	15500239	L02	23 15 46.8	-59 00 14	<0.18				<0.90		<1.42
IRAS 23128-5919	74201208	L02	23 15 46.9	-59 03 16	0.58±0.05						
NGC 7552	36903087	L01	23 16 10.8	-42 35 04	6.37±0.15		0.76±0.10	2.47±0.36	6.30±0.23		
NGC 7552	36903087	L01	23 16 10.8	-42 32 04	<0.15		<0.16	<1.05	<0.63		
NGC 7582	16700869	L01	23 18 23.7	-42 22 13	4.12±0.13			2.99±0.49	2.65±0.37		
NGC 7582	16700869	L01	23 18 23.7	-42 19 13	<0.23			<4.37	<1.40		
IC 5325	36902817	L02	23 28 43.2	-41 19 57	2.04±0.09		0.21±0.04				
III Zw 107	75800519	L01	23 30 09.9	+25 31 59	0.16±0.04		<0.14		<0.60		
NGC 7714	37501863	L01	23 36 14.7	+02 09 18	1.83±0.10			2.53±0.52	2.80±0.36		
IRAS F23365+3604	75201572	L02	23 39 01.3	+36 21 10	0.16±0.02				0.21±0.05		
NGC 7771	56500772	L02	23 51 24.8	+20 06 42	2.98±0.09		0.47±0.10	0.50±0.10	1.15±0.13	<0.36	
Mrk 331	56500637	L02	23 51 26.2	+20 35 08	1.48±0.08	<0.13	0.23±0.06	0.38±0.10	1.05±0.06		
NGC 7793	18700649 ^c	L02	23 57 42.8	-32 35 08	1.36±0.07						
NGC 7793	18700649 ^c	L02	23 57 47.5	-32 35 16	1.83±0.05						
NGC 7793	18700649 ^c	L02	23 57 52.2	-32 35 25	1.57±0.04						

Table 4—Continued

Galaxy	TDT ^a	AOT ^b	R.A. (J2000.0)	Dec. (J2000.0)	[CII] 158 μm	[OI] 145 μm	[NII] 122 μm	[OIII] 88 μm	[OI] 63 μm	[NIII] 57 μm	[OIII] 52 μm
NGC 7793	18700649 ^c	L02	23 57 56.9	−32 35 33	1.27±0.08						
NGC 7793	18700659 ^c	L02	23 57 42.8	−32 35 08					0.58±0.13		
NGC 7793	18700659 ^c	L02	23 57 47.5	−32 35 16					0.58±0.11		
NGC 7793	18700659 ^c	L02	23 57 52.2	−32 35 25					0.53±0.05		
NGC 7793	18700659 ^c	L02	23 57 56.9	−32 35 33					0.86±0.13		

Note. — Units of right ascension are hours, minutes, and seconds, and units of declination are degrees, arcminutes, and arcseconds. Line fluxes are in units of $10^{-15} \text{ W m}^{-2}$. Flux upper limits are 3σ .

^aTDT is the ISO observation number. It has the form RRRSSSOO where RRR=revolution number, SSS=sequence number within the revolution, and OO=observation number within an observer’s proposal

^bAOT = Astronomical Observation Template. L01 = medium-resolution ($R \sim 200$) spectrum covering the full LWS range (43–197 μm); L02 = medium-resolution line spectrum, producing an incomplete spectrum over the LWS range.

^cObservation considered an extended source in this paper. May require an extended source correction.

^dFlux measured is in absorption rather than emission.

Table 5. Molecular and Unidentified Line Fluxes

Galaxy	TDT ^a	R.A. (J2000.0)	Dec. (J2000.0)	OH 53 μ m	H ₂ O 59 μ m	OH 65 μ m	H ₂ O 67 μ m	unidentified 74 μ m	H ₂ O 75 μ m	OH 79 μ m	OH 84 μ m	H ₂ O 101 μ m	H ₂ O 108 μ m	OH 119 μ m	OH/CO 163 μ m
NGC 0253	24701103 ^b	00 47 33.3	-25 17 18												11.76 ^c
NGC 0253	56901708 ^b	00 47 33.3	-25 17 18	7.12 ^c											11.63 ^c
NGC 0253	79900508 ^b	00 47 33.3	-25 17 18												2.24
NGC 0891	61100256 ^b	02 22 33.0	+42 20 55												1.11 ^c
NGC 0891	61401144 ^b	02 22 33.2	+42 20 58												1.33 ^c
NGC 1068	82000605	02 42 40.6	-00 00 48										1.36		
NGC 1068	82000704	02 42 40.6	-00 00 48					1.32							1.31
NGC 1068	82001106	02 42 40.6	-00 00 48					1.24							1.60
M 82	18000501 ^b	09 55 52.4	+69 40 46												7.88 ^c
M 82	65800502 ^b	09 55 52.2	+69 40 46												8.17 ^c
M 82	65800611 ^b	09 55 52.2	+69 40 46												8.45 ^c
Mrk 231	05100540	12 56 14.6	+56 52 24										1.10 ^c		
Mrk 231	18001306	12 56 14.2	+56 52 24										1.09 ^c		0.31 ^c
Mrk 231	60300241	12 56 14.2	+56 52 24										0.65 ^c		0.34 ^c
NGC 4945	08101705 ^b	13 05 26.2	-49 28 15												13.8 ^c
NGC 4945	28000440 ^b	13 05 26.5	-49 27 54										7.44 ^c		11.62 ^c
Arp 220	27800202	15 34 57.2	+23 30 11	4.30 ^c			1.85 ^c					1.40 ^c	3.09 ^c	2.01 ^c	2.75 ^c
Arp 220	61001559	15 34 57.2	+23 30 11		0.68 ^c										0.76 ^c
Arp 220	64000801	15 34 57.2	+23 30 11	5.31 ^c			2.10 ^c	1.37 ^c		1.68 ^c		2.34 ^c			2.29 ^c
Arp 220	64000916	15 34 57.2	+23 30 11	4.62 ^c			1.55 ^c	1.36 ^c			1.00 ^c		2.97 ^c		2.84 ^c
															0.40

Note. — Units of right ascension are hours, minutes, and seconds, and units of declination are degrees, arcminutes, and arcseconds. Line fluxes are in units of 10^{-15} W m $^{-2}$. Upper limits are also available via L01 range scans, e.g., Arp 220 and Mkn 231.

^aTDT is the ISO observation number. It has the form RRRSSSOO where RRR=revolution number, SSS=sequence number within the revolution, and OO=observation number within an observer's proposal.

^bObservation considered an extended source in this paper. May require an extended source correction.

^cFlux measured is in absorption rather than emission.

Table 6. Serendipitous Galactic [C II] 158 μm Detections

Galaxy	TDT ^a	<i>l</i> ($^{\circ}$)	<i>b</i> ($^{\circ}$)	<i>cz</i> (km s $^{-1}$)	Galactic prediction ^b	Galactic observation ^c	extragalactic observation ^d	contamination ^f (%)
IC 10	45700606	118.89	−3.23	−344	25.38	20.73±0.48	70.93 ^g	23.4
	45700607	119.06	−3.45		23.76	12.44±0.48		
Maffei 2	85800683 ^e	136.48	−0.55	−17	148.97	27.47±0.87	112.62	24.4
NGC 1156	65300185	156.37	−29.28	375	2.92	2.51±0.58	17.54	14.3
UGC 02855	62902697	136.91	+12.33	1202	6.70	4.85±0.58	50.51	9.6
NGC 1569	64600490	143.61	+11.31	−104	7.29	8.22±0.86	65.99	12.5
3C 120	80901988	190.37	−27.40	9896	3.11	3.95±0.29	3.66	0
NGC 1614	85501010	204.45	−34.38	4778	2.53	4.44±0.39	21.80	0
NGC 3620	27600982	297.19	−14.32	1680	5.78	3.47±0.39	20.93	0
UGCA 332	25700705	310.84	+50.49	2107	1.85	0.87±0.10	0.66	0
ESO 173-G015	30601434	307.77	+5.04	3006	16.28	21.80±2.22	48.70	0
NGC 6821	31900733	32.89	−14.83	1525	5.59	3.49±0.58	9.43	0
NGC 6946	45100131	95.80	+12.14	48	6.80	2.69±0.49	20.58 ^g	13.1

Note. — [CII] 158m intensities are in 10^{-6} ergs cm $^{-2}$ s $^{-1}$ sr $^{-1}$ assuming a 75'' aperture diameter.

^aTDT is the ISO observation number. It has the form RRRSSSOO where RRR=revolution number, SSS=sequence number within the revolution, and OO=observation number within an observer's proposal.

^bMilky Way [CII] 158 μm predicted by Equation 1.

^cMilky Way [CII] 158 μm measured by ISOLWS.

^d[CII] 158 μm measured for external target galaxy.

^eObservation considered an extended source in this paper. May require an extended source correction.

^fPercent of observed [CII] arising from the Milky Way. This foreground contamination has been removed from the [CII] fluxes listed in Table 4 for these galaxies.

^gAn average value measured in the LWS aperture from multiple observations.

Table 7. Extended Source Aperture Corrections

Detector	Aperture Radius ('')	Correction
SW1	39	0.88
SW2	42	0.88
SW3	43	0.84
SW4	41	0.73
SW5	40	0.70
LW1	38	0.69
LW2	39	0.69
LW3	35	0.62
LW4	34	0.55
LW5	33	0.48

Note. — The fluxes listed in Tables 3 and 4 for extended sources are based on a point source calibration. The multiplicative correction listed here may need to be applied to these fluxes.

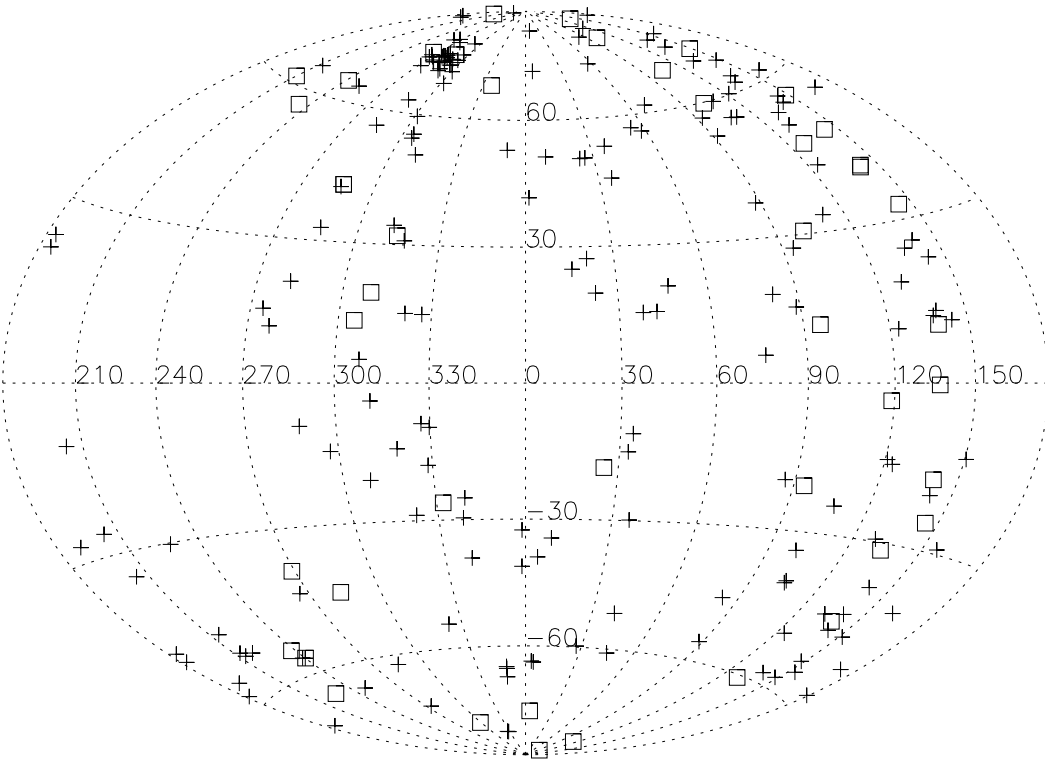


Fig. 1.— Aitoff projection of the galaxies selected for this sample. The galaxies in this sample are distributed across the sky. Galaxies unresolved by the LWS in the far-infrared are displayed with crosses. Resolved galaxies by the LWS in the far-infrared are shown with open squares. The clump of galaxies at RA, Dec (70° , 280°) are members of the Virgo Cluster.

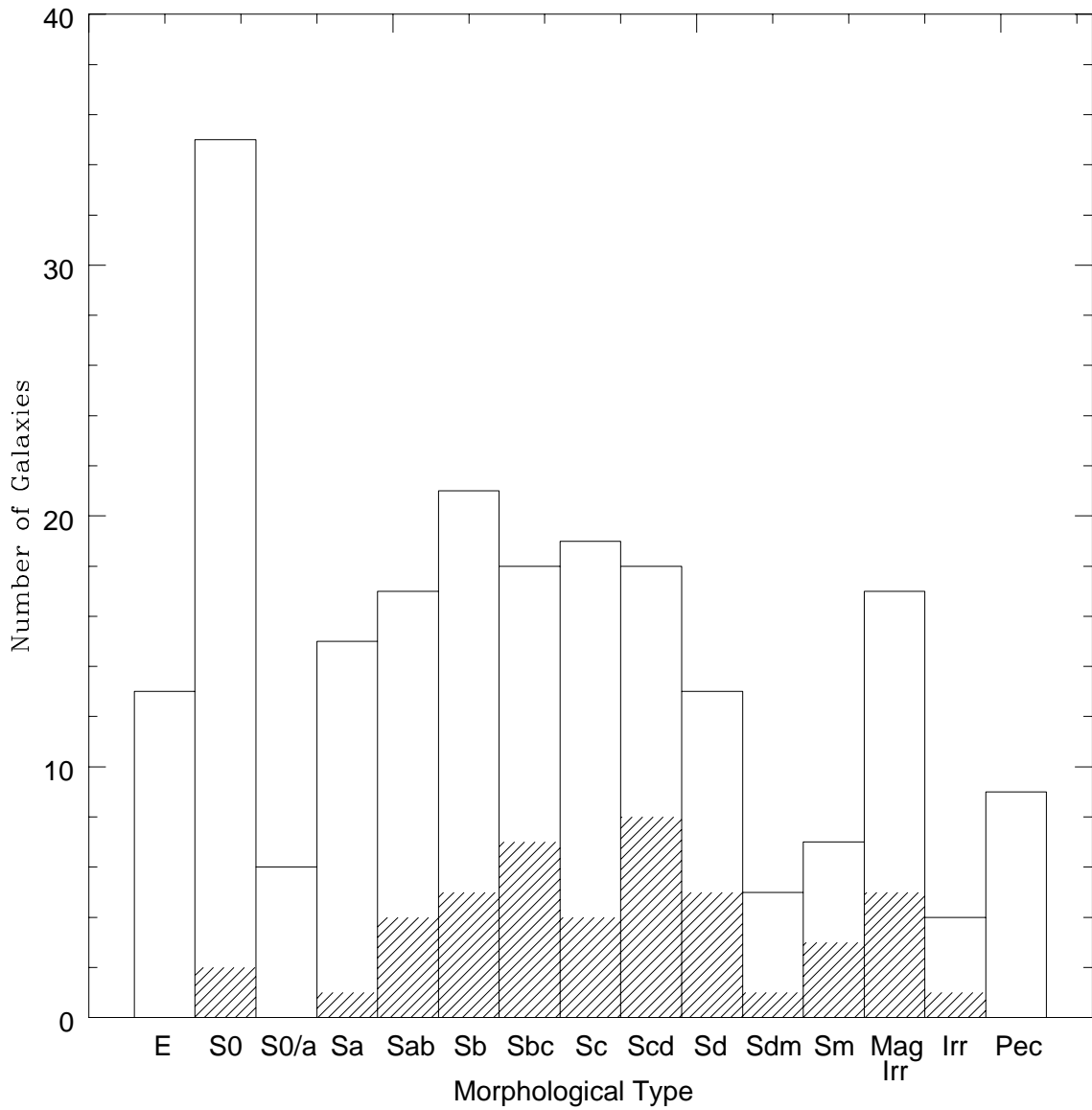


Fig. 2.— The distributions of the optical morphologies of the resolved and unresolved subsets of galaxies. The resolved subset is cross-shaded.

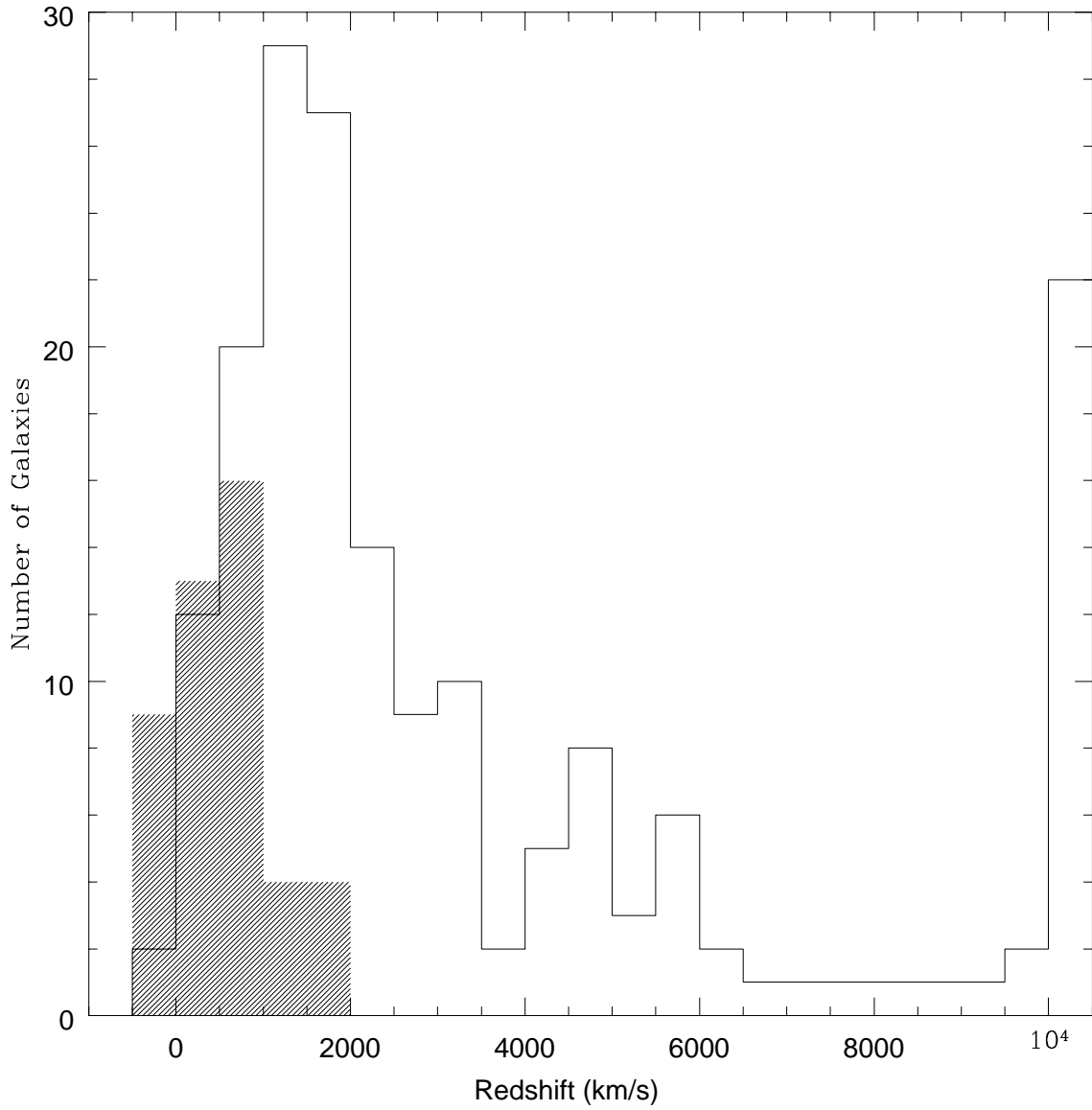


Fig. 3.— The distributions of redshifts for the resolved and unresolved subsets. The resolved galaxy redshifts are cross-shaded.

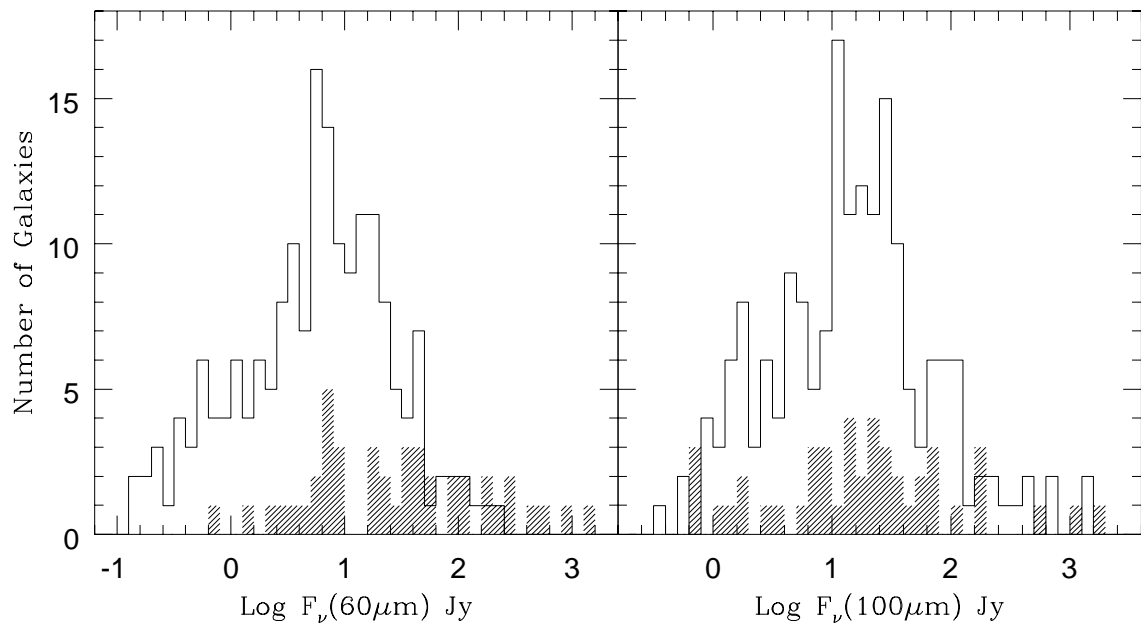


Fig. 4.— The distributions of *IRAS* 60 μm and 100 μm flux densities. The resolved galaxy subset is cross-shaded.

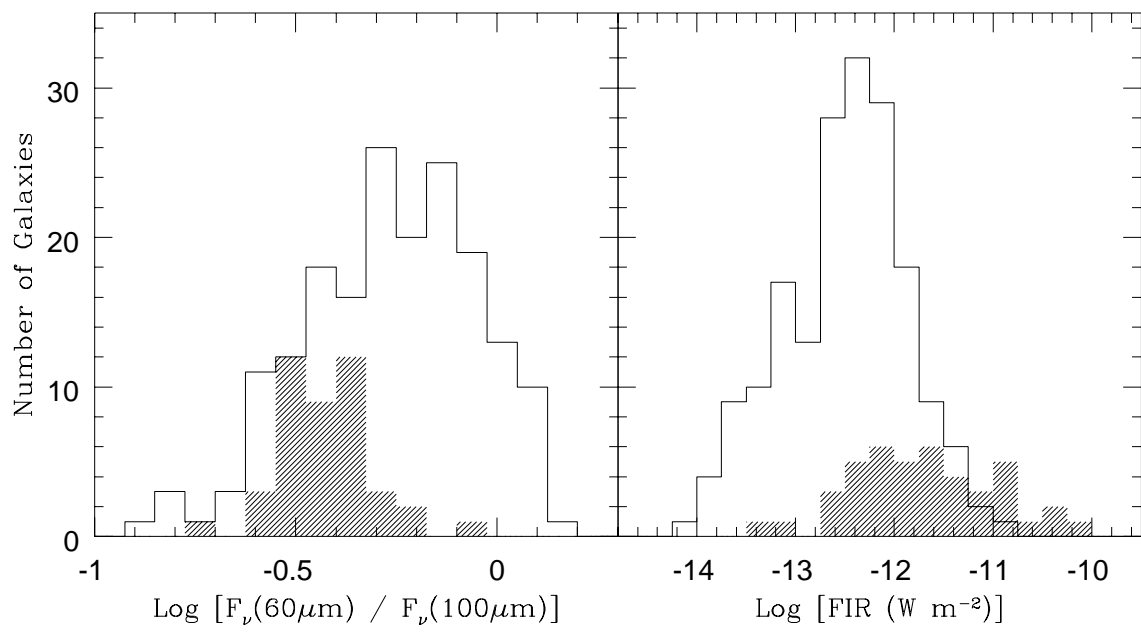


Fig. 5.— The distributions of *IRAS* 60 μm /100 μm ratio and *FIR*. The resolved galaxy subset is cross-shaded.

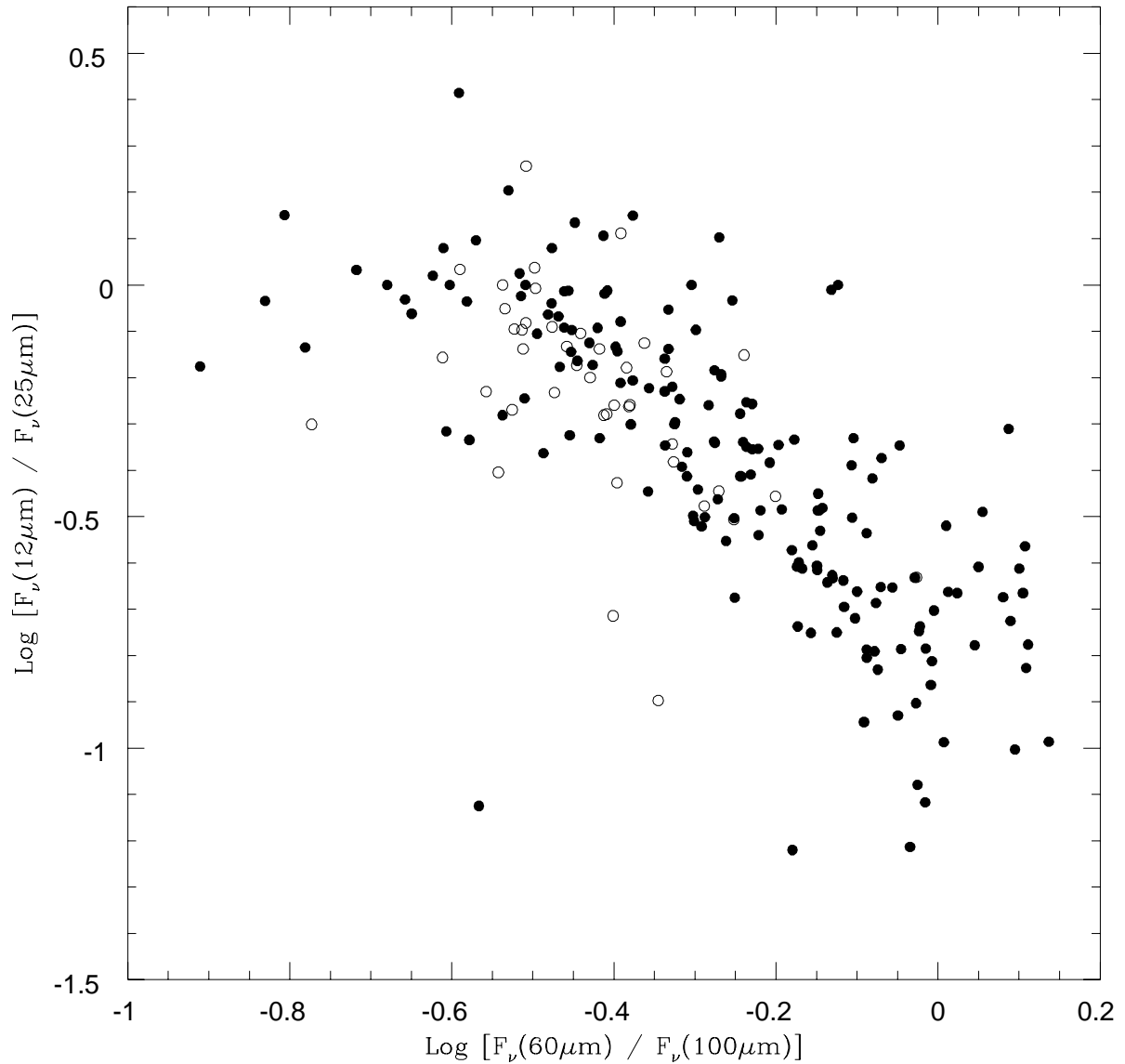


Fig. 6.— The *IRAS* color-color diagram for the galaxies in this sample. Quiescent galaxies are located towards the upper left and actively star-forming galaxies towards the lower right. Filled circles are galaxies in the unresolved subset. Open circles are galaxies in the resolved subset.

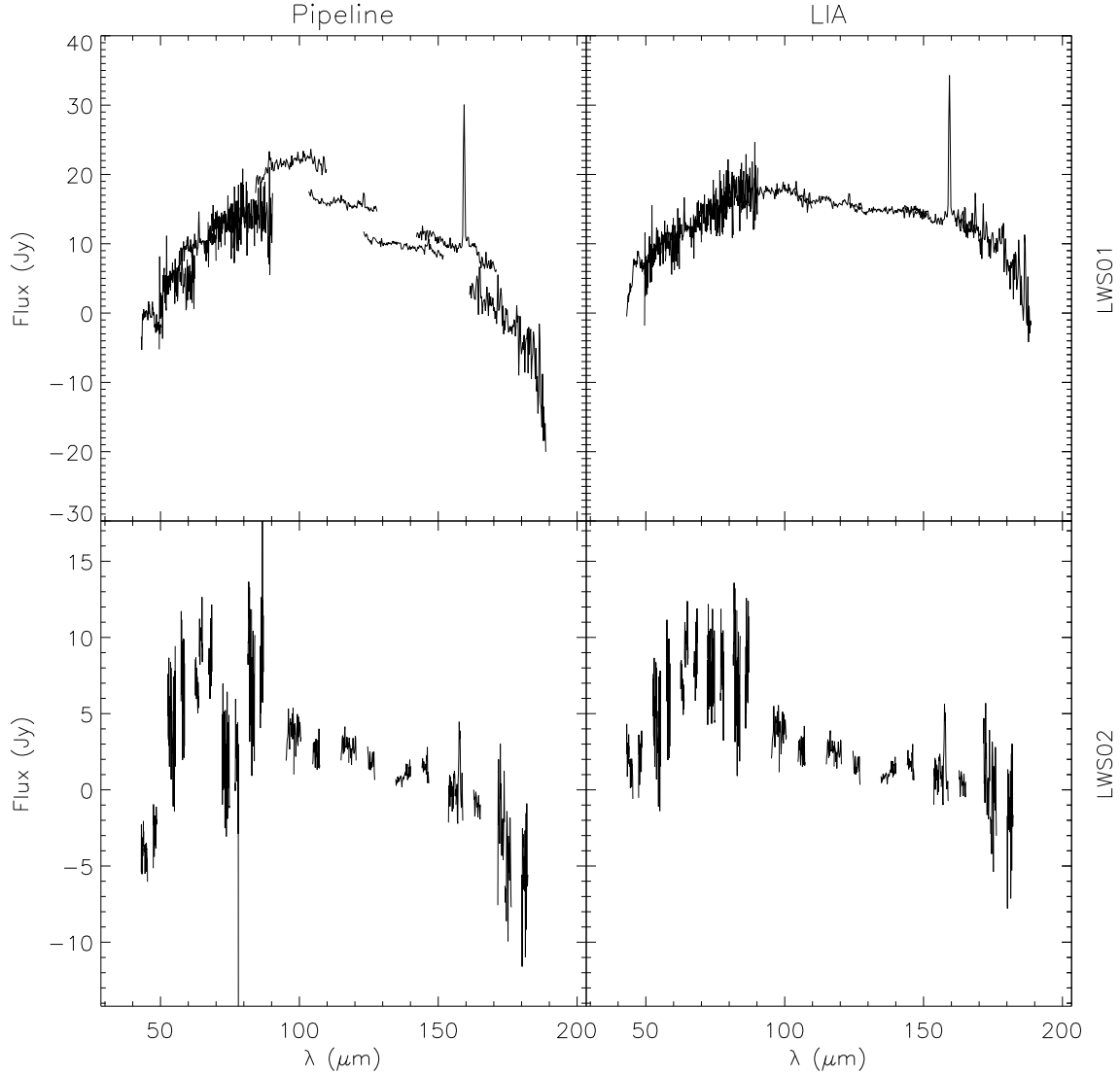


Fig. 7.— Two example LWS spectra representing the pipeline product L01 and L02 AOTs displayed before and after using the LIA and ISAP reduction. Improvements from using LIA and ISAP include not only the removal of fringes and glitch removal but also the reduction of negative continuum fluxes and misaligned adjacent detectors.

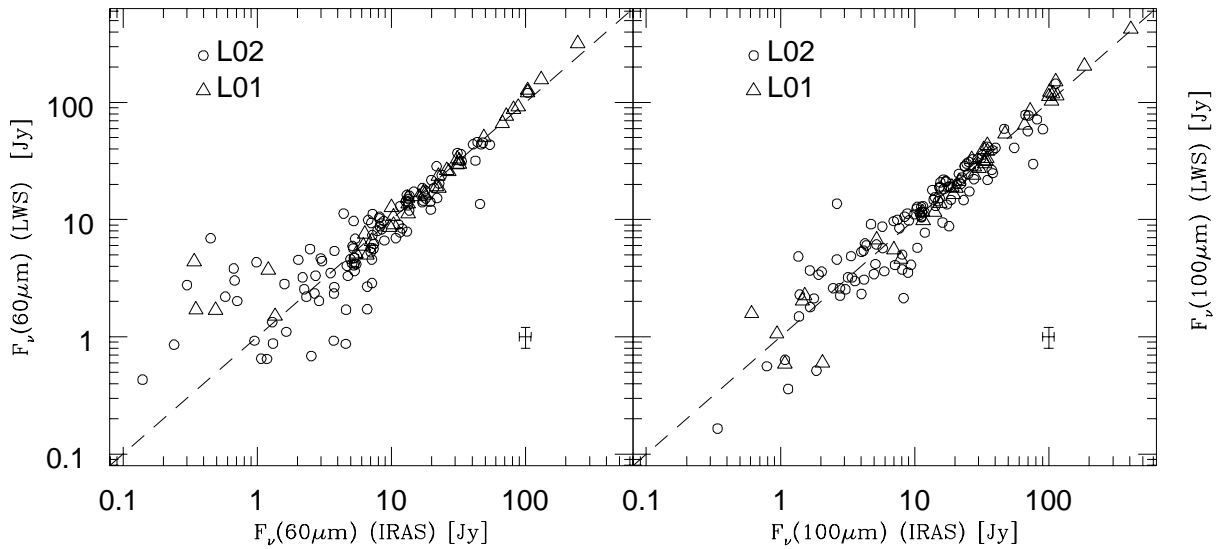


Fig. 8.— Comparison of LWS continuum fluxes to the *IRAS* fluxes at $60\mu\text{m}$ and $100\mu\text{m}$. Triangles (circles) are continuum fluxes from L01 (L02) observations. A typical error bar is plotted in the lower right of each plot. The LWS error bar is calculated from the combination of the systematic and measured flux uncertainties and represents an average 20% uncertainty. The *IRAS* flux error bar is taken from the *IRAS* Point Source Catalog and represents an average 10% uncertainty. The dashed line is the one-to-one correlation.

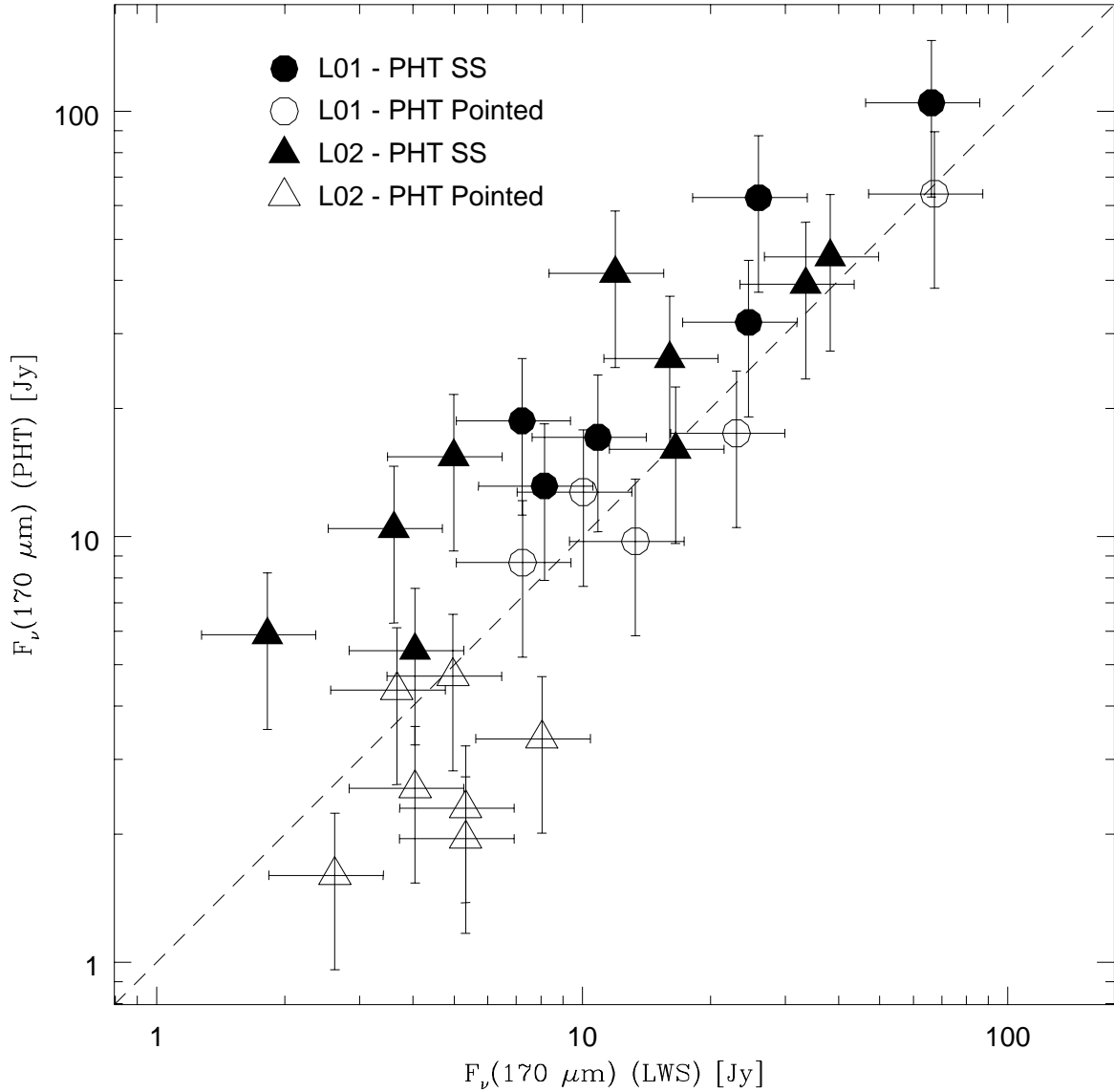


Fig. 9.— Comparison of LWS continuum fluxes to ISOPHOT Serendipity Survey fluxes (Stickel et al. 2000) at 170 μm for galaxies unresolved by the LWS. Filled circles are measurements from L01 observations and open triangles are from L02 observations. The ISOPHOT error bars represent 40% calibration uncertainties quoted by Stickel et al. (2000) and the LWS error bars represent 30% calibration uncertainties at 170 μm . The dashed line is the one-to-one correlation.

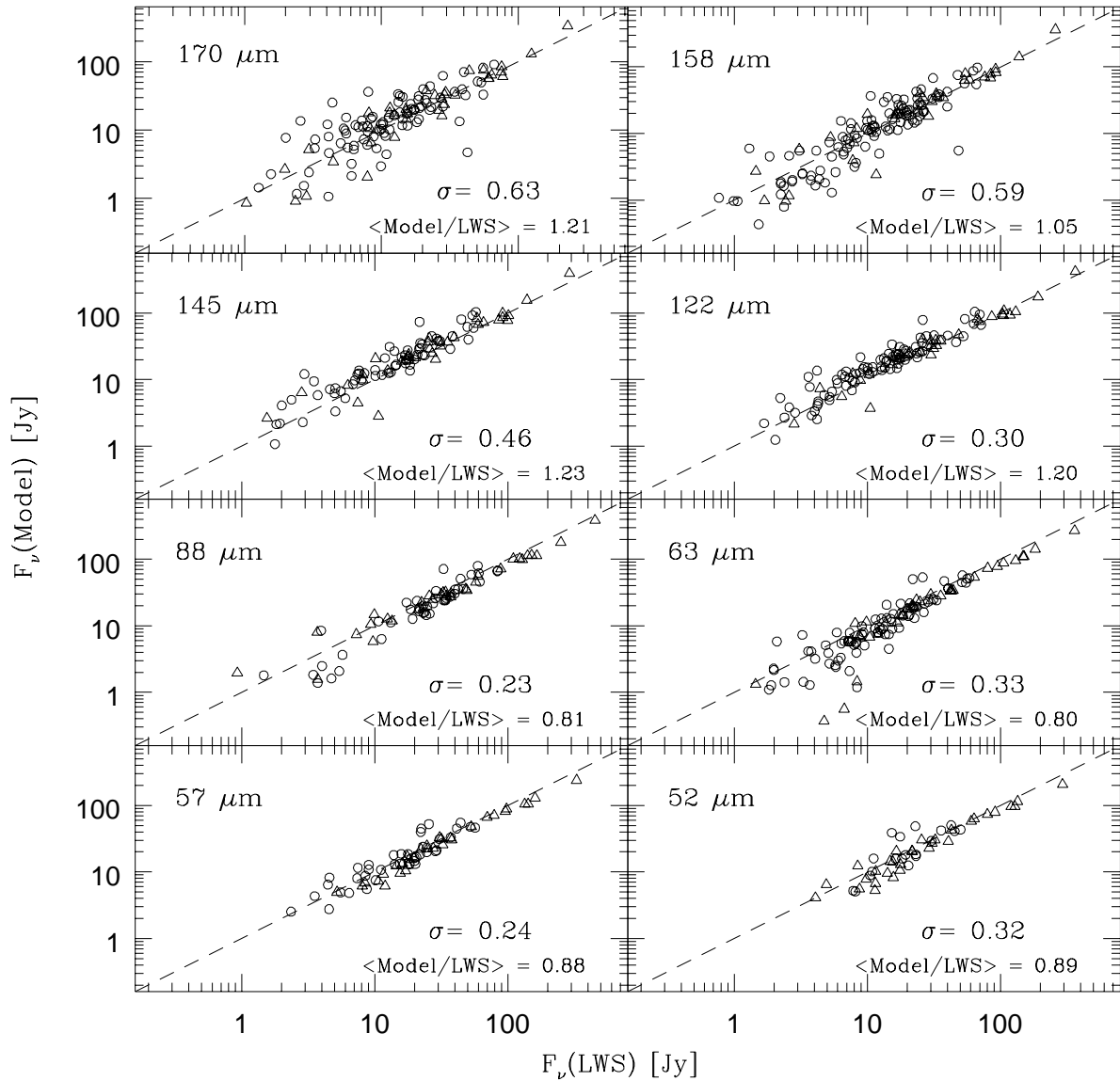


Fig. 10.— Comparison of the LWS continuum fluxes of galaxies unresolved by the LWS beam and the Dale & Helou (2002) model prediction for eight far-infrared wavelengths. Triangles (circles) represent continuum fluxes taken from a fully sampled L01 (fitted L02 line) spectrum. The dashed line is the one-to-one correlation.

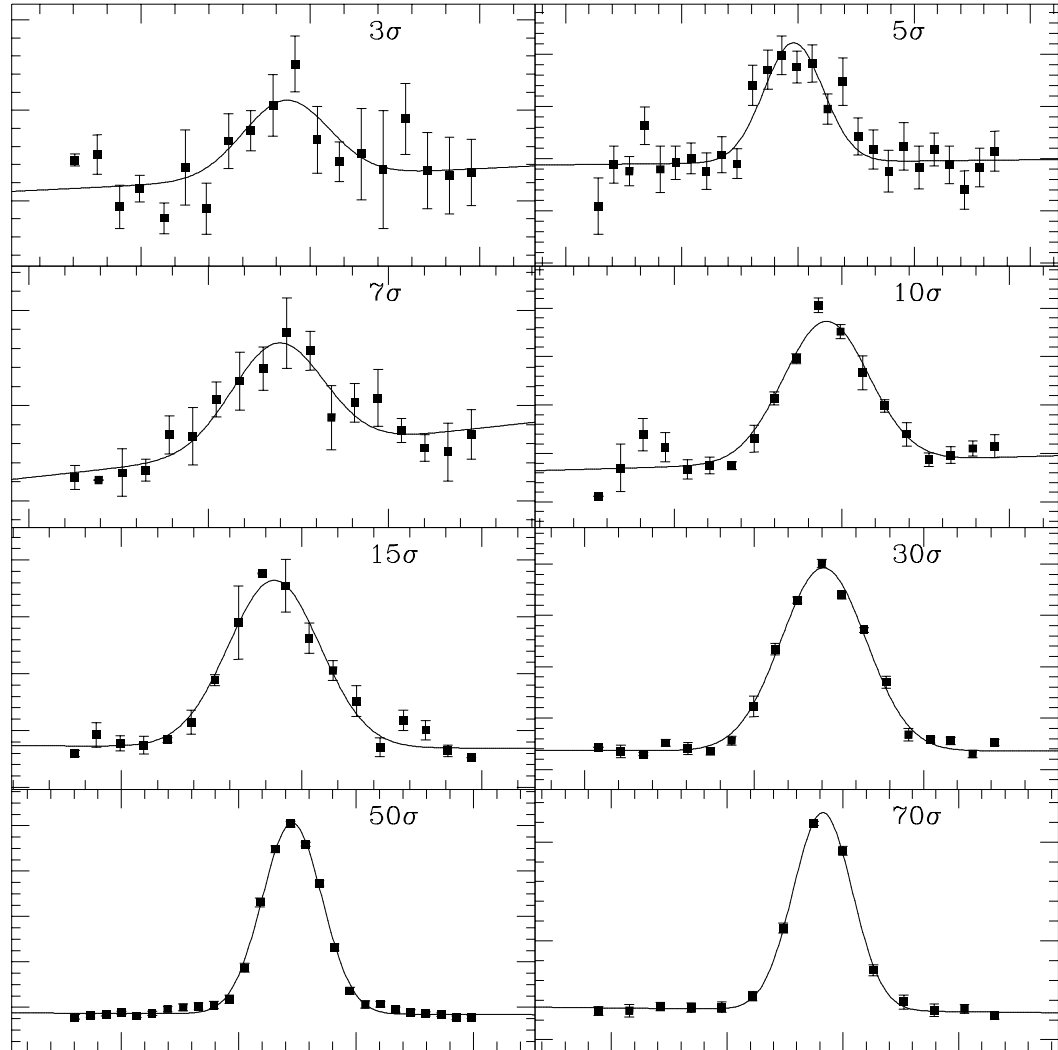


Fig. 11.— Examples of the [C II] 158 μm line found in this sample. This figure is a representative selection of varying signal-to-noise detections and shows how well a Gaussian with the effective instrumental width fits the line data. Error bars are taken from the uncertainty in the averaging of the spectral scans in each bin.

Fig. 12.— Three LWS spectra with both Milky Way [C II] 158 μm and C⁺ emission at the redshift of the observed galaxy is plotted along with the corresponding $1^\circ \times 1^\circ$ *IRAS* 100 μm images. The LWS observation for each galaxy was located at the center of each *IRAS* image. The line through the spectra is a best fit using a linear baseline and two instrumental width Gaussians.

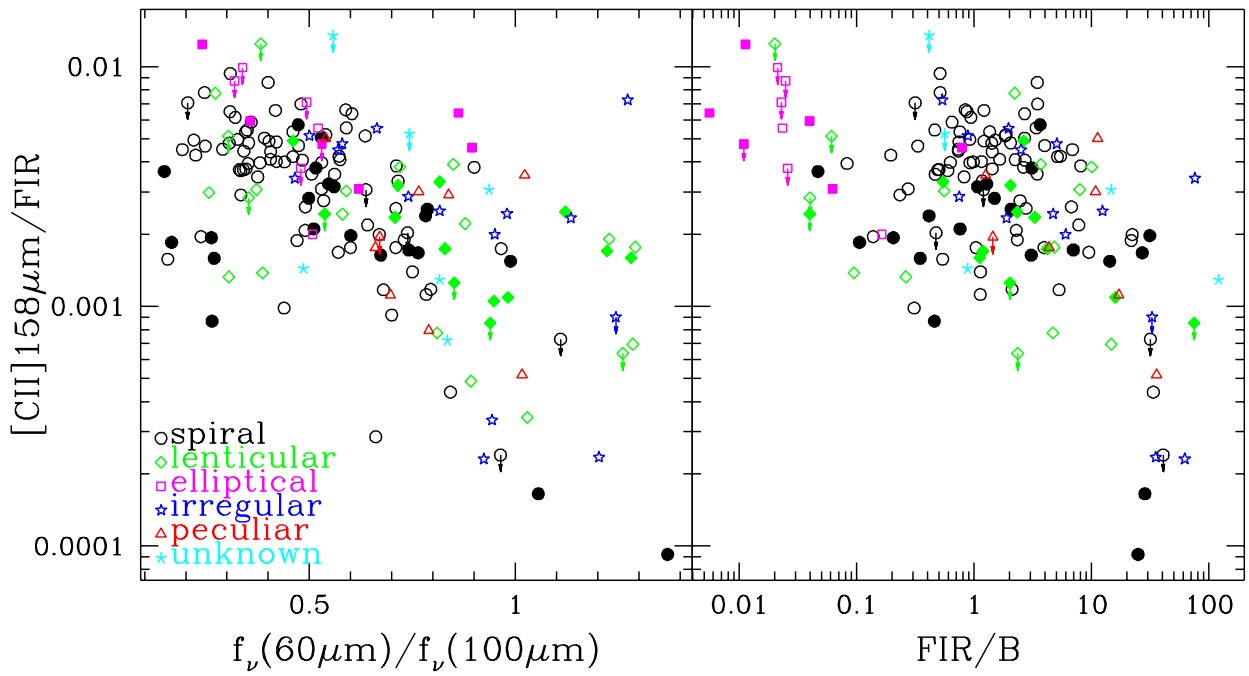


Fig. 13.— The ratio of [C II] 158 μm to far-infrared continuum is plotted against the *IRAS* 60 $\mu\text{m}/100 \mu\text{m}$ and *FIR/B* ratios for galaxies unresolved by the LWS. Galaxies of spiral ($T = 0 - 9$), lenticular ($T = -3, -2, -1$), elliptical ($T = -6, -5, -4$), irregular ($T = 10, 11, 90$), peculiar ($T = 99$), and unknown morphology are respectively plotted as circles, diamonds, squares, stars, and asterisks. AGN are indicated by filled symbols. Regardless of morphology, the [C II] 158 $\mu\text{m}/\text{FIR}$ ratio decreases as the 60 $\mu\text{m}/100 \mu\text{m}$ and *FIR/B* ratios increase.

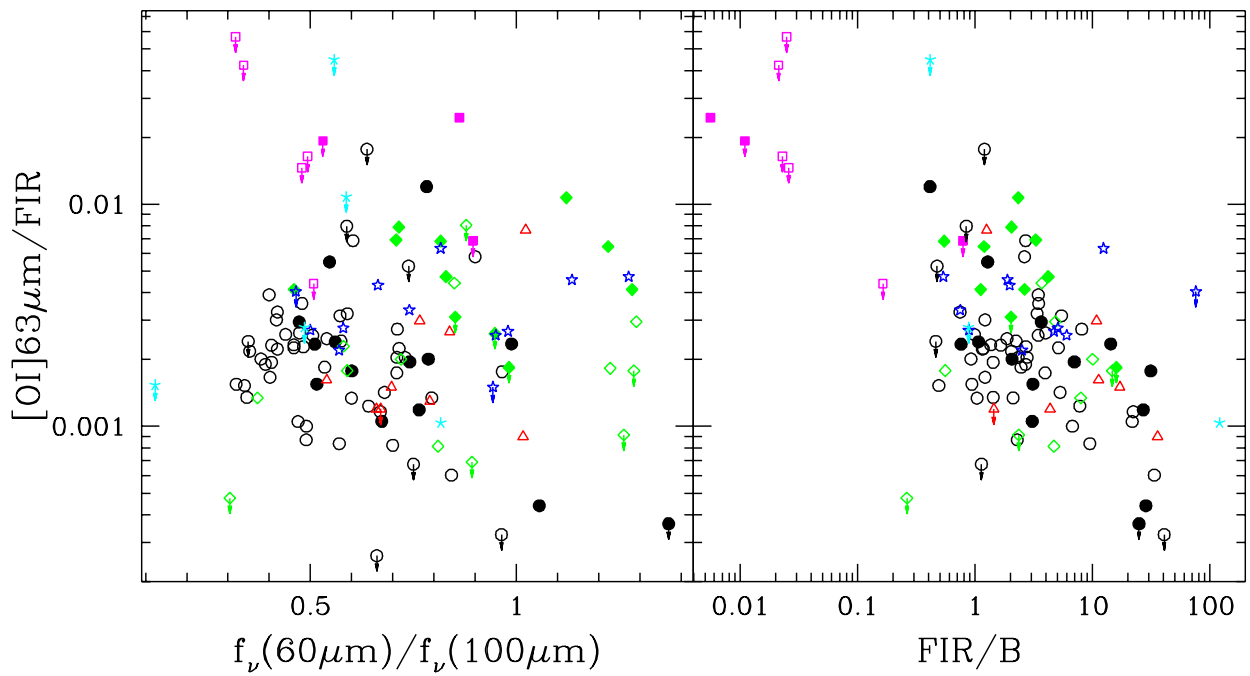


Fig. 14.— The ratio of [O I] 63 μm to far-infrared continuum is plotted against the *IRAS* 60 μm /100 μm and *FIR/B* ratios for galaxies unresolved by the LWS. The [O I] 63 μm /*FIR* shows no trend with either 60 μm /100 μm or *FIR/B*. The symbols are the same as those in Figure 13.

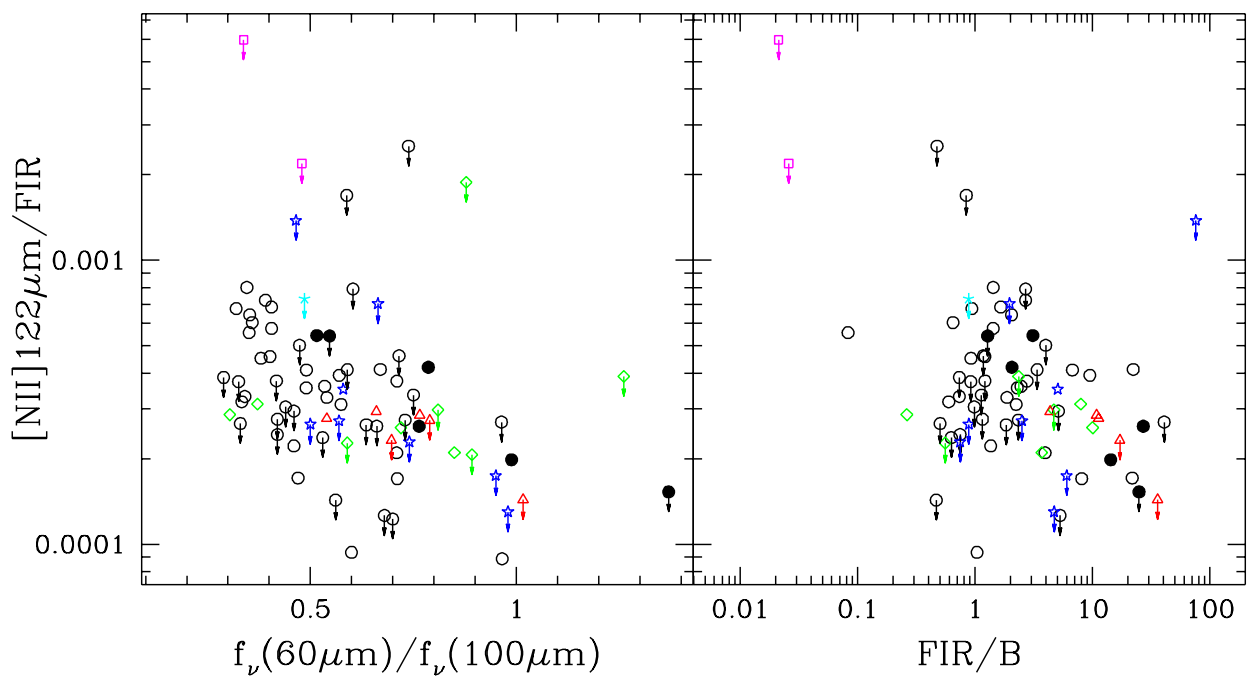


Fig. 15.— The ratio of [N II] 122 μm to far-infrared continuum is plotted against the *IRAS* 60 $\mu\text{m}/100 \mu\text{m}$ and *FIR/B* ratios for galaxies unresolved by the LWS. The [N II] 122 $\mu\text{m}/\text{FIR}$ ratio decreases as the 60 $\mu\text{m}/100 \mu\text{m}$ and *FIR/B* ratios increase, similar to the behavior of [C II] 158 $\mu\text{m}/\text{FIR}$ line. The symbols are the same as those in Figure 13.

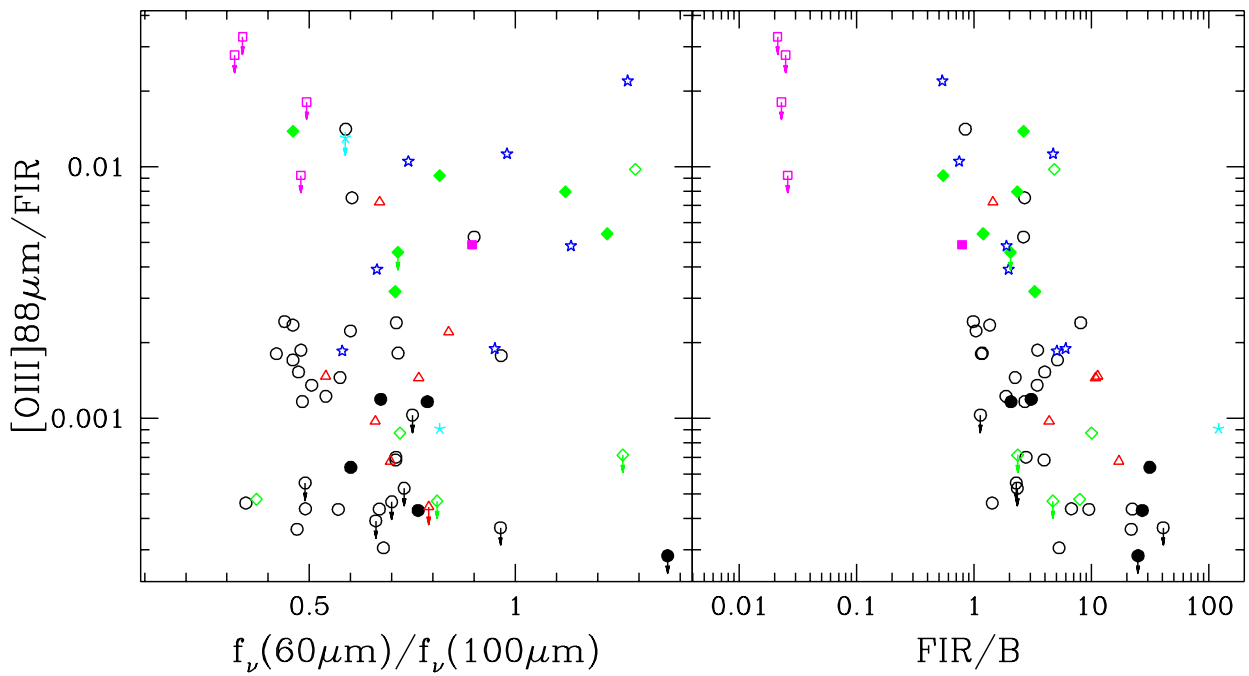


Fig. 16.— The ratio of [O III] 88 μm to far-infrared continuum is plotted against the *IRAS* 60 $\mu\text{m}/100 \mu\text{m}$ and *FIR/B* ratios for galaxies unresolved by the LWS. The [O III] 88 $\mu\text{m}/\text{FIR}$ ratio increases with increasing 60 $\mu\text{m}/100 \mu\text{m}$ ratio and decreases with increasing *FIR/B* ratio. The symbols are the same as those in Figure 13.

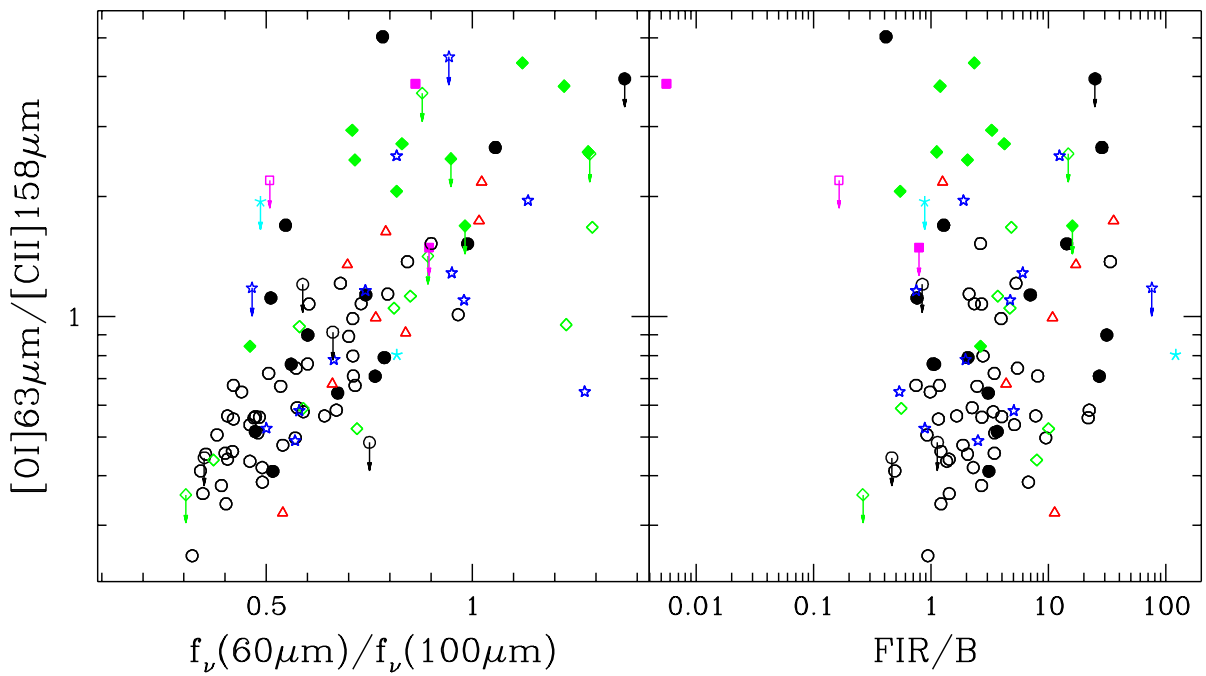


Fig. 17.— The ratio of [O I] 63 μm /[C II] 158 μm is plotted against the *IRAS* 60 μm /100 μm and *FIR/B* ratios for galaxies unresolved by the LWS. The [O I] 63 μm /[C II] 158 μm ratio increases as the 60 μm /100 μm ratio increases, but shows no correlation with the *FIR/B* ratio. The symbols are the same as those in Figure 13.

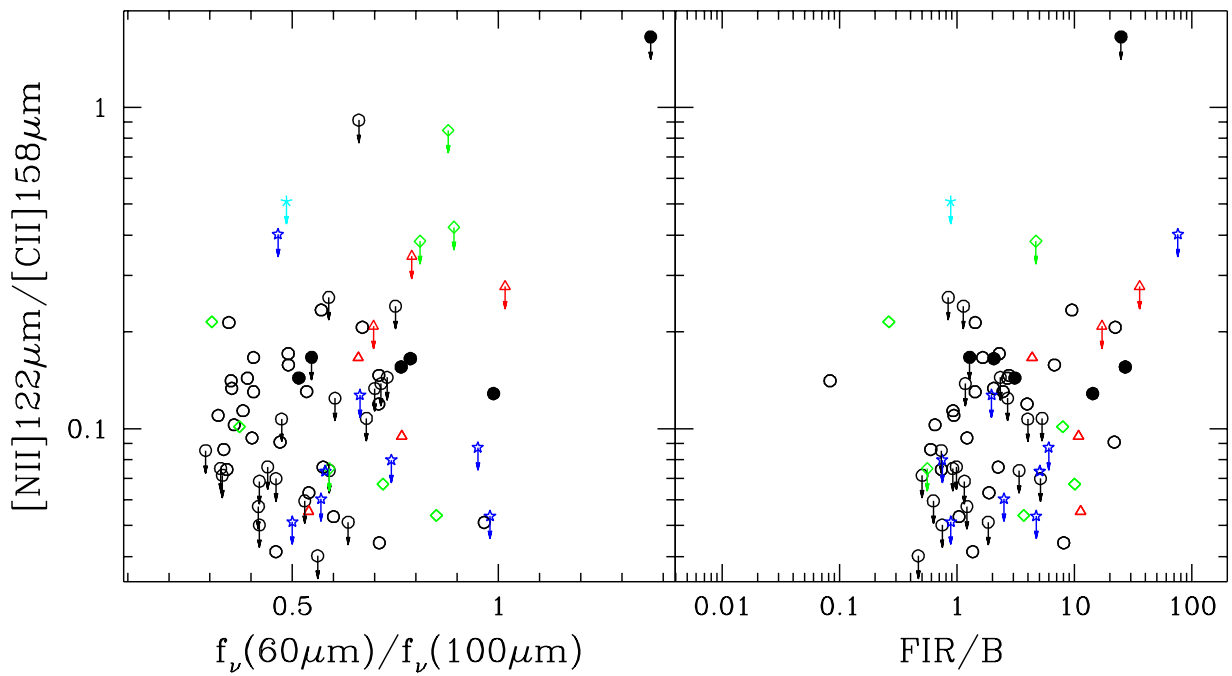


Fig. 18.— The ratio of [N II] 122 μm /[C II] 158 μm is plotted against the *IRAS* 60 $\mu\text{m}/100 \mu\text{m}$ and *FIR/B* ratios for galaxies unresolved by the LWS. The symbols are the same as those in Figure 13.

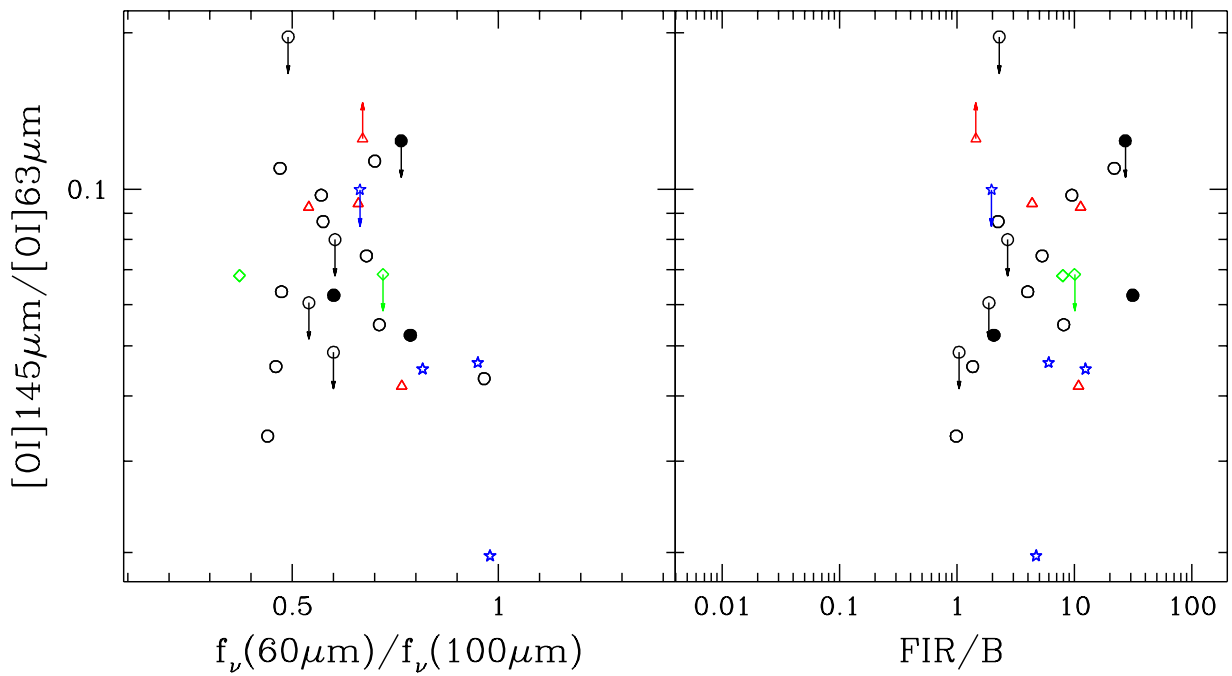


Fig. 19.— The ratio of [O I] 145 μm /[O I] 63 μm is plotted against the *IRAS* 60 μm /100 μm and *FIR/B* ratios for galaxies unresolved by the LWS. The symbols are the same as those in Figure 13.

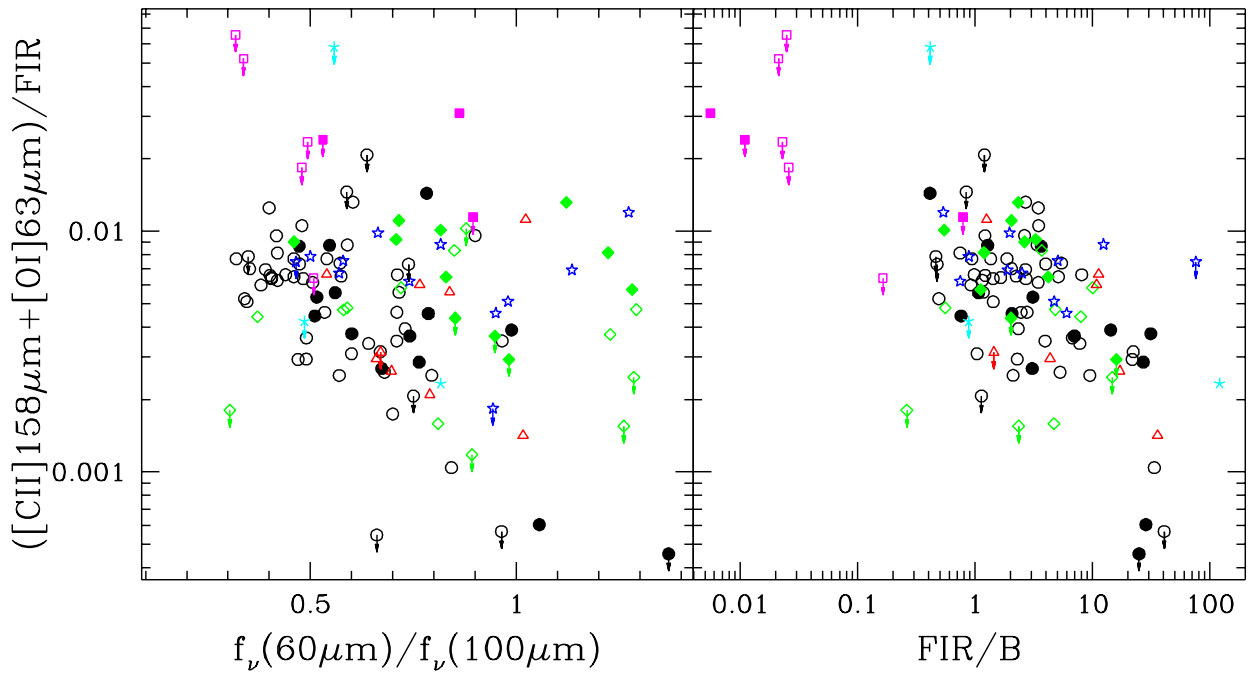


Fig. 20.— The ratio of ($[O\ I]$ 63 μm + [$C\ II$] 158 μm)/ FIR is plotted against the $IRAS$ 60 μm /100 μm and FIR/B ratios for galaxies unresolved by the LWS. The symbols are the same as those in Figure 13.

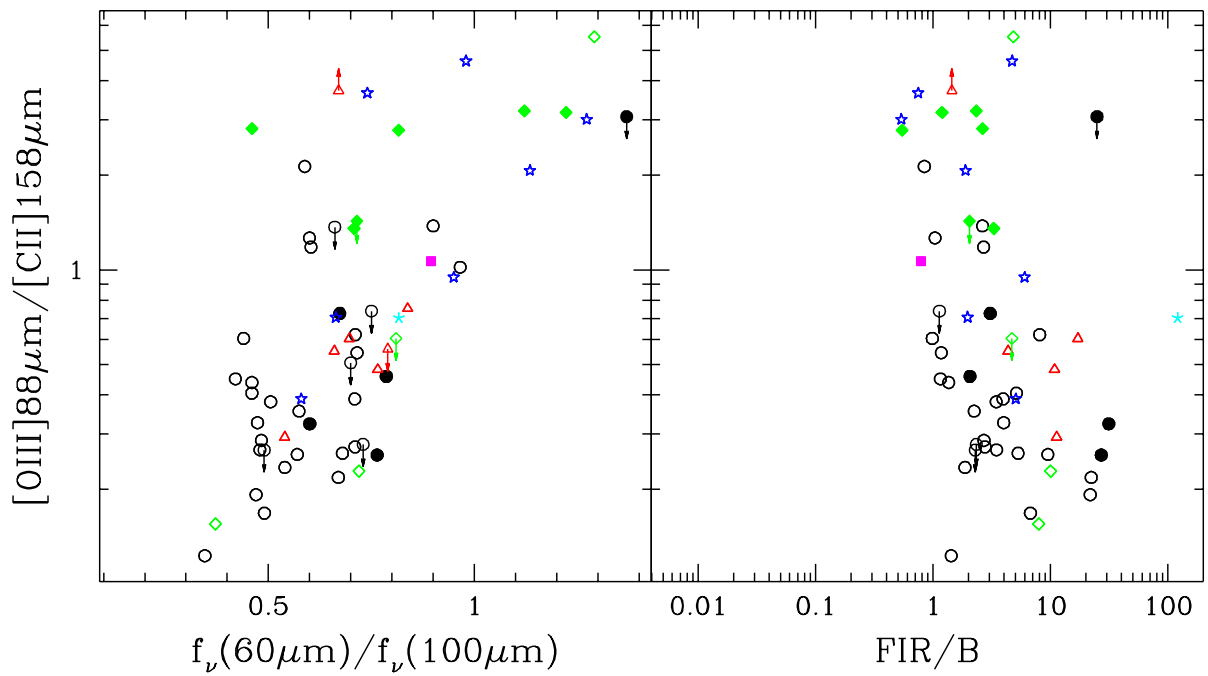


Fig. 21.— The ratio of [O III] 88 μm /[C II] 158 μm is plotted against the *IRAS* 60 μm /100 μm and *FIR/B* ratios for galaxies unresolved by the LWS. The [O III] 88 μm /[C II] 158 μm ratio increases with increasing 60 μm /100mm ratio, but shows no correlation with *FIR/B*. The symbols are the same as those in Figure 13.

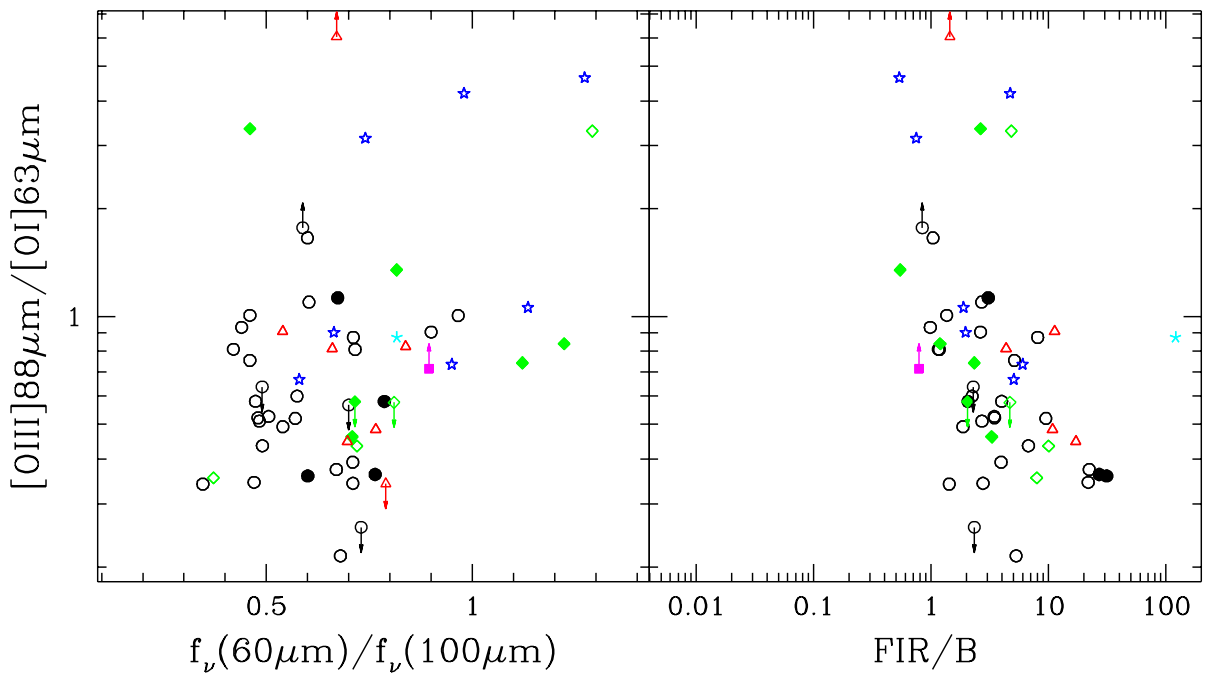


Fig. 22.— The ratio of [O III] 88 μm /[O I] 63 μm is plotted against the *IRAS* 60 μm /100 μm and *FIR/B* ratios for galaxies unresolved by the LWS. The symbols are the same as those in Figure 13.

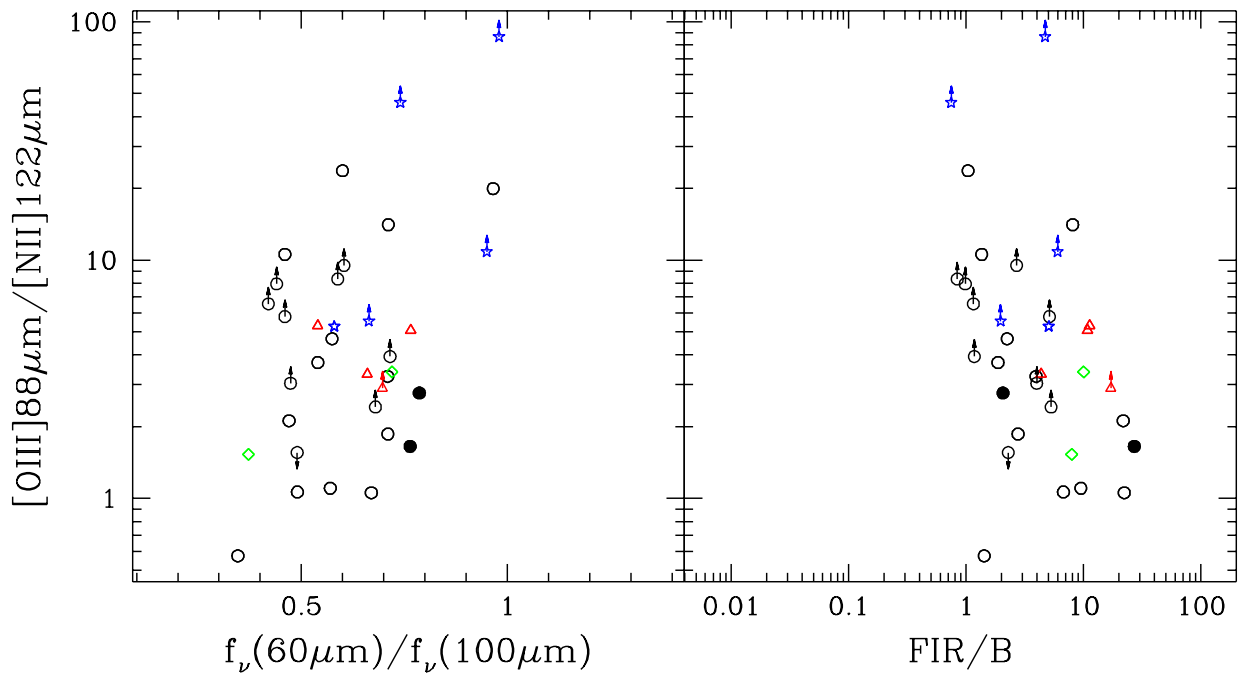


Fig. 23.— The ratio of [O III] 88 μm /[N II] 122 μm is plotted against the *IRAS* 60 μm /100 μm and *FIR/B* ratios for galaxies unresolved by the LWS. The symbols are the same as those in Figure 13.

This figure "f12.jpg" is available in "jpg" format from:

<http://arxiv.org/ps/0805.2930v1>